AD-A248 046

STUDIES OF NEAR-SOURCE AND NEAR-RECEIVER SCATTERING AND LOW-FREQUENCY Lg FROM EAST KAZAKH AND NTS EXPLOSIONS

I. N. Gupta
C. S. Lynnes
R. A. Wagner

Teledyne Geotech Alexandria Laboratories
314 Montgomery Street
Alexandria, VA 22314-1581

4 DECEMBER 1991

DTIC
ELECTE
MAR 10 1992
S B D

FINAL REPORT
16 APRIL 1989 - 15 JULY 1991

92-06131

92 3 09 059
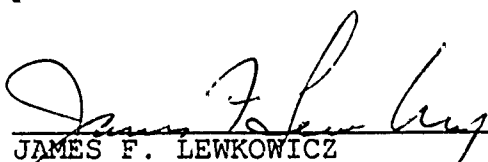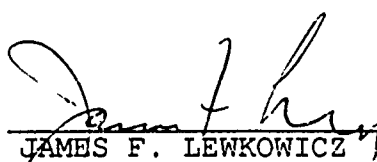
The views and conclusions contained in this document are those of the authors and should not be interpreted as representing the official policies, either expressed or implied, of the Defense Advanced Research Projects Agency or the U.S. Government.

This technical report has been reviewed and is approved for publication.

JAMES F. LEWKOWICZ
Contract Manager
Solid Earth Geophysics Branch
Earth Sciences Division

JAMES F. LEWKOWICZ
Branch Chief
Solid Earth Geophysics Branch
Earth Sciences Division

DONALD H. ECKHARDT, Director
Earth Sciences Division

This report has been reviewed by the ESD Public Affairs Office (PA) and is releasable to the National Technical Information Service (NTIS).

Qualified requestors may obtain additional copies from the Defense Technical Information Center. All others should apply to the National Technical Information Service.

If your address has changed, or if you wish to be removed from the mailing list, or if the addressee is no longer employed by your organization, please notify PL/IMA, Hanscom AFB, MA 01731-5000. This will assist us in maintaining a current mailing list.

Do not return copies of this report unless contractual obligations or notices on a specific document requires that it be returned.

REPORT DOCUMENTATION PAGE

Form Approved
OMB No. 0704-0188

1. AGENCY USE ONLY (Leave blank)	2. REPORT DATE 4 December 1991	3. REPORT TYPE AND DATES COVERED Final Report, 16 April 1989 - 15 July 1991

4. TITLE AND SUBTITLE
Studies of Near-Source and Near-Receiver Scattering and Low-Frequency Lg from East Kazakh and NTS Explosions

5. FUNDING NUMBERS
Contract F19628-89-C-0036
PE62714E
P9A10 TADA WUBC

6. AUTHOR(S)
I. N. Gupta, C. S. Lynnes, and R. A. Wagner

7. PERFORMING ORGANIZATION NAME(S) AND ADDRESS(ES)
Teledyne Geotech
314 Montgomery Street
Alexandria, VA 22314-1581

8. PERFORMING ORGANIZATION REPORT NUMBER
TGAL-91-08

9. SPONSORING / MONITORING AGENCY NAME(S) AND ADDRESS(ES)
DARPA/NMRO
(Attn: Dr. A. Ryall)
3701 North Fairfax Drive
Arlington, VA 22203-1714

Phillips Laboratory
Hanscom AFB, MA 01731-5000
Contract Manager: J. Lewkowicz/GEH

10. SPONSORING / MONITORING AGENCY REPORT NUMBER
PL-TR-91-2287

11. SUPPLEMENTARY NOTES

12a. DISTRIBUTION / AVAILABILITY STATEMENT
Approved for Public Release; Distribution Unlimited

12b. DISTRIBUTION CODE

13. ABSTRACT (Maximum 200 words)

This report consists of three sections: (A) Evidence for Rg-to-P Scattering in Teleseismic P-coda and Rg-to-S Scattering in Regional Lg of East Kazakh Explosions, (B) Generation of Low-frequency Lg from NTS Explosions, and (C) An Array Study of the Effects of a Known Local Scatterer on Regional Phases. In Section A, analysis of teleseismic data from Degelen and Shagan River explosions recorded at NORSAR and EKA arrays suggests that the low-frequency P-coda is dominated by near-source scattering of the explosion-generated Rg into P. Regional data from Shagan River explosions recorded at WMQ indicates that the low-frequency Lg is probably due to the scattering of explosion-generated Rg into S. In Section (B), analysis of regional data from Yucca Flat and Pahute Mesa explosions suggests that Rg-to-S makes a significant contribution to the low-frequency Lg. Strong support for this comes from a comparison of data from closely spaced explosions. In Section C, f-k analysis of regional events recorded at NORESS provides evidence for scattered arrivals Pn-to-Rg, Pg-to-Rg, and Lg-to-Rg, originating from a known prominent scatterer in the region of Lake Mjosa.

14. SUBJECT TERMS
Rg, Lg, Rg-to-P scattering, Rg-to-S scattering, Low-frequency Lg, f-k analysis, scattering, Degelen explosions, Shagan River explosions

15. NUMBER OF PAGES
108

16. PRICE CODE

17. SECURITY CLASSIFICATION OF REPORT	18. SECURITY CLASSIFICATION OF THIS PAGE	19. SECURITY CLASSIFICATION OF ABSTRACT	20. LIMITATION OF ABSTRACT
Unclassified	Unclassified	Unclassified	UL

SECTION A

EVIDENCE FOR Rg-TO-P SCATTERING IN TELESEISMIC P-CODA AND Rg-TO-S SCATTERING IN REGIONAL Lg OF EAST KAZAKH EXPLOSIONS

SUMMARY

Analysis of teleseismic data from both Degelen and Shagan River (East Kazakh, U.S.S.R.) underground nuclear explosions recorded at two seismic arrays suggests that the low-frequency teleseismic P-coda is dominated by near-source scattering of fundamental-mode Rayleigh-to-P ($Rg \rightarrow P$). The data set consisted of 22 Degelen (including 8 with announced shot depths) and 40 Shagan River explosions recorded at the NORSAR and EKA arrays, respectively. Good agreement between the observed and expected variation of the amplitude ratio P/P-coda (averaged over the frequency range of 0.5-2.0 Hz) with shot depth indicates that scattering of the explosion-generated Rg, apparently due to heterogeneities in the source region, makes significant contributions to teleseismic P-coda. Similarly, regional data from Shagan River explosions recorded at the CDSN station, WMQ, indicates that the low-frequency Lg is probably due to the scattering of explosion-generated Rg into S. The scattering mechanisms provide possible explanations for the stability of P-coda and Lg as estimators of explosive yields because the scattering is expected to occur over a large region of the shallow crust. An understanding of the generation of teleseismic P-coda and low-frequency Lg from underground nuclear explosions not only provides useful source information including shot depth but is also essential for improving yield estimates and source discrimination.

SECTION B

GENERATION OF LOW-FREQUENCY Lg FROM NTS EXPLOSIONS

SUMMARY

Analysis of regional data from Yucca Flat and Pahute Mesa regions of NTS suggests that near-source scattering makes a significant contribution to the large-amplitude low-frequency Lg observed at regional distances. A possible mechanism for generation of low-frequency Lg appears to be the scattering of explosion-generated Rg into S. Variations of low-frequency amplitude ratios Pn/Lg and Pg/Lg with shot depth are not always consistent with the expected depth-dependence of Rg generated by a point source within a homogeneous half space. The lack of good agreement in certain cases may, however, be due to the complexity of sub-surface geology at the NTS where large lateral and vertical variations in physical properties of rock are common. For closely spaced shots at both Yucca Flat and Pahute Mesa, a comparison of the low-frequency spectra of their regional phases at common recording stations shows variation with shot depth that agrees well with the theoretically expected dependence on shot depth and therefore supports the Rg-to-S mechanism. The generation of Lg appears to be considerably influenced by azimuthal direction, perhaps because the scattering function Rg-to-S varies significantly with direction. The observed strong dependence on azimuth appears to support near-source scattering rather than spall as the main contributor to the low-frequency Lg. Observed differences in the Lg spectra of normal and overburied shots may also be explained in terms of Rg-to-S scattering. The known stability of Lg as an estimator of explosive yields may be due to scattering occurring over a relatively large volume of the uppermost crust.

SECTION C

AN ARRAY STUDY OF THE EFFECTS OF A KNOWN LOCAL SCATTERER ON REGIONAL PHASES

SUMMARY

Our f-k analyses of NORESS array recordings of teleseismic events first indicated a prominent secondary source about 25-30 km southwest of the array, in the region of Lake Mjosa with large topographical relief. The use of residual seismograms derived by subtracting the beamed record from each array channel provided an effective method for isolating the secondary source from the effects of the primary source. In this study, similar f-k techniques are used to investigate the effects of this known scatterer on the regional phases Pn, Pg, and Lg from several events at regional distances. The beamed record for each regional phase is obtained by incorporating steering delays based on the known azimuthal direction and phase velocity from the f-k analysis of raw data. Both explosion and earthquake sources along various azimuthal directions to NORESS provide evidence for scattered arrivals Pn-to-Rg, Pg-to-Rg, and Lg-to-Rg, originating from the same region of Lake Mjosa. These scattered arrivals are observed with remarkable clarity and closeness to the expected arrival times and are rich in low frequencies, as expected for Rg. Their presence in various regional phases indicates that near-receiver scattering plays an important role in the composition of regional phases.

(THIS PAGE INTENTIONALLY LEFT BLANK)

vi

TABLE OF CONTENTS

Section A

EVIDENCE FOR Rg-TO-P SCATTERING IN TELESEISMIC P-CODA AND Rg-TO-S SCATTERING IN REGIONAL Lg OF EAST KAZAKH EXPLOSIONS

Section B

GENERATION OF LOW-FREQUENCY Lg FROM NTS EXPLOSIONS

Section C

AN ARRAY STUDY OF THE EFFECTS OF
A KNOWN LOCAL SCATTERER ON REGIONAL PHASES

SECTION A

EVIDENCE FOR Rg-TO-P SCATTERING IN TELESEISMIC P-CODA AND

Rg-TO-S SCATTERING IN REGIONAL Lg OF EAST KAZAKH EXPLOSIONS

INTRODUCTION

Theoretical (e.g. Garvin, 1956) and observational studies (e.g. Rulev, 1965) indicate that, in the vicinity of a shallow explosion, the largest amount of ground surface motion is generally due to Rayleigh waves. An analysis of teleseismic P arrivals from underground nuclear explosions at Novaya Zemlya, U.S.S.R., known for its rugged topography, led Greenfield (1971) to suggest that a significant portion of arrivals in P-coda (taken to be between 10 and 40 sec after first P) may be due to near-surface scattering of explosion-generated Rayleigh waves into teleseismic P. Gupta et al. (1985a, 1991b) proposed that near-source scattering of fundamental-mode Rayleigh waves (Rg) into teleseismic P (referred to as Rg→P hereafter) may be responsible for the large arrivals immediately following P and pP on NORSAR records of Nevada Test Site (NTS) shots. Theoretical studies of near-source scattering by explosion sources in the Yucca Flat (NTS) region by McLaughlin et al. (1987) and Stead and Helmberger (1988) also demonstrated that locally scattered Rayleigh waves may be responsible for the large arrivals immediately following P and pP. F-k analyses of teleseismic recordings of both U.S. and U.S.S.R. explosions provided evidence in favor of both near-receiver P→Rg and near-source Rg→P scattering (Gupta et al., 1990a; Gupta et al., 1990b). Observations of the spectra of Rg signals from both explosions and very shallow-focus earthquakes indicate the dominant energy in Rg to be confined to frequencies less than about 2 Hz and the most important parameter for influencing its generation to be the

1

- source-depth (e.g. Kafka, 1990).

Several investigators (e.g. Frasier, 1972; Bakun and Johnson, 1973; McLaughlin et al., 1990) have suggested that spall makes a significant contribution to the low-frequency component of teleseismic P arrivals. It is important to understand the generation of teleseismic P-coda, especially because of its usefulness as an effective measure of the seismic yield of nuclear explosions (Gupta et al., 1985b). Moreover, an understanding of the various arrivals in teleseismic P from nuclear explosions may provide useful source information such as shot depth, medium velocity, and geological environment. In this study, we analyze the spectra of teleseismic P and P-coda from underground nuclear explosions at Degelen Mountain and Shagan River test sites in Eastern Kazakh, U.S.S.R., recorded at the NORSAR and EKA arrays, respectively. Least squares inversion of array data allows the results to be relatively free from recording site effects. Use is made of the recently released information on Soviet nuclear explosions by Bocharov et al. (1989). A comparison of the observed dependence of the amplitude ratio P/P-coda on shot depth with the theory of explosion-generated Rg shows good agreement, suggesting that the low-frequency content of teleseismic P-coda consists mainly of Rg→P arrivals. Similarly, analysis of regional data from 14 Shagan River explosions recorded at the CDSN station, WMQ, indicates that the low-frequency component of the observed Lg is probably due to the scattering of explosion-generated Rg into S. It is expected that Rg→P scattering should be accompanied by even larger Rg→S scattering (e.g. Stead and Helmberger, 1988).

DEPENDENCE OF EXPLOSION-GENERATED Rg AND P-CODA ON SHOT DEPTH

For an explosion source with source function S(f) within a homogeneous half space, the fundamental-mode Rayleigh wave amplitude $R_g(f)$ is given by the expression (Hudson and Douglas, 1975):

$$R_g(f) = \frac{A \, \overline{\phi}(\omega)}{r^{0.5} \, \rho \, \alpha^{3.5}} \, f^{1.5} \, 10^{-4.4 \frac{h}{\alpha} f} \tag{1}$$

where $\overline{\phi}(\omega)$ is the Fourier transform of the source RDP $\phi(t)$, h is the shot depth, $\omega = 2\pi f$, α is the compressional-wave velocity of the shot medium, ρ is the density, r is the epicentral distance, A is a numerical constant, and a Poisson's ratio of 0.25 is assumed. The far-field P-wave displacement, in the frequency domain, may be written as (Hudson and Douglas, 1975):

$$P(f) = \frac{1}{4 \pi \rho \, \alpha^3 \, R} \, \omega \, \overline{\phi}(\omega) \tag{2}$$

where R is the teleseismic source-receiver distance. If the source-receiver path and the medium velocity do not change, equations (1) and (2) yield

$$\frac{Rg \rightarrow P}{P} (f) = k \, C(f) \, f^{0.5} \, 10^{-4.4 \frac{h}{\alpha} f} \tag{3}$$

where k is a constant and C(f) denotes the scattering function Rg→P. Assuming that the low-frequency P-coda in teleseismic data is mainly due to the scattering of Rg, we replace Rg→P in equation (3) by P-coda and obtain

$$\log \frac{P}{P-coda} (f) = 4.4 \frac{h}{\alpha} f - \log k - \log C(f) - 0.5 \log f \tag{4}$$

This shows that if we consider explosions for which the Rg→P scattering function may be assumed to be the same (such as closely spaced explosions) and the frequency is kept fixed

(i.e. for a narrow frequency band), a plot of log P/P-coda versus shot depth, h should have a slope of about 4.4 f/α.

P AND P-CODA FROM DEGELEN EXPLOSIONS RECORDED AT NORSAR ARRAY

We first examined short-period, vertical component teleseismic P arrivals from 22 Degelen explosions (Table 1) recorded at 22 center element sensors of the NORSAR array, providing over 400 observations. In Table 1, data for the first 8 shots is from Bocharov et al. (1989) and those for the remaining explosions is from P. D. Marshall (written communication, 1987). The epicentral distance is about 38° along the azimuth of about 313° or N 47° W. This testing area is dominated by the Degelen mountain, with local relief of a few hundred meters and locally steep slopes. Figure 1, based on topographic data in Bonham et al. (1980), shows the main features along with the eight known locations of shots from Bocharov et al. (1989). The emplacement of nuclear devices was made possible by tunneling into the mountain.

As compared to results from a single receiver, use of multichannel data has the advantage that receiver effects, which can drastically influence the observed signals, can be eliminated or at least suppressed. Excluding a few channels with spikes or clipped data, spectra and spectral ratios P/P-coda were obtained for each record by selecting a window length of 12.8 sec (beginning 4 sec before the onset of P) as the P-window and the following 25.6 sec signal as the P-coda, and applying Parzen taper to each (see Figure 1 of Gupta and Blandford, 1987 for examples). A correction for noise was made by selecting a sample of noise before the onset of P, obtaining its spectra, and subtracting its power from that of the observed signal. The average amplitude ratio of P/P-coda, over the frequency range of 0.5-2.0 Hz, was obtained by using only those data points for which the signal/noise power ratio was at least 2 for each of P and P-coda. All available amplitude ratios P/P-coda were used as input to a least squares inversion that separated the source and receiver terms.
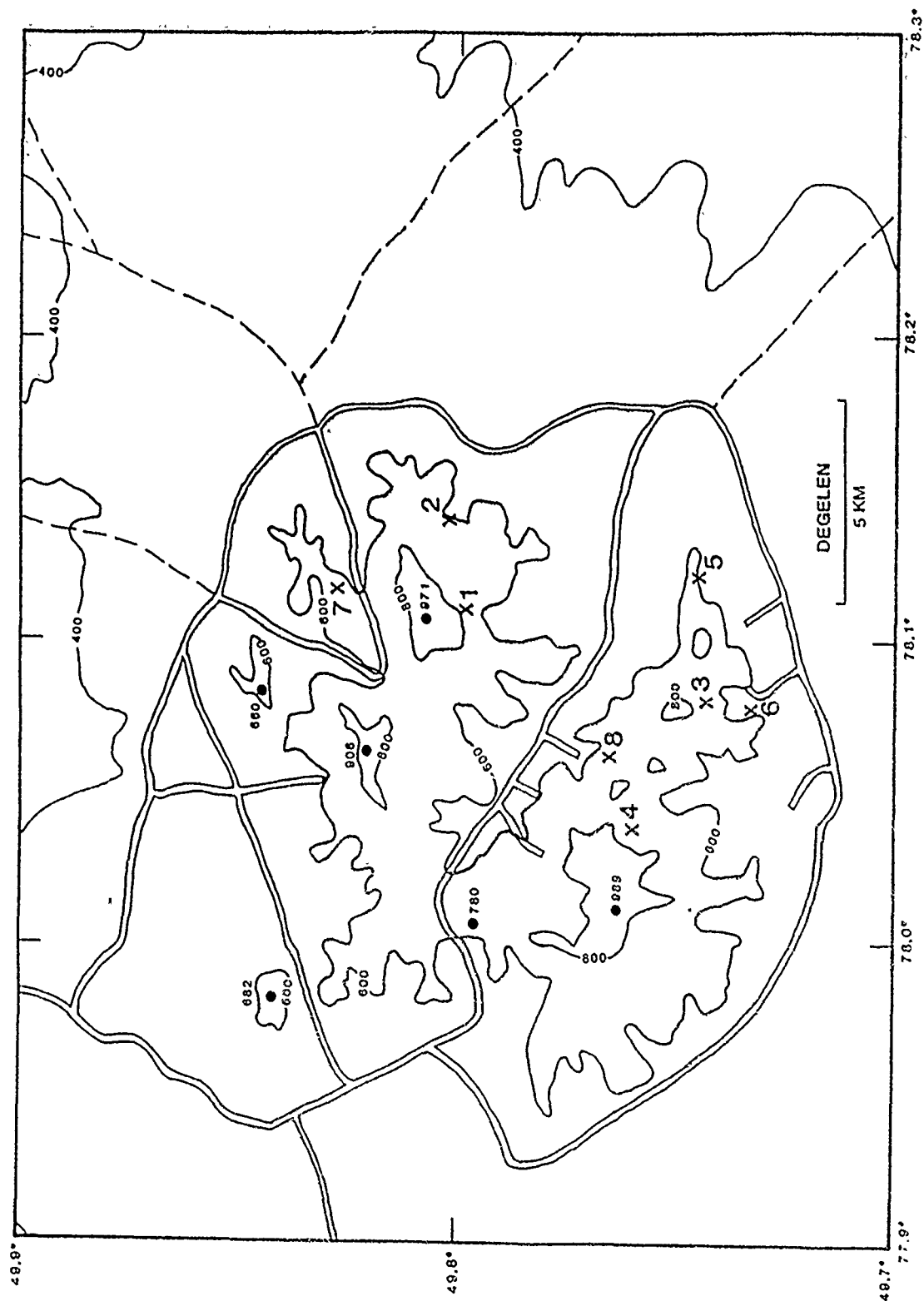
5

Figure 1. Topographic map of the Degelen mountain region with locations of 8 explosions numbered as in Table 1. The contour interval is 200 m.

6

TABLE 1

22 DEGELEN MOUNTAIN SHOTS RECORDED AT NORSAR ARRAY

No.	DATE	ORIGIN TIME	LAT (N)	LON (E)	m_b	DEPTH (M)	YIELD (KT)
1	22 Mar 1971	04:33:00.3	49.79847	78.10897	5.767	283.0	20-150
2	25 May 1971	04:03:00.4	49.80164	78.13883	5.048	132.0	<20
3	29 Nov 1971	06:02:59.9	49.74342	78.07850	5.462	203.0	<20
4	30 Dec 1971	06:21:00.2	49.76003	78.03714	5.838	249.0	20-150
5	10 Mar 1972	04:56:59.8	49.74531	78.11969	5.453	171.0	<20
6	28 Mar 1972	04:22:00.1	49.73306	78.07569	5.177	124.0	6
7	07 Jun 1972	01:28:00.0	49.82675	78.11547	5.422	208.0	20-150
8	16 Aug 1972	03:16:59.8	49.76547	78.05883	5.105	139.0	8
9	16 Feb 1973	05:02:57.6	49.822	78.158	5.477	-	-
10	26 Oct 1973	04:26:57.7	49.759	78.164	5.228	-	-
11	16 May 1974	03:02:57.7	49.752	78.093	5.242	-	-
12	25 Jun 1974	03:56:57.7	49.840	78.166	4.419	-	-
13	10 Jul 1974	02:56:57.6	49.783	78.130	5.168	-	-
14	13 Sep 1974	03:02:57.6	49.778	78.081	5.144	-	-
15	16 Dec 1974	06:40:58.0	49.867	78.087	4.887	-	-
16	20 Feb 1975	05:32:57.6	49.789	78.062	5.765	-	-
17	11 Mar 1975	05:42:57.6	49.747	78.146	5.424	-	-
18	07 Aug 1975	03:56:57.7	49.812	78.161	5.187	-	-
19	15 Jan 1976	04:46:57.6	49.824	78.201	5.182	-	-
20	21 Apr 1976	04:57:57.8	49.776	78.146	4.940	-	-
21	19 May 1976	02:56:57.8	49.796	78.058	4.722	-	-
22	23 Jul 1976	02:32:57.8	49.779	78.085	4.961	-	-

A plot of the source-term amplitude ratio P/P-coda versus shot depth for 8 Degelen explosions for which shot depths are known (Bocharov *et al.*, 1989) is shown in Figure 2a whereas a plot of the source term versus m_b for all 22 shots is shown in Figure 2b. Assuming the P-wave velocity in the Degelen testing region to be about 4 km/sec (Bonham *et al.*, 1980), 4.4 $f/\alpha \approx 1.4$, if f is taken to be the average of 0.5 and 2.0, or 1.25 Hz. Good agreement between the mean slope expected from simple theory and observation (Figure 2a) suggests that the low-frequency P-coda is mainly due to the scattering of explosion-generated Rg.
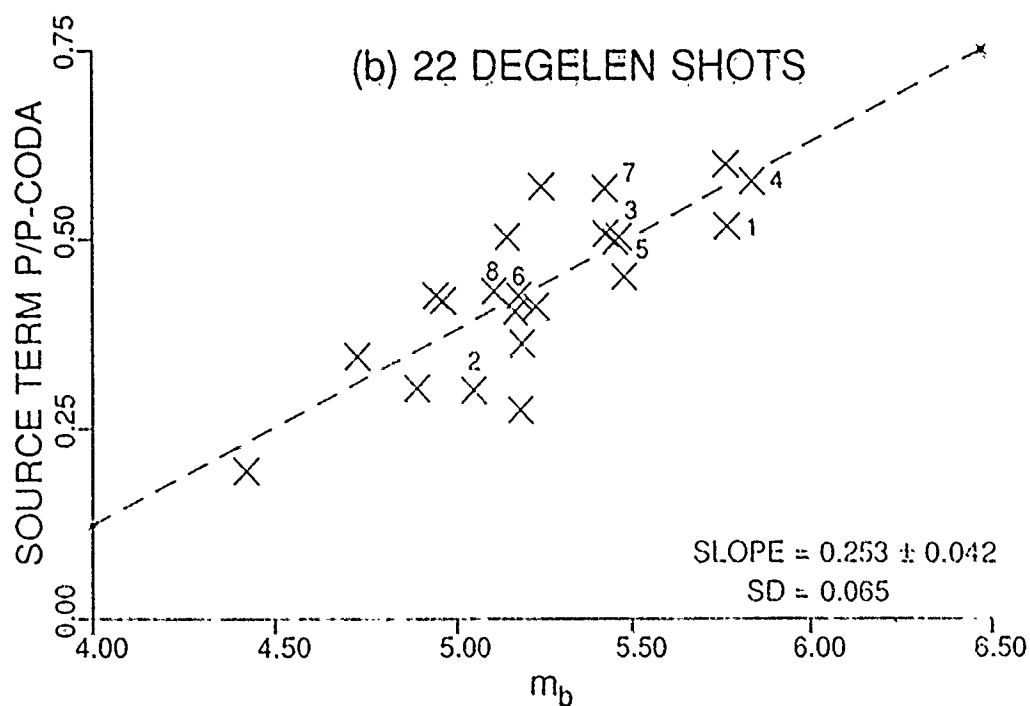
7
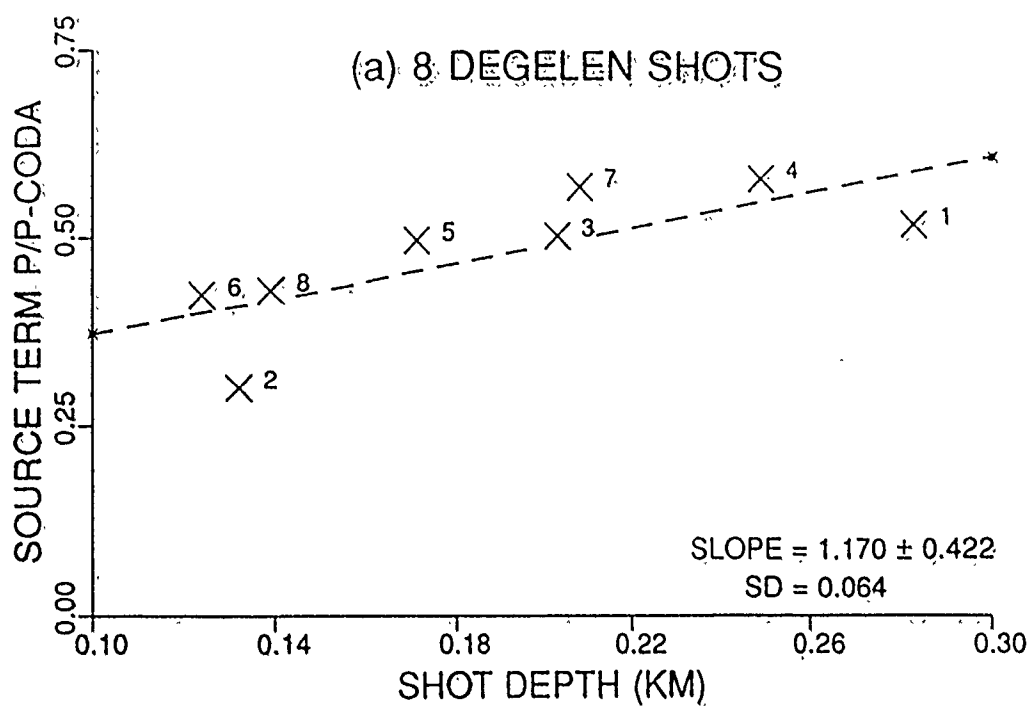
Figure 2. Source term amplitude ratio P/P-coda (log units), averaged over the frequency range of 0.5-2.0 Hz and derived from NORSAR array data, plotted versus (a) shot depth for 8 Degelen explosions (numbered as in Table 1), and (b) versus m_b for 22 Degelen explosions. The least squares linear regression (dashed line), mean slope (with associated standard deviation), and one standard deviation of residuals (SD) are indicated on each plot.

8

Results in Figure 2b, in which the 8 explosions used in Figure 2a have been identified, suggest generally larger P/P-coda for larger explosions and a dependence on shot depth that appears to be similar to that in Figure 2a.

On the basis of the known locations of 8 Degelen shots (Bocharov *et al.*, 1989), Figure 2a includes results from three pairs of explosions (nos. 1 and 2, 3 and 6, 4 and 8) that are within about 2 km of each other. Since differences in propagation paths are known to exert significant influence on various seismic arrivals, results from closely spaced seismic sources recorded at a common station should be considered more reliable than others. It is important to note that the slope from each of the three pairs of closely spaced shots in Figure 2a is nearly the same as that derived from the average of all (8) shots and is in good agreement with the theoretically expected value.

P AND P-CODA FROM SHAGAN RIVER EXPLOSIONS RECORDED AT EKA ARRAY

We examined the short-period, vertical-component data from 40 Shagan River explosions (28 from SW and 12 from NE region) recorded at the Eskdalemuir (EKA) array. These shots are listed in Table 2 in which data for the first 4 shots is from Bocharov $et\ al.$ (1989) and those for the remaining explosions is from P. D. Marshall (written communication, 1987). The array has 20 elements arranged in an "L" configuration with element spacing of 0.9 km and maximum spacing of 9.8 km (Bache $et\ al.$, 1985). The epicentral distance of Shagan explosions to the array is about $47°$ along the azimuth of about $310°$ or $N50°W$. The Shagan River test site is believed to be underlain by about 100 m of unconsolidated sediments with the thickness decreasing gradually towards southwest (Bonham $et\ al.$, 1980). A plot of the source-term amplitude ratio P/P-coda versus m_b (Figure 3a) suggests generally larger P/P-coda for larger explosions and the mean slope is close to that obtained in Figure 2b. For a fixed value of m_b, the NE Shagan shots in Figure 3a have generally smaller values of P/P-coda than the SW shots. This will be consistent with generally larger P-coda and greater complexity for the NE shots than for the SW shots observed by Bache $et\ al.$ (1984) and Marshall $et\ al.$ (1985).

TABLE 2

40 SHAGAN RIVER EXPLOSIONS RECORDED AT EKA ARRAY

| No.	DATE	ORIGIN TIME	LAT (N)	LON (E)	m_b	DEPTH (M)	YIELD (KT)
1	15 Jan 1965	06:00:00.8	49.93500	79.00936	5.87	178.0	100-150
2	19 Jun 1968	05:05:59.8	49.98025	78.98550	5.28	316.0	<20
3	30 Nov 1969	03:32:59.7	49.92428	78.95575	6.02	472.0	125
4	30 Jun 1971	03:56:59.8	49.94600	78.98047	4.94	217.0	<20
5	31 May 1974	03:27:00.4	49.950	78.852	5.81	-	-
6	16 Oct 1974	06:33:00.5	49.979	78.898	5.41	-	-
7	27 Dec 1974	05:46:59.8	49.943	79.011	5.50	-	-
8	27 Apr 1975	05:37:00.2	49.949	78.926	5.51	-	-
9	30 Jun 1975	03:27:00.5	50.004	78.957	4.52	-	-
10	29 Oct 1975	04:47:00.3	49.946	78.878	5.61	-	-
11	25 Dec 1975	05:17:00.1	50.044	78.814	5.69	-	-
12	04 Jul 1976	02:57:00.4	49.909	78.911	5.85	-	-
13	28 Aug 1976	02:57:00.4	49.969	78.930	5.74	-	-
14	07 Dec 1976	04:57:00.3	49.922	78.846	5.80	-	-
15	29 May 1977	02:57:00.5	49.937	78.770	5.75	-	-
16	29 Jun 1977	03:07:00.7	50.006	78.869	5.20	-	-
17	05 Sep 1977	03:03:00.3	50.035	78.921	5.73	-	-
18	30 Nov 1977	04:07:00.3	49.958	78.885	5.89	-	-
19	11 Jun 1978	02:57:00.5	49.898	78.797	5.83	-	-
20	05 Jul 1978	02:47:00.4	49.887	78.871	5.77	-	-
21	15 Sep 1978	02:37:00.3	49.916	78.879	5.89	-	-
22	04 Nov 1978	05:06:00.2	50.034	78.943	5.56	-	-
23	23 Jun 1979	02:57:00.4	49.903	78.855	6.16	-	-
24	07 Jul 1979	03:47:00.2	50.026	78.991	5.84	-	-
25	04 Aug 1979	03:57:00.0	49.894	78.904	6.13	-	-
26	18 Aug 1979	02:52:00.0	49.943	78.938	6.13	-	-
27	28 Oct 1979	03:16:59.9	49.973	78.997	5.98	-	-
28	02 Dec 1979	04:37:00.4	49.891	78.796	5.99	-	-
29	23 Dec 1979	04:57:00.4	49.916	78.755	6.13	-	-
30	29 Jun 1980	02:33:00.6	49.939	78.815	5.69	-	-
31	12 Oct 1980	03:34:17.0	49.961	79.028	5.88	-	-
32	14 Dec 1980	03:47:09.3	49.899	78.938	5.93	-	-
33	27 Dec 1980	04:09:11.0	50.057	78.981	5.87	-	-
34	29 Mar 1981	04:03:52.9	50.007	78.982	5.49	-	-
35	22 Apr 1981	01:17:14.3	49.885	78.810	5.94	-	-
36	13 Sep 1981	02:17:21.2	49.910	78.915	6.06	-	-
37	18 Oct 1981	03:57:05.6	49.923	78.859	6.00	-	-
38	29 Nov 1981	03:35:11.5	49.887	78.860	5.62	-	-
39	31 Aug 1982	01:31:03.6	49.924	78.761	5.20	-	-
40	26 Dec 1982	03:35:17.1	50.071	78.988	5.58	-	-
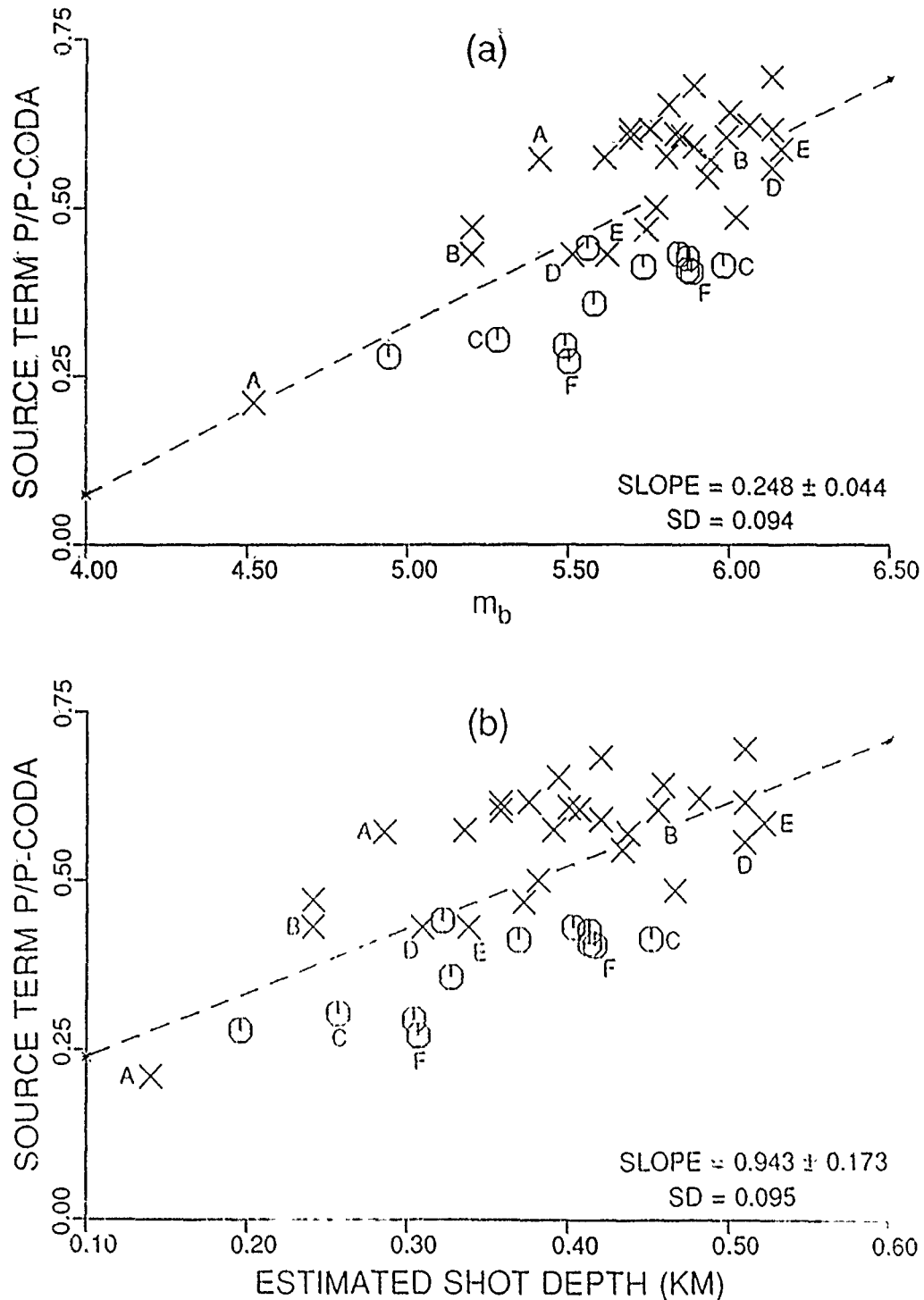
Figure 3. Source term amplitude ratio P/P-coda (log units), averaged over the frequency range of 0.5-2.0 Hz, for 40 Shagan River explosions recorded at the EKA array plotted versus (a) m_b and (b) estimated shot depth. The least squares linear regression (dashed line), mean slope (with associated standard deviation), and one standard deviation of residuals (SD) are indicated on each plot. Six pairs of closely spaced explosions are identified by the letters A through F and the SW and NE explosion populations are denoted by X and O, respectively.

12

A relationship between the average ratio P/P-coda and shot depth was obtained by converting the known m_b into shot depth by using empirical relationships based on the information on shot depths and yields recently released by Bocharov *et al.* (1989). These relationships, derived from the Shagan River and Konystan (Murzhik) explosions are (R. S. Jih, written communications, 1990):

$$m_b = 0.690 \log Y + 4.605 \qquad (5)$$

where Y is the yield in kt, and

$$\log h = 0.241 \log Y + 2.174 \qquad (6)$$

where h is shot depth in meters. These two equations would indicate an explosion of $m_b = 6.0$ to have a yield of about 105 kt and a depth of 458 m. Using equations (5) and (6), one obtains

$$\log h = 0.349 \, m_b + 0.567 \qquad (7)$$

which can be used to estimate shot depth for an explosion with known m_b. A plot of the amplitude ratio P/P-coda versus estimated shot depth in km (Figure 3b) indicates a mean slope of 0.943 with one standard deviation of residuals of only 0.095. Assuming the P-wave velocity for the uppermost 0.5 km of the crust in the Shagan test site region to be 5 km/sec, 4.4 $f/\alpha = 1.1$, if f is taken to be the average of 0.5 and 2.0, or 1.25 Hz. Good agreement between the mean slope expected from simple theory and observation (Figure 3b) suggests that the low-frequency P-coda is mainly due to the scattering of explosion-generated Rg.

Figures 3a and 3b include results from six (including two from NE Shagan) pairs of explosions within less than 2 km of each other and with their m_b differing by at least 0.4

m.u.; these are identified by the letters A through F. Note that the slope from each of the six pairs of shots in Figure 3b is nearly the same as derived from the average of all (40) shots and is in good agreement with the theoretically expected value.

Results similar to those in Figure 3 but for the frequency range of 3.0-5.0 Hz are shown in Figure 4 which shows good separation between explosions from the SW and NE regions of the Shagan River test site. The lack of any systematic variation with shot depth is consistent with the suggestion of explosion-generated Rg contributing to P-coda because Rg is important only for frequencies less than about 2 Hz.
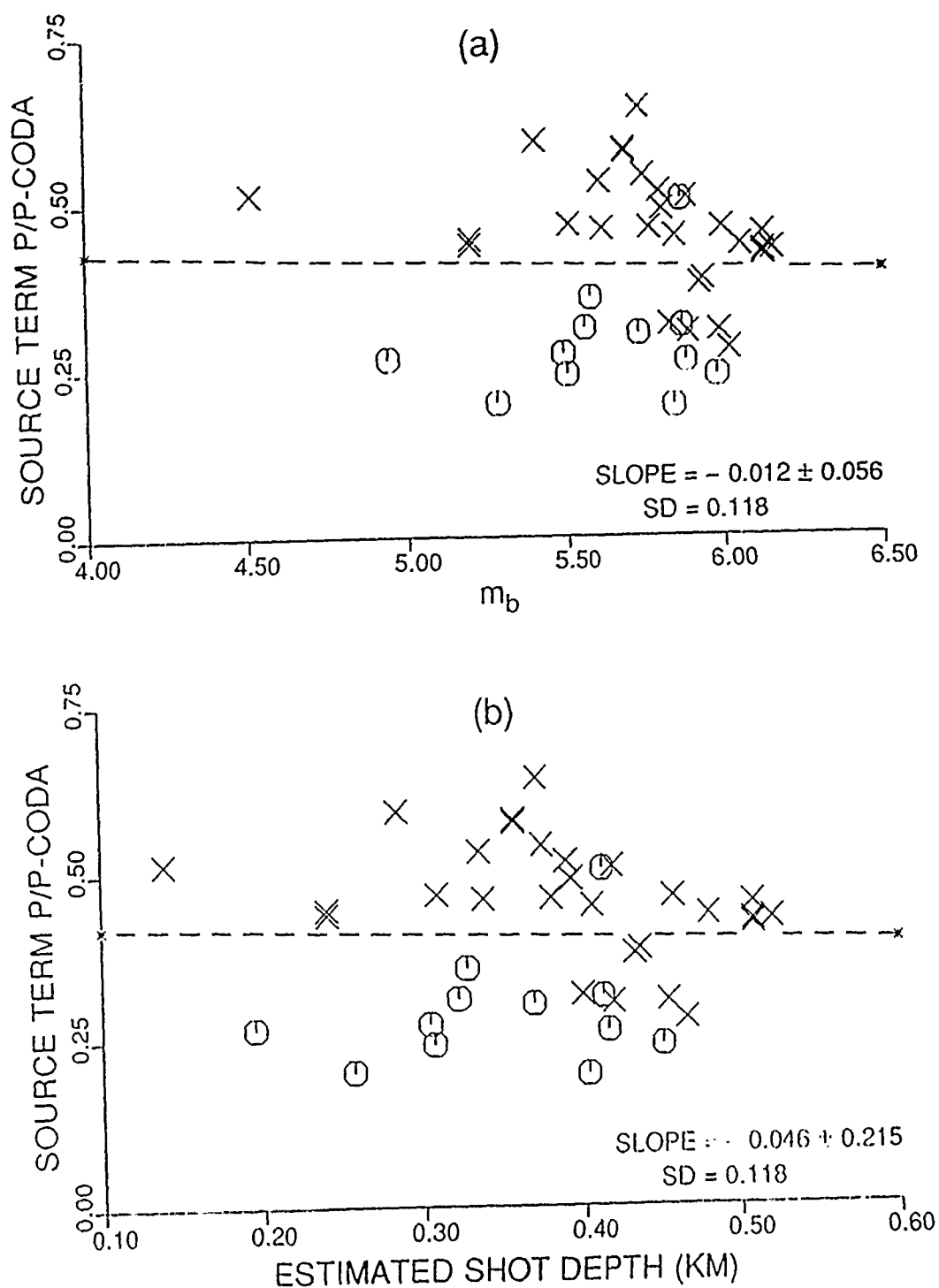
Figure 4. Similar to Figure 3 but for the frequency range of 3.0-5.0 Hz. There is no significant dependence of P/P-coda on mb or estimated shot depth but the SW and NE explosion populations appear well separated.

Pn AND Lg FROM SHAGAN RIVER EXPLOSIONS RECORDED AT WMQ

We examined the spectra of the regional phases Pn and Lg from Shagan River nuclear explosions in order to understand their dependence on source depth and crustal structure (Gupta et al., 1991a). The data set included 14 shots from the southwest region of the test site recorded on the broadband instrument at the Chinese network station Urumchi (WMQ), located about 950 km southeast of the test site. The explosions are listed in Table 3, which includes data from Ringdal and Marshall (1989) for 12 explosions prior to the year 1989. The first arrival Pn was distinct on all records, and the beginning of Lg was assumed to be at a group velocity of 3.5 km/sec, in agreement with the observed data. Spectra of Pn and Lg were obtained by applying a 10% cosine taper to time windows of 12.8 and 51.2 sec for Pn and Lg, respectively. Average Pn/Lg amplitude ratios, with correction for noise and no smoothing, were computed for desired ranges of frequency.

TABLE 3

14 SHAGAN RIVER (SOUTHWEST) EXPLOSIONS RECORDED AT WMQ

No.	DATE	ORIGIN TIME	LAT (N)	LON (E)	m_b
1	12 Mar 1987	01:57:17.2	49.939	78.823	5.31
2	03 Apr 1987	01:17:08.0	49.928	78.829	6.12
3	20 Jun 1987	00:53:04.8	49.913	78.735	6.03
4	02 Aug 1987	00:58:06.8	49.880	78.917	5.83
5	15 Nov 1987	03:31:06.7	49.871	78.791	5.98
6	13 Dec 1987	03:21:04.8	49.989	78.844	6.06
7	27 Dec 1987	03:05:04.7	49.864	78.758	6.00
8	13 Feb 1988	03:05:05.9	49.954	78.910	5.97
9	03 Apr 1988	01:33:05.8	49.917	78.945	5.99
10	04 May 1988	00:57:06.8	49.928	78.769	6.09
11	14 Sep 1988	04:00:00.0	49.870	78.820	6.03
12	17 Dec 1988	04:18:06.8	49.818	78.910	5.80
13	12 Feb 1989	04:15:06.8	49.93	78.74	5.9
14	08 Jul 1989	03:46:57.6	49.87	78.82	5.6

In order to explore the possibility that the low-frequency Lg from the underground nuclear explosions at Shagan River test site is mainly due to the scattering of explosion-generated Rg into S, we again compare common-station results from explosions with significantly different shot depths. Assuming the medium velocity to be the same for all explosions, equations (1) and (2) give

$$\frac{Rg \rightarrow S}{P} (f) = k\ C_1(f)\ f^{0.5}\ 10^{-4.4\frac{h}{\alpha}f} \tag{8}$$

where $C_1(f)$ denotes the scattering function Rg→S. If the low-frequency Lg in regional data is mainly due to the scattering of Rg→S, we can replace Rg→S and P in equation (8) by Lg and Pn, respectively and obtain

$$\log \frac{Pn}{Lg} (f) = 4.4\ \frac{h}{\alpha}\ f - \log k - \log C_1(f) - 0.5 \log f \tag{9}$$

Thus if we consider explosions for which the Rg→S scattering function may be assumed to be the same (such as closely spaced explosions) and the frequency is kept fixed (i.e. for a narrow frequency band), a plot of log Pn/Lg versus shot depth, h should have a slope of about 4.4 f/α.

Figure 5a shows a plot of average amplitude ratio Pn/Lg over the low-frequency range of 0.5-2.0 Hz versus m_b for 14 explosions from the southwest region of the Shagan River test site for which the assumption of the same Rg→S scattering function may be approximately valid. Shot depths for these Shagan River explosions may again be estimated by using equation (7). A plot of the amplitude ratio Pn/Lg versus estimated shot depth (Figure 5b) shows a mean slope of about 1.08, in excellent agreement with the slope of about 1.1 expected from theory.
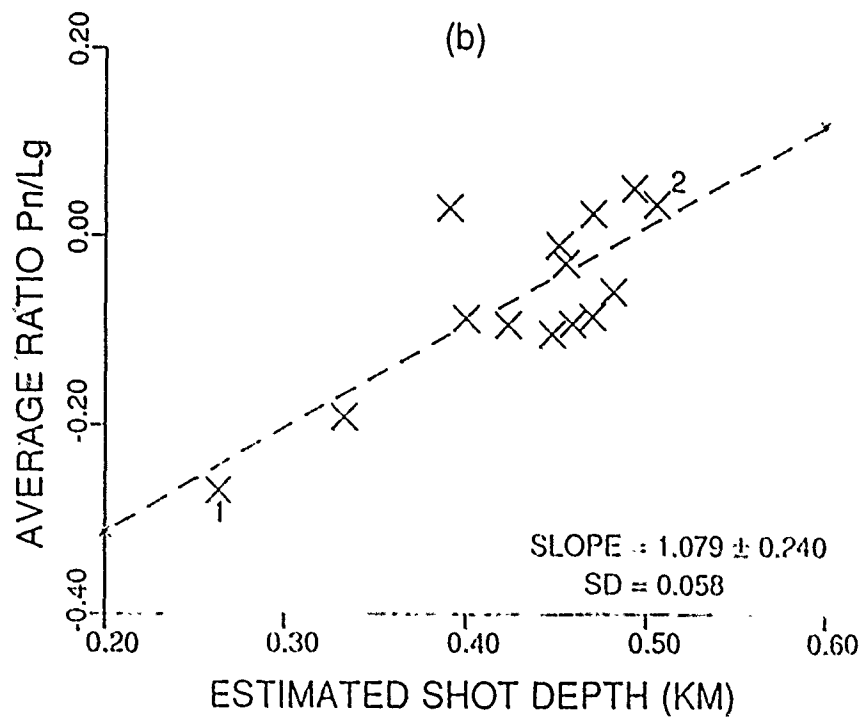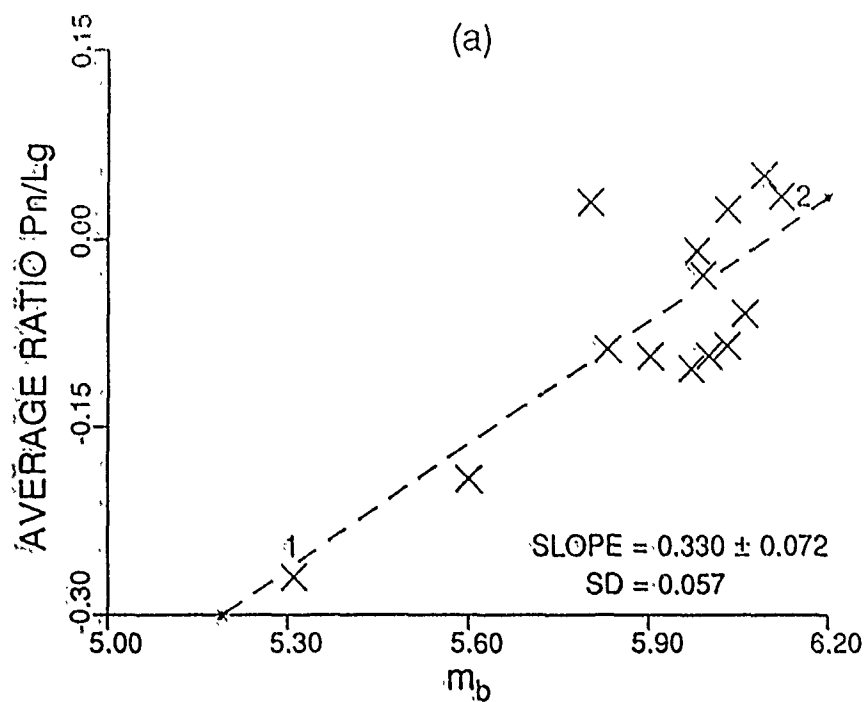
17

Figure 5. Average amplitude ratio Pn/Lg over the frequency range of 0.5-2.0 Hz versus (a) m_b and (b) estimated shot depth for 14 explosions from the southwest Shagan test site. Data from two closely spaced shots (nos. 1 and 2) are identified. Each plot indicates the least squares linear regression (dashed line), mean slope (with associated standard deviation), and one standard deviation of residuals (SD).

18

Figures 5a and 5b include results from two explosions (nos. 1 and 2) that are within a few km of each other. Regional phases are extremely sensitive to differences in propagation paths (Blandford, 1981). In a study of regional data from earthquakes and explosions in the Western United States, Lynnes *et al.* (1990) found that for frequencies up to 4 Hz, the source-station path is more important than the source type in determining the Pg/Lg ratios. Therefore, results from seismic sources with nearly common paths should be given more weight than others. Note that the slope from the two closely spaced shots in Figure 5b is nearly the same as that derived from the average of all (14) shots and is in good agreement with the theoretically expected value. It seems therefore that the low-frequency Lg is generated by the scattering of explosion-generated Rg into S.

CONCLUSIONS

Analysis of a large amount of teleseismic and regional data from East Kazakh underground nuclear explosions suggests that the low-frequency teleseismic P-coda and Lg are dominated by the near-source scattering of fundamental-mode Rayleigh (Rg) to P and S, respectively. The amplitude ratios P/P-coda and Pn/Lg, averaged over the frequency range of 0.5-2.0 Hz and derived from teleseismic and regional data, respectively, vary with shot depths with a mean slope in good agreement with that expected from theory. Scattering occurring over a large region of the uppermost crust may also contribute to the observed stability of P-coda and Lg over teleseismic P and regional Pn, respectively. Results of this study not only provide new insight into the generation of teleseismic P-coda and low-frequency Lg but also improved methods for estimating shot depths of underground nuclear explosions. It will be useful to apply these techniques to more teleseismic and regional data and estimate shot depths of U.S.S.R. explosions. Similar analysis should also be carried out for NTS explosions for which the near-source environmental conditions (including shot depth) are known but the shallow crustal structure is considerably more complex than in East Kazakh.

ACKNOWLEDGMENTS

REFERENCES

Bache, T. C., P. D. Marshall, and L. B. Bache (1985). Q for teleseismic P waves from Central Asia, *J. Geophys. Res. 90*, 3575-3587.

Bache, T. C., P. D. Marshall, and J. B. Young (1984). Q and its effect on short-period P-waves from explosions in Central Asia, *AWRE O 17/84*, Atomic Weapons Research Establishment, H. M. Stationery Office, London,

Bakun, W. H. and L. R. Johnson (1973). The deconvolution of teleseismic P waves from explosions MILROW and CANNIKIN, *Geophys. J. 34*, 321-342.

Blandford, R. R. (1981). Seismic discrimination problems at regional distances, in *Identification of Seismic Sources - Earthquake or Underground Explosions*, E. S. Husebye and S. Mykkeltveit, Editors, D. Reidel Publishing Co., Dordrecht, Holland, 695-740.

Bocharov, V. S., S. A. Zelentsoz, and V. N. Mikhailov (1989). Characteristics of 96 underground nuclear explosions at the Semipalatinsk test site, *Atomic Energy 67(3)*.

Bonham, S., W. J. Dempsey, and J. Rachlin (1980). Geologic environment of the Semipalatinsk area, U.S.S.R. *(Preliminary Report)*, U. S. Geological Survey, Reston, Virginia.

Frasier, C. W. (1972). Observations of pP in the short-period phases of NTS explosions recorded at Norway, *Geophys. J. 31*, 99-109.

Garvin, W. W. (1956). Exact transient solution of the buried line source problem, *Proc. Roy. Soc. (London) A 234*, 528-541.

Greenfield, R. J. (1971). Short-period P-wave generation by Rayleigh-wave scattering at Novaya Zemlya, *J. Geophys. Res. 76*, 7988-8002.

Gupta, I. N. and R. R. Blandford (1987). A study of P waves from Nevada Test Site explosions: near-source information from teleseismic observations?, *Bull. Seism. Soc. Am. 77*, 1041-1056.

Gupta, I. N., R. R. Blandford, R. A. Wagner, and J. A. Burnetti (1985a). Use of P-coda for explosion medium and improved yield determination, in *The Vela Program*, A. U. Kerr, Editor, Executive Graphic Services, Virginia, 711-720.

Gupta, I. N., R. R. Blandford, R. A. Wagner, J. A. Burnetti, and T. W. McElfresh (1935b). Use of P-coda for determination of yield of nuclear explosions, *Geophys. J. 83*, 541-553.

Gupta, I. N., C. S. Lynnes, T. W. McElfresh, and R. A. Wagner (1990a). F-k analysis of NORESS array and single-station data to identify sources of near-receiver and near-source scattering, *Bull. Seism. Soc. Am. 80*, 2227-2241.

Gupta, I. N., C. S. Lynnes, and R. A. Wagner (1990b). Broadband f-k analysis of array data to identify sources of local scattering, *Geophys. Res. Lett. 17*, 183-186.

Gupta, I. N., W. W. Chan, and R. A. Wagner (1991a). A comparison of regional phases from underground nuclear explosions at East Kazakh and Nevada Test Sites, *Bull. Seism. Soc. Am. 81* (in press).

Gupta, I. N., T. W. McElfresh, and R. A. Wagner (1991b). Near-source scattering of Rayleigh to P in teleseismic arrivals from Pahute Mesa (NTS) shots, *AGU Monograph on Explosion Source Phenomenology* (in press).

Hudson, J. A. and A. Douglas (1975). On the amplitudes of seismic waves, *Geophys. J. 42*, 1039-1044.

Kafka, A. L. (1990). Rg as a depth discriminant for earthquakes and explosions: a case study in New England, *Bull. Seism. Soc. Am. 80*, 373-394.

Lynnes, C. S., R. Baumstark, R. K. Cessaro, and W. W. Chan (1990). Pg/Lg discrimination in the Western United States, *GL-TR-90-0167*, Geophysics Laboratory, Hanscom Air Force Base, Massachusetts. ADA226819

Marshall, P. D., T. C. Bache, and R. C. Lilwall (1985). Body wave magnitudes and locations of Soviet underground explosions at the Semipalatinsk Test Site, *AWRE O 16/84 (re-issue)*, Atomic Weapons Research Establishment, H. M. Stationery Office, London, U.K.

McLaughlin, K. L., L. M. Anderson, and A. C. Lees (1987). Effects of local geologic structure on Yucca Flats, Nevada Test Site, explosion waveforms: two-dimensional linear finite-difference simulations, *Bull. Seism. Soc. Am. 77*, 1211-1222.

McLaughlin, K. L., T. G. Barker, and S. M. Day (1990). Implications of explosion generated spall models: regional seismic signals, *GL-TR-90-0133*, Geophysics Laboratory, Hanscom Air Force Base, Massachusetts. ADA227273

Ringdal, F. and P. D. Marshall (1989). Yield determination of Soviet underground nuclear explosions at the Shagan River test site, *NORSAR Scientific Rep. 2-88/89*, 36-67, Kjeller, Norway.

Rulev, B. G. (1965). The energy in a Rayleigh surface wave from explosions in different kinds of rock, *Izvestiya*, Earth Physics Series, 233-241.

Stead, R. J. and D. V. Helmberger (1988). Numerical-analytical interfacing in two dimensions with applications to modeling NTS seismograms, *PAGEOPH 128*, Nos. 1/2, 157-193.

(THIS PAGE INTENTIONALLY LEFT BLANK)

SECTION B

GENERATION OF LOW-FREQUENCY Lg FROM NTS EXPLOSIONS

INTRODUCTION

At regional distances, the S-wave group known as Lg is often the largest amplitude arrival from both earthquake and explosion sources. Since Lg has proven useful for detection, source discrimination, and yield estimation of underground nuclear explosions, it is important to understand the generation, propagation, and spectral characteristics of Lg. Perhaps the most puzzling aspect of Lg from explosions is their spectra's relative richness in low-frequency content compared to corresponding earthquake Lg spectra, at least for the Nevada Test Site (NTS) shots (Murphy and Bennett, 1982). Gupta and Blandford (1983) suggested that the low-frequency Lg from explosions may be due to preferential scattering of low frequencies in P to S scattering near the source. Theoretical studies of Lg generation (e.g. Campillo *et al.*, 1984) indicate that explosions do not generate large Lg amplitudes unless they are located close to strong interfaces such as the free surface. There are several other possible mechanisms that can generate large S waves and low-frequency Lg; these include spall (Taylor and Randall, 1989; McLaughlin *et al.*, 1990) and interaction of the spherical P-wavefront emanating from an explosion with the free-surface, resulting in shear waves referred to as S* (Gutowski *et al.*, 1984; Lilwall, 1988). Pg is also a prominent phase from both explosion and earthquake sources, especially in the WUS, and its generation is also not fully understood. Murphy and Bennett (1982) found the Pg spectra also to be deficient in high-frequency energy as compared to those from earthquakes whereas the Pn spectra for the two types of sources were found to be indistinguishable.

25

As shown in Part A of this report, our analysis of regional data from Shagan River explosions recorded at the CDSN station, WMQ, indicates that the low-frequency Lg is probably due to the scattering of explosion-generated Rg into S. In this study, we examine the possibility that a similar mechanism is responsible for generating the large low-frequency Lg observed from NTS explosions for which the near-source parameters (including shot depth) are known but the shallow crustal structure is considerably more complex than in East Kazakh. Regional data from 66 NTS explosions recorded mostly at two broadband digital stations at regional distances are analyzed for their dependence on shot depth and other geological and geophysical parameters.

LATERAL VARIATIONS IN MEDIUM VELOCITY AND OTHER PARAMETERS AT NTS

Extreme lateral and vertical variations in medium velocity exist at both Yucca Flat and Pahute Mesa test regions of the NTS. At Yucca Flat, the large variations are due to the presence of low velocity alluvium and tuffs within a basin structure and the presence of Yucca Fault and other geological features (Hays and Murphy, 1971). Variations in medium velocity are even more dramatic at Pahute Mesa because of the presence of alternating layers of various tuffs and rhyolites of irregular thickness. In a study of geophysical properties of shot media at NTS, Ramspott and Howard (1975) observed that, "of the various media, Yucca Flat and Pahute Mesa above the water table are the most variable. In these areas, it is possible to find individual past sites with extreme values of reported parameters. The other media are relatively uniform." It is interesting to note that nearly all explosions with large low-frequency (0.5-1.0 Hz) Lg, used in Murphy and Bennett's (1982) study, were above the water table (AWT) and shallow (shot depth less than 500m) or within a region where scattering is expected to be large.

Table 1 provides a chronological list of 66 NTS (including 39 Yucca Flat and 27 Pahute Mesa) shots used in this study. The Yucca Flat shots include 13 explosions detonated below the water table (BWT) and 26 above the water table (AWT) whereas the Pahute Mesa shots include 17 BWT and 10 AWT explosions. The m_b values are maximum-likelihood estimates from P. D. Marshall (written communication, 1988) and the medium velocity in the table is the overburden velocity or the average compressional-wave velocity between the shot point and the surface as measured by sonic logs. Most explosions were recorded at both broadband digital stations ELK and KNB operated by the Lawrence Livermore National Laboratory. Figures 1 and 2 show the geographical locations of these shots along with their shot depths. It is
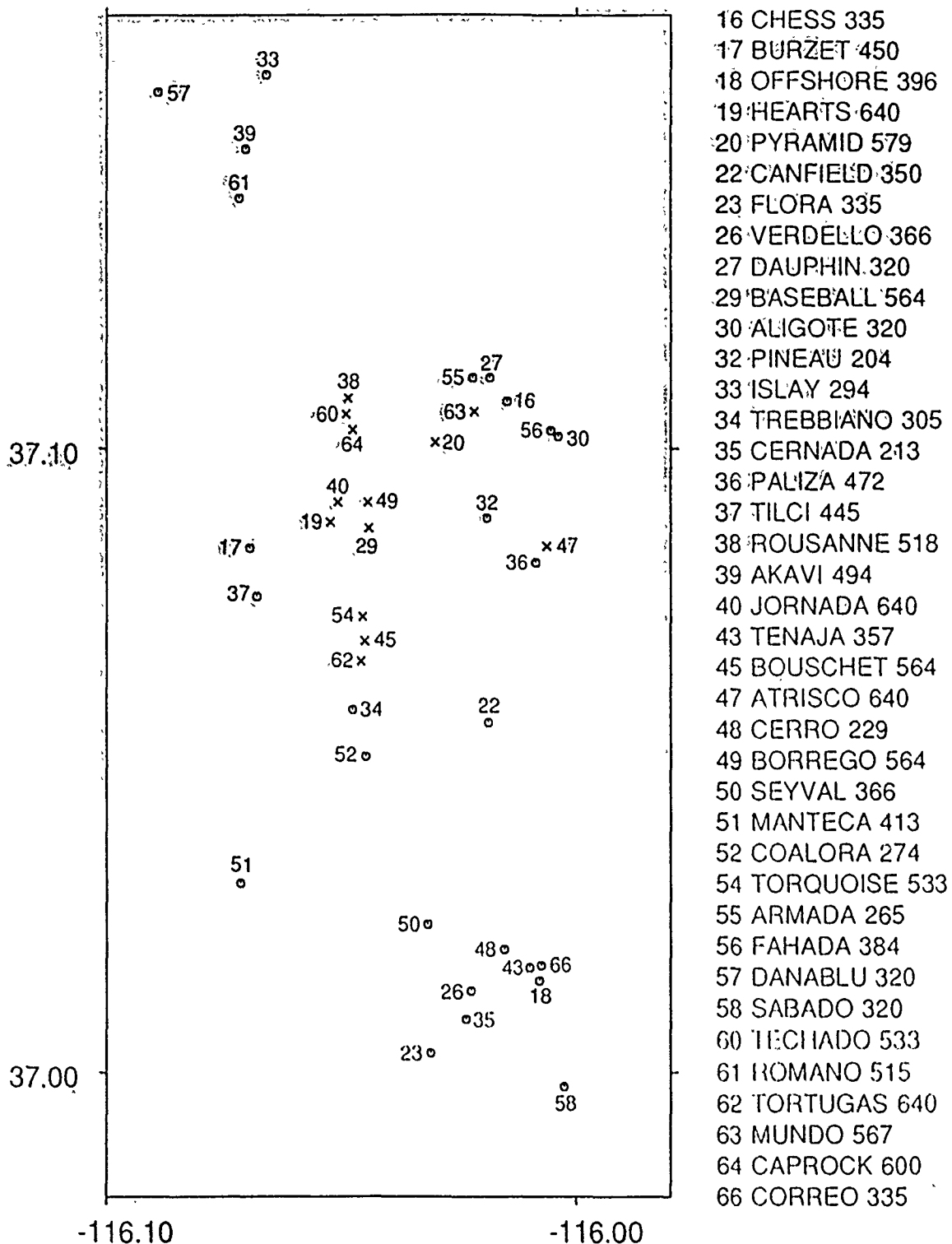
Figure 1. Location map of 39 Yucca Flat shots with 13 BWT and 26 AWT explosions denoted by x and o, respectively. The numbers correspond to those in Table 1. Shot names and depths (in meters) are indicated on the right of the figure. Note several pairs of closely spaced explosions with considerably different shot depths.
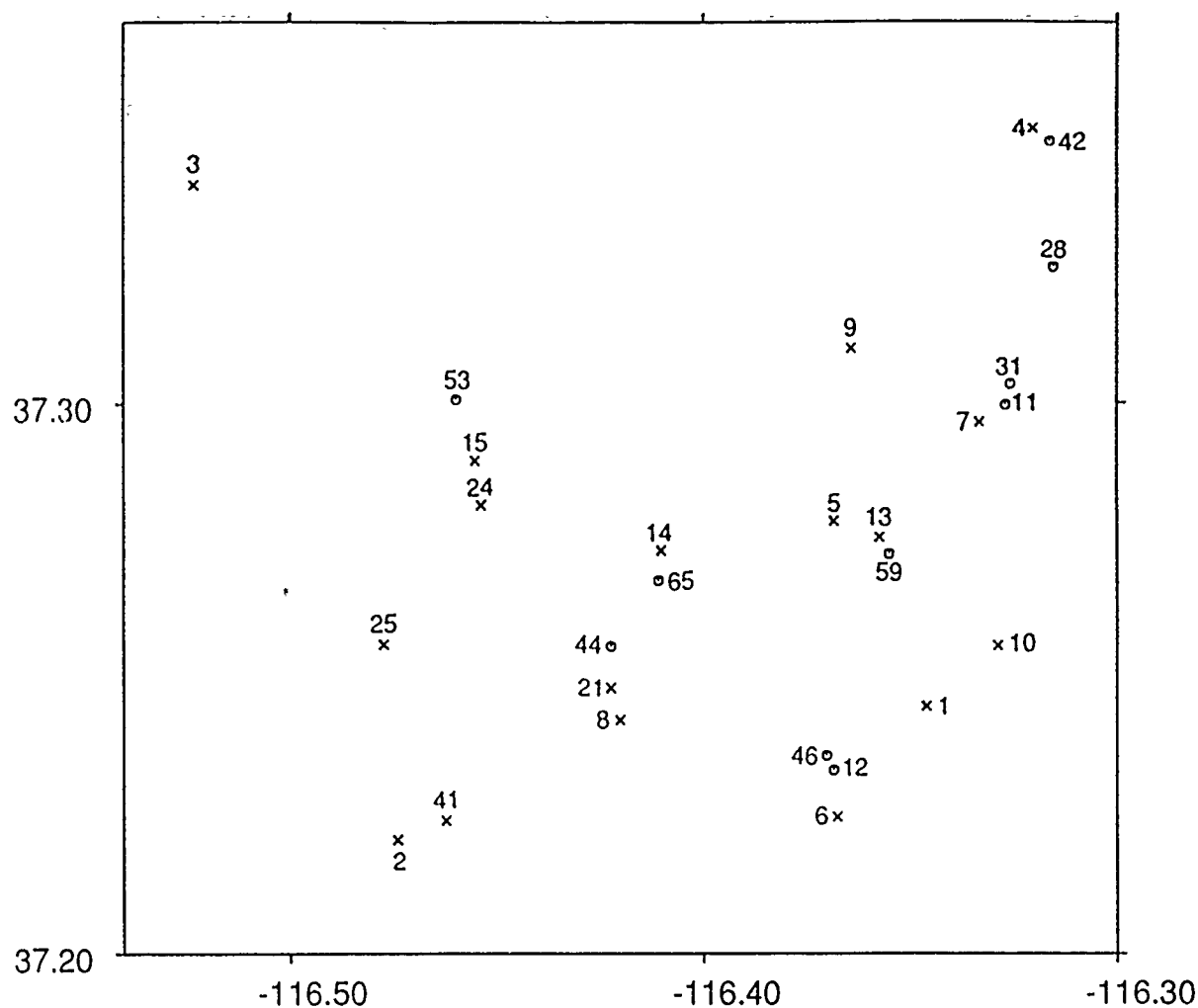
Figure 2. Location map of 27 Pahute Mesa shots with 17 BWT and 10 AWT explosions denoted by x and o, respectively. The numbers correspond to those in Table 1. Shot names and depths (in meters) are indicated at the bottom of the figure. Note several pairs of closely spaced explosions with considerably different shot depths.

1 ALMENDRO 1064	10 POOL 879	28 SERPA 573
2 TYBO 765	11 FONDUTTA 633	31 HARZER 637
3 STILTON 732	12 BACKBEACH 672	41 MOLBO 638
4 MAST 911	13 PANIR 681	42 HOSTA 640
5 CAMEMBERT 1311	14 FARM 689	44 GIBNE 570
6 INLET 819	15 PEPATO 681	46 NEBBIOLO 640
7 MUENSTER 1452	21 COLWICK 633	53 CABRA 543
8 CHESHIRE 1167	24 KASH 645	59 CHANCELLOR 625
9 ESTUARY 868	25 TAFI 680	65 KAPPELI 640

interesting to note that several explosions are within a few hundred meters of each other so that propagation paths to a common recording station should be almost identical. Two such examples in which BWT and AWT shots are closely spaced are the Yucca Flat shots PALIZA (no. 36) and ATRISCO (no. 47) in Figure 1 and the Pahute Mesa shots MAST (no. 4) and HOSTA (no. 42) in Figure 2.

TABLE 1

66 NTS EXPLOSIONS USED IN STUDY

No.	DATE	NAME	m_b	VEL (KM/S)	SHOT DEPTH (KM)	DEPTH OF WT (KM)
1	06 Jun 1973	ALMENDRO (E,K)	6.166	3.083	1.0638	0.6860
2	14 May 1975	TYBO (K)	6.046	2.275	0.7650	0.6300
3	03 Jun 1975	STILTON (E,K)	5.831	2.150	0.7315	0.2720
4	19 Jun 1975	MAST (E,K)	6.060	3.877	0.9113	0.6660
5	26 Jun 1975	CAMEMBERT (E)	6.212	2.900	1.3106	0.6680
6	20 Nov 1975	INLET (E,K)	5.981	3.042	0.8190	0.7030
7	03 Jan 1976	MUENSTER (E)	6.288	2.900	1.4524	0.6760
8	14 Feb 1976	CHESHIRE (E,K)	5.942	3.210	1.1670	0.6250
9	09 Mar 1976	ESTUARY (E,K)	5.974	2.660	0.8681	0.6270
10	17 Mar 1976	POOL (E,K)	6.061	2.865	0.8793	0.6900
11	11 Apr 1978	FONDUTTA (E,K)	5.499	2.299	0.6330	0.6680
12	11 Apr 1978	BACKBEACH (E,K)	5.551	2.043	0.6721	0.7150
13	31 Aug 1978	PANIR (K)	5.667	2.096	0.6810	0.6450
14	16 Dec 1978	FARM (K)	5.634	2.125	0.6890	0.6490
15	11 Jun 1979	PEPATO (E)	5.568	1.887	0.6810	0.5790
16	20 Jun 1979	CHESS (E)	4.161	1.520	0.3353	0.5730
17	03 Aug 1979	BURZET (E,K)	4.863	1.589	0.4500	0.5100
18	08 Aug 1979	OFFSHORE (E,K)	4.820	1.393	0.3962	0.4670
19	06 Sep 1979	HEARTS (E,K)	5.892	1.763	0.6400	0.5070
20	16 Apr 1980	PYRAMID (E,K)	5.423	1.553	0.5791	0.5400
21	26 Apr 1980	COLWICK (E,K)	5.547	2.070	0.6330	0.6300
22	02 May 1980	CANFIELD (K)	4.411	1.247	0.3505	0.4970
23	22 May 1980	FLORA (E,K)	3.820	1.257	0.3353	0.4730
24	12 Jun 1980	KASH (K)	5.671	1.837	0.6450	0.6020
25	25 Jul 1980	TAFI (E,K)	5.571	1.872	0.6800	0.6070
26	31 Jul 1980	VERDELLO (E)	4.473	1.337	0.3658	0.4700

27	14 Nov 1980	DAUPHIN (E,K)	4.554	1.420	0.3200	0.5800
28	17 Dec 1980	SERPA (E,K)	5.294	2.000	0.5730	0.6270
29	15 Jan 1981	BASEBALL (E,K)	5.725	1.970	0.5639	0.5120
30	29 May 1981	ALIGOTE (E,K)	4.368	1.400	0.3200	0.6050
31	06 Jun 1981	HARZER (E,K)	5.625	2.056	0.6370	0.6680
32	16 Jul 1981	PINEAU (E,K)	3.290	1.125	0.2042	0.5350
33	27 Aug 1981	ISLAY (E)	4.360	1.440	0.2940	0.5670
34	04 Sep 1981	TREBBIANO (E,K)	3.820	1.465	0.3048	0.4980
35	24 Sep 1981	CERNADA (E,K)	3.500	1.060	0.2130	0.4720
36	01 Oct 1981	PALIZA (E,K)	5.115	1.497	0.4724	0.5300
37	11 Nov 1981	TILCI (E,K)	5.035	1.600	0.4450	0.4940
38	12 Nov 1981	ROUSANNE (E,K)	5.458	1.580	0.5182	0.4950
39	03 Dec 1981	AKAVI (E,K)	4.749	1.730	0.4940	0.5800
40	28 Jan 1982	JORNADA (E,K)	5.932	1.695	0.6400	0.5070
41	12 Feb 1982	MOLBO (E,K)	5.412	2.005	0.6380	0.6140
42	12 Feb 1982	HOSTA (E,K)	5.599	2.020	0.6401	0.6680
43	17 Apr 1982	TENAJA (E,K)	4.454	1.310	0.3570	0.4680
44	25 Apr 1982	GIBNE (E,K)	5.364	1.920	0.5700	0.6100
45	07 May 1982	BOUSCHET (E,K)	5.730	1.740	0.5639	0.5000
46	24 Jun 1982	NEBBIOLO (E,K)	5.636	2.027	0.6400	0.7080
47	05 Aug 1982	ATRISCO (E,K)	5.738	1.604	0.6400	0.5380
48	02 Sep 1982	CERRO (E,K)	3.290	1.165	0.2286	0.4720
49	29 Sep 1982	BORREGO (E,K)	4.150	1.860	0.5639	0.5010
50	12 Nov 1982	SEYVAL (K)	4.545	1.320	0.3660	0.482
51	10 Dec 1982	MANTECA (E,K)	4.741	1.610	0.4130	0.5290
52	11 Feb 1983	COALORA (E,K)	4.150	1.340	0.2740	0.5010
53	26 Mar 1983	CABRA (E,K)	5.275	1.757	0.5430	0.5710
54	14 Apr 1983	TORQUOISE (E,K)	5.742	1.868	0.5330	0.5000
55	22 Apr 1983	ARMADA (E,K)	3.977	1.313	0.2650	0.5790
56	26 May 1983	FAHADA (E,K)	4.647	1.500	0.3840	0.6000
57	09 Jun 1983	DANABLU (E)	4.519	1.578	0.3200	0.5840
58	11 Aug 1983	SABADO (E)	4.391	1.315	0.3200	0.4600
59	01 Sep 1983	CHANCELLOR (E)	5.445	1.970	0.6250	0.6470
60	22 Sep 1983	TECHADO (E,K)	4.150	1.610	0.5334	0.5000
61	16 Dec 1983	ROMANO (K)	5.140	1.699	0.5150	0.563
62	01 Mar 1984	TORTUGAS (K)	5.848	1.769	0.6400	0.497
63	01 May 1984	MUNDO (K)	5.474	1.670	0.5670	0.558
64	31 May 1984	CAPROCK (K)	5.743	1.585	0.6000	0.500
65	25 Jul 1984	KAPPELI (E,K)	5.385	2.100	0.6400	0.6520
66	02 Aug 1984	CORREO (E,K)	4.669	1.305	0.3350	0.4700

Note: Stations recording the event are denoted by E (ELK) and K (KNB).

31

Plots of delay time ($= 2h/\alpha$ where h is the shot depth and α the overburden velocity) versus shot depth for 39 Yucca Flat and 27 Pahute Mesa shots are shown in Figure 3. The Yucca Flat data (Figure 3a) shows an approximately linear trend suggesting gradual increase in velocity with depth. But the Pahute Mesa data in Figure 3b indicate extreme variations in medium velocity with depth. Large lateral variations in velocity are mainly responsible for the lack of an approximately linear relationship. For example, the explosions MAST and HOSTA, within about 500 m of each other (Figure 2), have overburden velocities of about 3.9 and 2.0 km/sec so that the delay time for the deeper (911 m) shot, MAST, is *smaller* than that for the shallower (640 m) shot, HOSTA. Most of these drastic variations are perhaps of limited spatial extent and therefore not "seen" by seismic waves of low frequency or long wavelength. This means that, if only low frequencies are being used, a deeper shot should almost always be considered to have a larger delay time than a shallower explosion. In other words, delay times derived from the linear regression relationships in Figures 3a and 3b for shots with known depths, referred to hereafter as "estimated delay times", may be expected to provide better estimates than those from sonic logs in the immediate vicinity of the shot holes.

(a) 39 YF SHOTS

SLOPE = 0.836 ± 0.051
SD = 0.042, CC = 0.937

BWT + AWT ⊙

(b) 27 PM SHOTS

SLOPE = 0.315 ± 0.065
SD = 0.076, CC = 0.698

BWT ✕ AWT ⧌
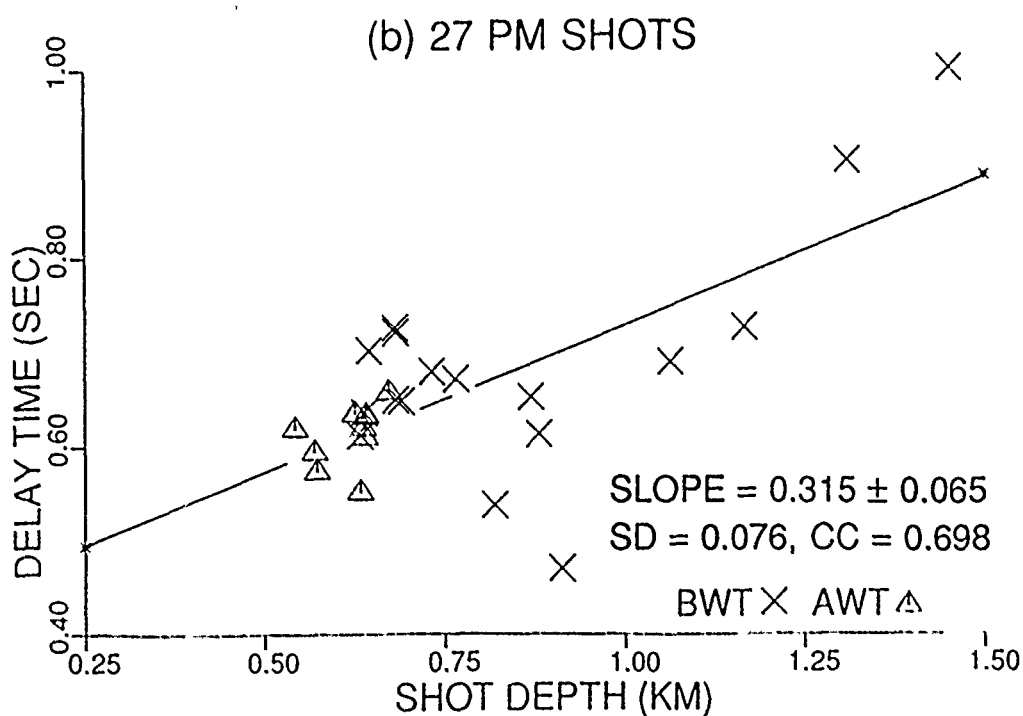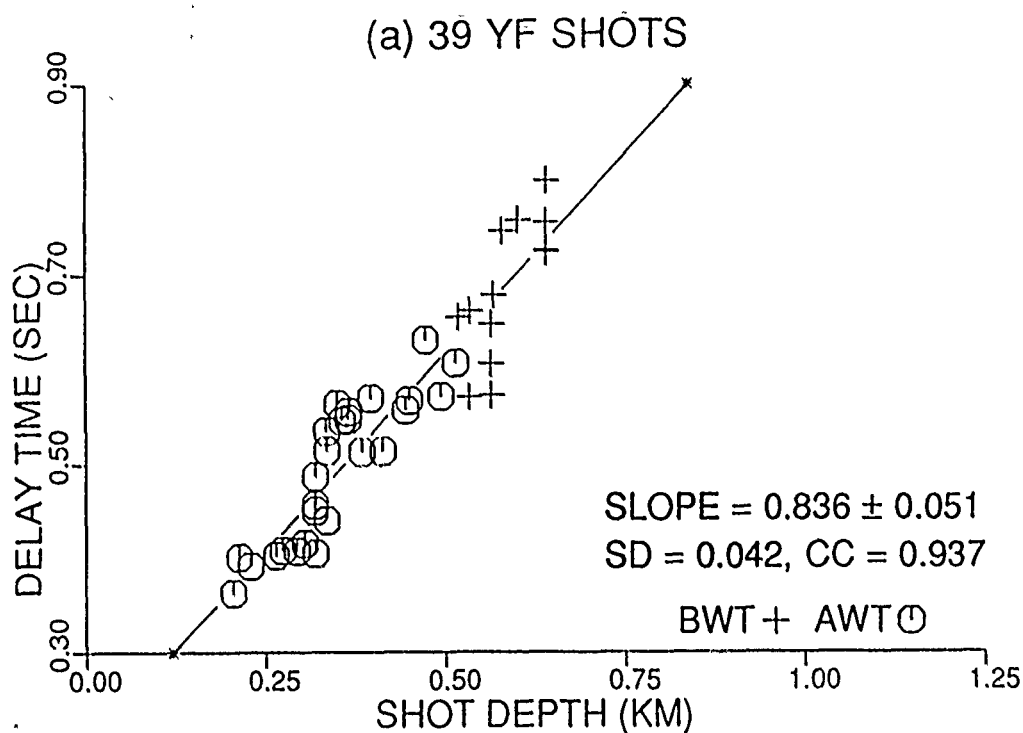
Figure 3. Delay time versus shot depth for (a) 39 Yucca Flat and (b) 27 Pahute Mesa shots used in the study. The least squares linear regression line, mean slope (with associated standard deviation), one standard deviation of residuals (SD), and the correlation coefficient (CC) are indicated on each plot.

33

COMPARISON OF LOW FREQUENCY Pn, Pg, AND Lg

We first examined spectra of the regional phases Pn, Pg, and Lg from a fairly large number of NTS explosions recorded at two common stations, ELK and KNB, located at epicentral distances of about 410 and 290 km, respectively. In order to isolate source effects, it is important to use common source-receiver paths because of the extreme sensitivity to propagation paths of the regional phases, especially Pn (Langston, 1982) and Lg (Gupta and Blandford, 1983). Source characteristics derived from closely spaced explosions should therefore be given more importance than others. The window lengths used for spectral analysis of Pn, Pg, and Lg on the vertical component records were 6.4, 12.8, and 25.6 sec, respectively, and a 10% cosine taper was used. The beginning of Pn was quite sharp for nearly all explosions and the onsets of Pg and Lg phases were selected in the same manner as in Murphy and Bennett (1982).

Amplitude ratios Pn/Lg and Pg/Lg, averaged over the frequency ranges of 0.3-1.0 Hz and 0.5-2.0 Hz, were computed for all explosions recorded at both ELK and KNB and plotted versus shot depth, delay time, and estimated delay time. In order to avoid possible effects of large variations in scaled depth on regional phases, 7 overburied shots (all from Yucca Flat) were excluded from plots. Moreover, results from these overburied shots appeared as outliers on most plots. Plots of all available amplitude ratios Pn/Lg and Pg/Lg from the remaining 59 shots versus shot depth, delay time, and estimated delay time, derived from ELK data, are shown in Figures 4 through 7. The figures include results of linear regression such as the mean slope, standard deviation of residuals (SD), and the correlation coefficient values (CC). Results from Yucca Flat shots alone (Figures 4 and 6) and those from a combination of Yucca Flat and Pahute Mesa shots (Figures 5 and 7) are shown. The scattering functions at Yucca

34
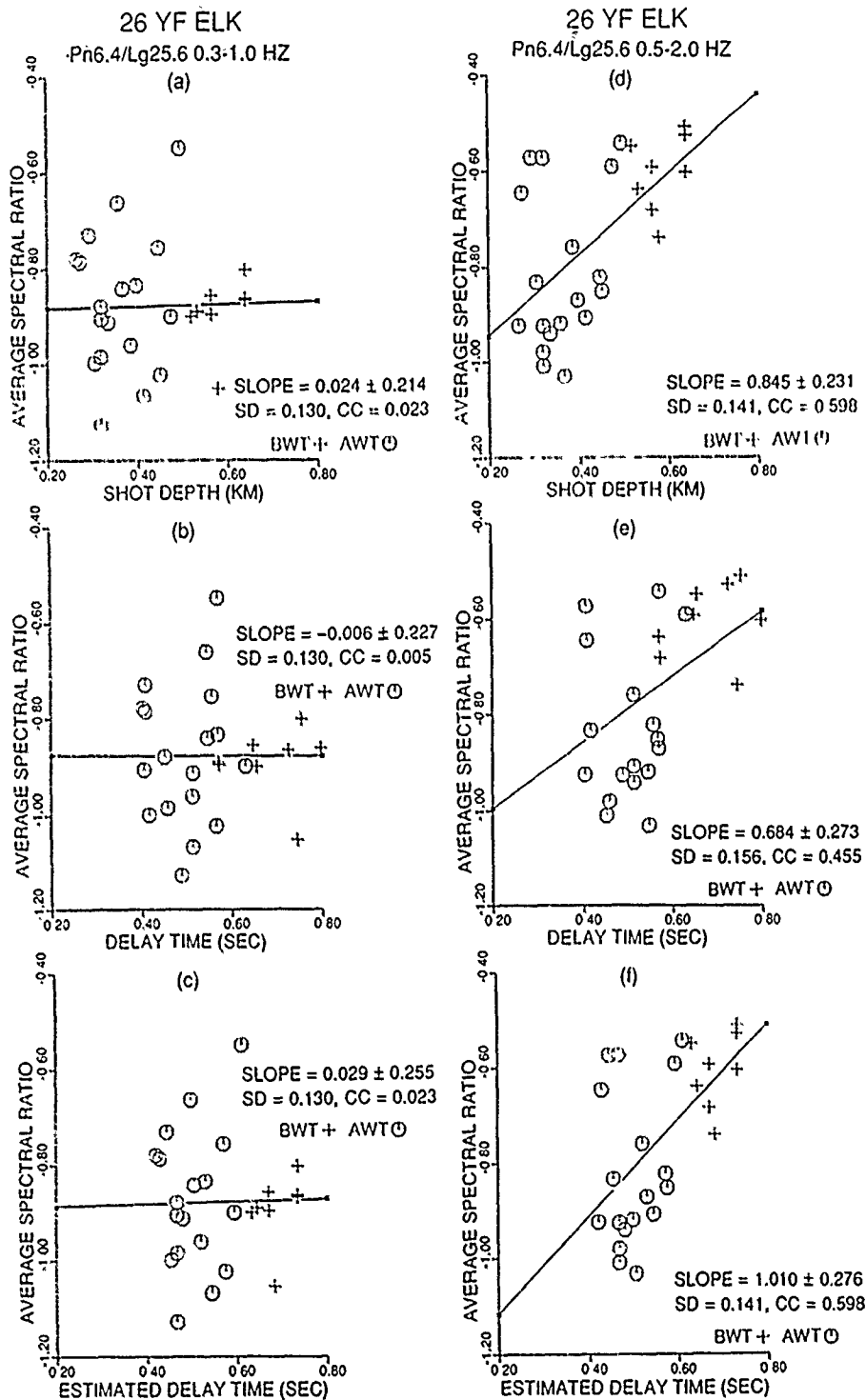
Figure 4. Average amplitude ratio Pn/Lg (log units) over the frequency ranges of 0.3-1.0 Hz and 0.5-2.0 Hz for 26 Yucca Flat shots recorded at ELK versus shot depth, delay time, and estimated delay time. Each plot indicates the least squares linear regression, mean slope (with associated standard deviation), one standard deviation of residuals (SD), and the correlation coefficient (CC).
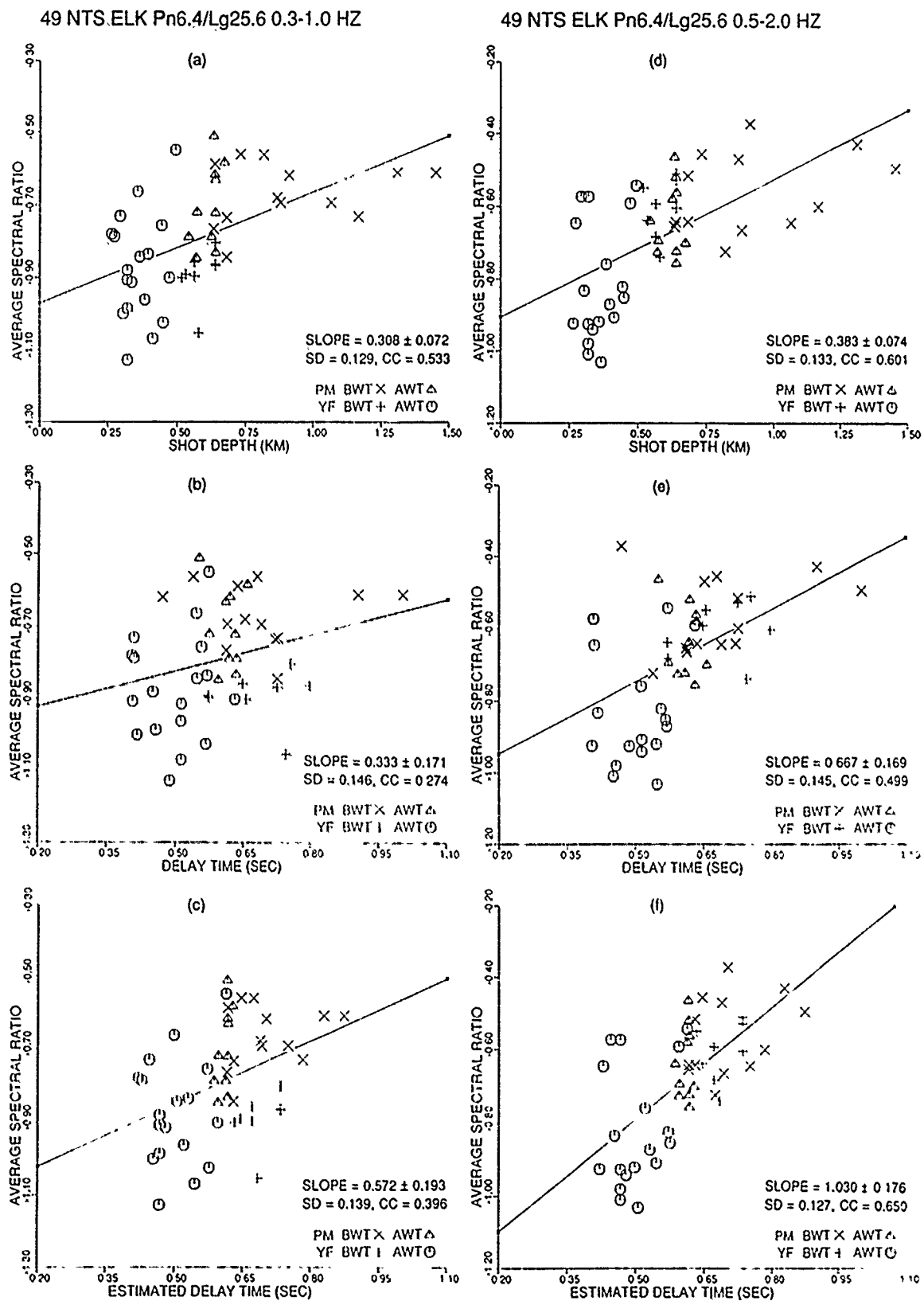
Figure 5. Similar to Figure 4 for 49 NTS (26 Yucca Flat and 23 Pahute Mesa) shots.
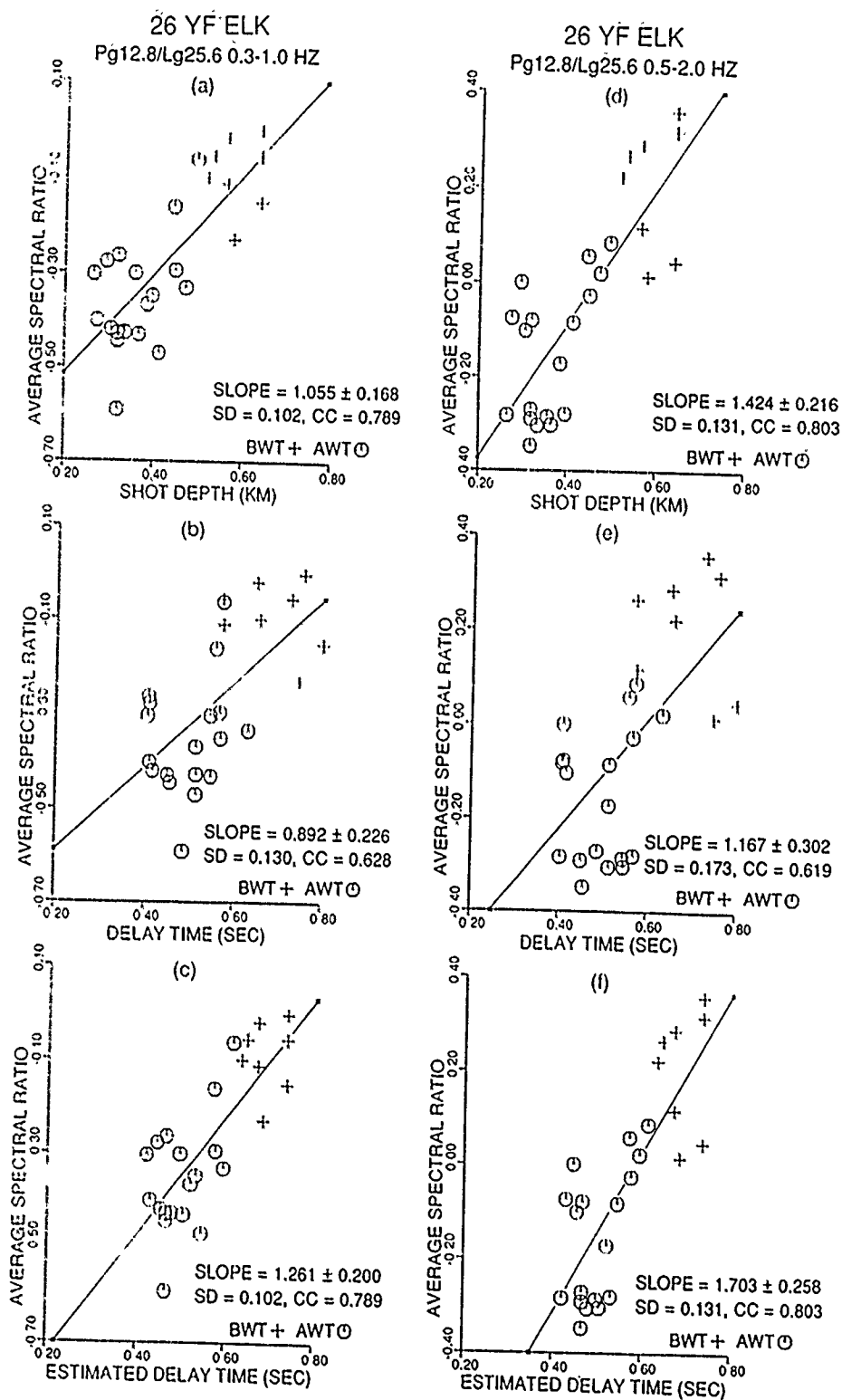
Figure 6. Similar to Figure 4 for Pg/Lg derived from 26 Yucca Flat shots.
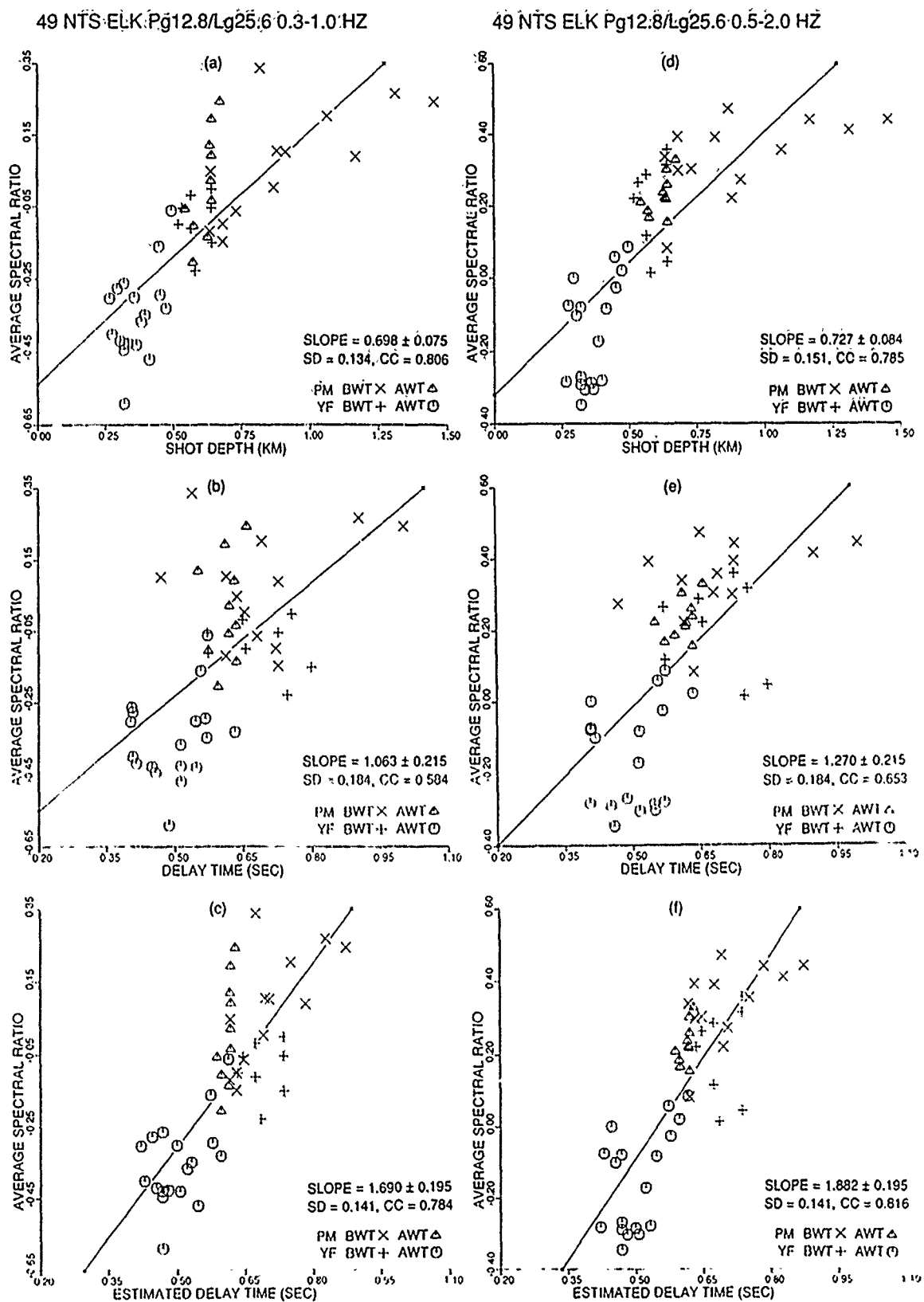
Figure 7. Similar to Figure 4 for Pg/Lg derived from 49 NTS (26 Yucca Flat and 23 Pahute Mesa) shots.

38

Flat and Pahute Mesa may not be the same but the combined results are included so that a bigger range of source parameters can be examined.

The correlations in several figures, such as Figures 6f and 7f, both for Pg/Lg versus estimated delay time, are good whereas those in Figures 4c and 5c are poor. In general, linear relationships for the frequency range of 0.5-2.0 Hz are better than those for 0.3-1.0 Hz and those for Pg/Lg are better than those for Pn/Lg. Possible reasons for the latter are greater stability of Pg over Pn, use of signal time window that is twice as long as for Pn, and much better S/N for Pg than for Pn (especially for the low frequencies). Theoretical considerations (Gupta *et al.*, 1991) would suggest the mean slopes of Pn/Lg versus delay time to be about 2.2 f where f is the frequency, or about 1.4 for the frequency range 0.3-1.0 if f is taken to be the average of 0.3 and 1.0, or 0.65 Hz. Similarly, theory would suggest a mean slope of about 2.8 for the frequency range of 0.5-2.0 Hz. One may assume that the depth dependence of low-frequency Pg/Lg is similar to that for Pn/Lg because Pg is derived mainly from P waves trapped within the crust. Thus theory would suggest the mean slopes in Figures 6c and 7c to be about 1.4 and those in Figures 6f and 7f to be about 2.8. It should be noted that the mean slopes indicated in Figures 4 through 7 are all based on the assumption that values on the x-axis (shot depth, delay time, or estimated delay time) are error-free and that all error lies in the measurement of the average spectral ratios. This assumption is unrealistic for several reasons such as finite (rather than a point) source size and large lateral variations. It is, however, known that a linear regression that incorporates an error in values on the x-axis will always *increase* the mean slope (see, for example, Bolt, 1978) and thus bring the slope values indicated on linear regressions such as those in Figures 6c, 6f, 7c, and 7f close to the theoretically predicted values.

All available values of amplitude ratios Pn/Lg and Pg/Lg, averaged over the frequency ranges of 0.3-1.0 Hz and 0.5-2.0 Hz, are plotted at their epicentral (ground zero) locations in Figures 8 and 9 for 26 Yucca Flat shots recorded at ELK. Location plots of shot depth and delay times for the same 26 explosions are included in Figure 10. These data include several pairs of closely spaced explosions for which the Rg-to-S scattering functions are expected to be similar. Pairs of closely spaced shots with their depths differing by at least 50 m are identified in Figures 8, 9, and 10. When the shallower shot is AWT and the deeper explosion is BWT, they are denoted by the letters A and B, respectively. Other pairs are marked by the letters S and D denoting the relatively shallower and deeper shots, respectively. A comparison of the four plots in Figures 8 and 9 with the two plots in Figure 10 show considerable similarity. Moreover, for closely spaced shots, the deeper shot (marked B or D) almost always has relatively larger Pn/Lg and Pg/Lg for both ranges of frequency than those for the shallower shot (denoted by A or S). It seems therefore that, for closely spaced shots, the observed values of Pn/Lg and Pg/Lg are in agreement with the theoretically expected dependence on shot depth and delay time. These observations also suggest that the near-source Rg-to-S scattering functions are perhaps nearly the same only for closely spaced shots. The lack of a linear relationship for many plots in Figures 4 through 7 may therefore be due to the scattering functions being significantly different from one shot region to another, presumably due to the lateral variations that exist at the Yucca Flat test site.

Plots of amplitude ratios Pn/Lg and Pg/Lg, averaged over the frequencies ranges of 0.3-1.0 Hz and 0.5-2.0 Hz and obtained from 23 Pahute Mesa shots recorded at ELK, are plotted at their epicentral locations in Figures 11 and 12. Figure 13 shows plots of shot depth and delay time values for the same 23 Pahute Mesa shots. Unlike the remarkable similarity

40
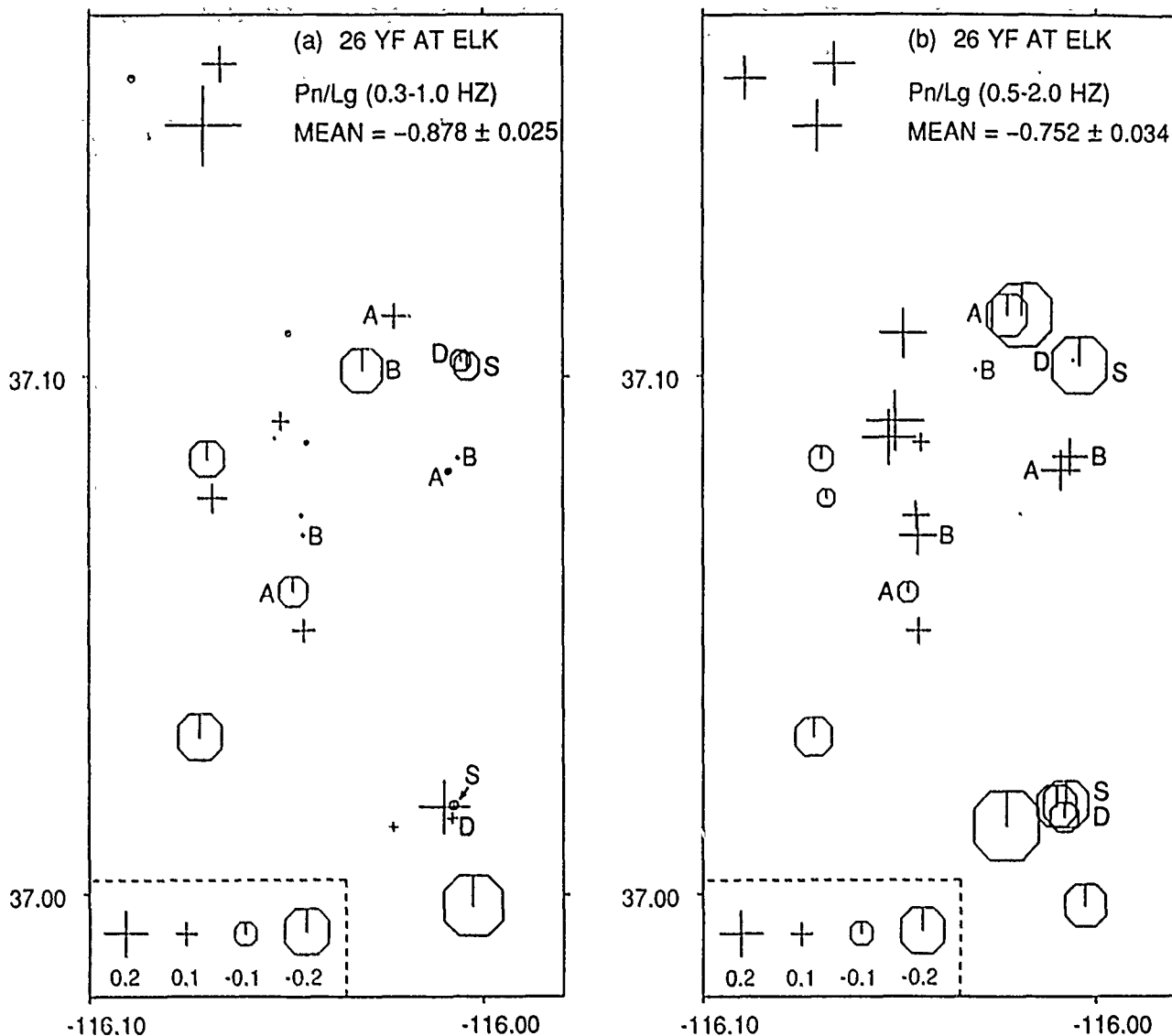
Figure 8. Average amplitude ratio Pn/Lg (in log units and relative to the indicated mean value) derived from ELK records of 26 Yucca Flat shots plotted at their known epicentral locations for the frequency range of (a) 0.3-1.0 Hz and (b) 0.5-2.0 Hz. Three pairs of closely spaced A (AWT)and B (BWT) shots and two pairs of S (shallower) and D (deeper) shots are identified. For nearly all pairs, the deeper shot (B or D) has relatively larger Pn/Lg than the shallower (A or S) explosion.
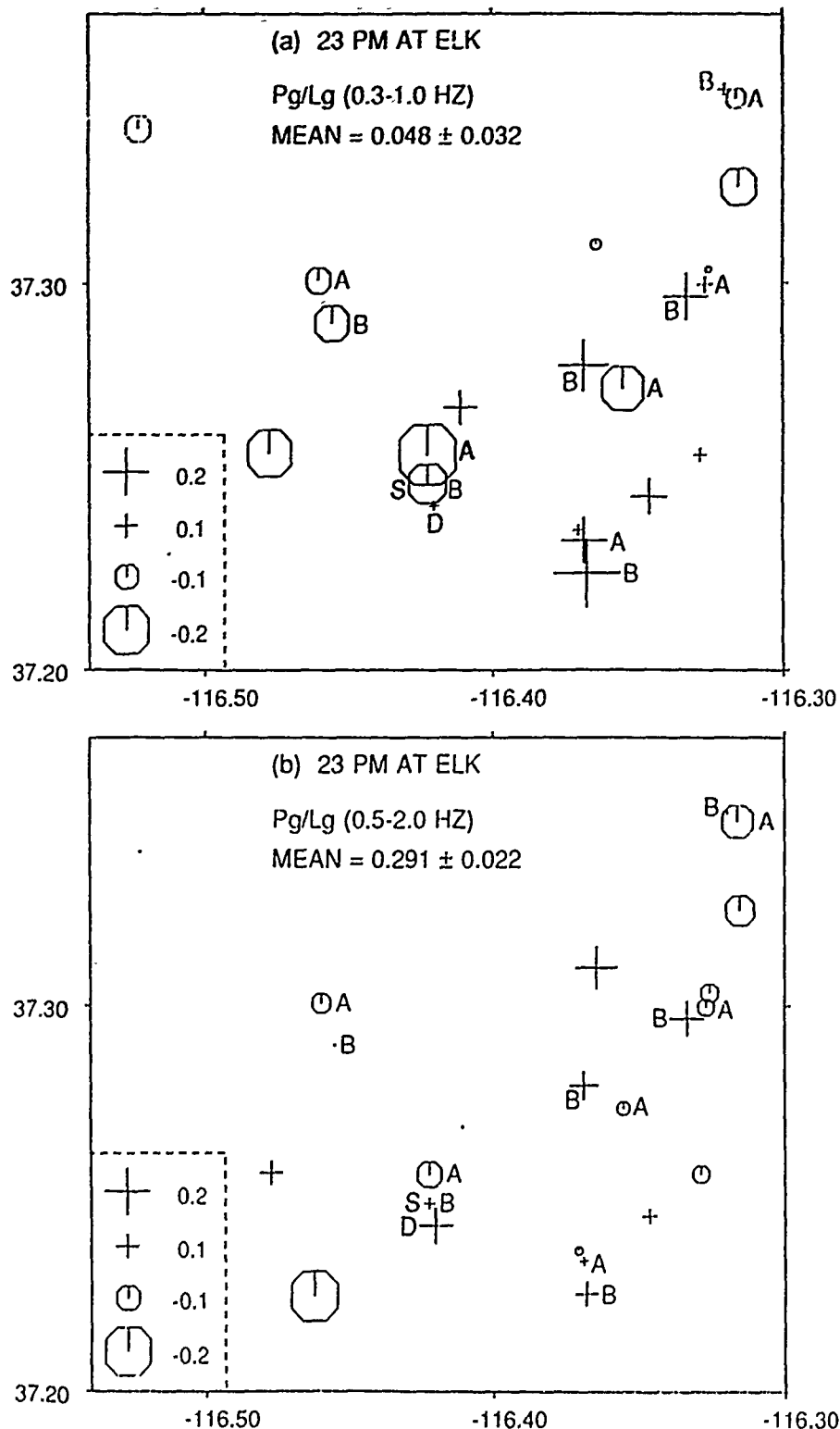
41
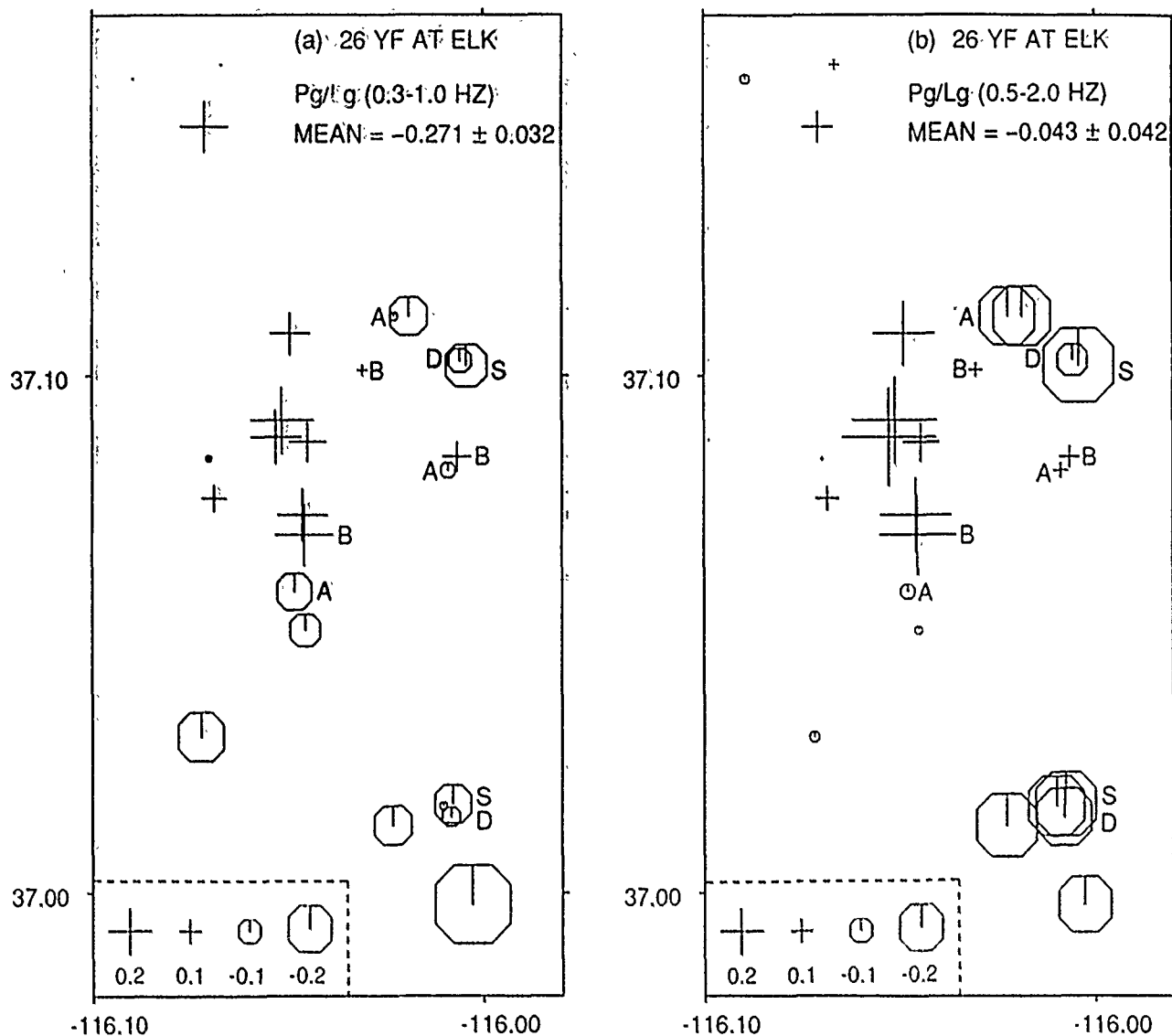
Figure 9. Similar to Figure 8 for Pg/Lg. For nearly all pairs, the deeper shot (B or D) has larger Pg/Lg than the shallower (A or S) explosion.
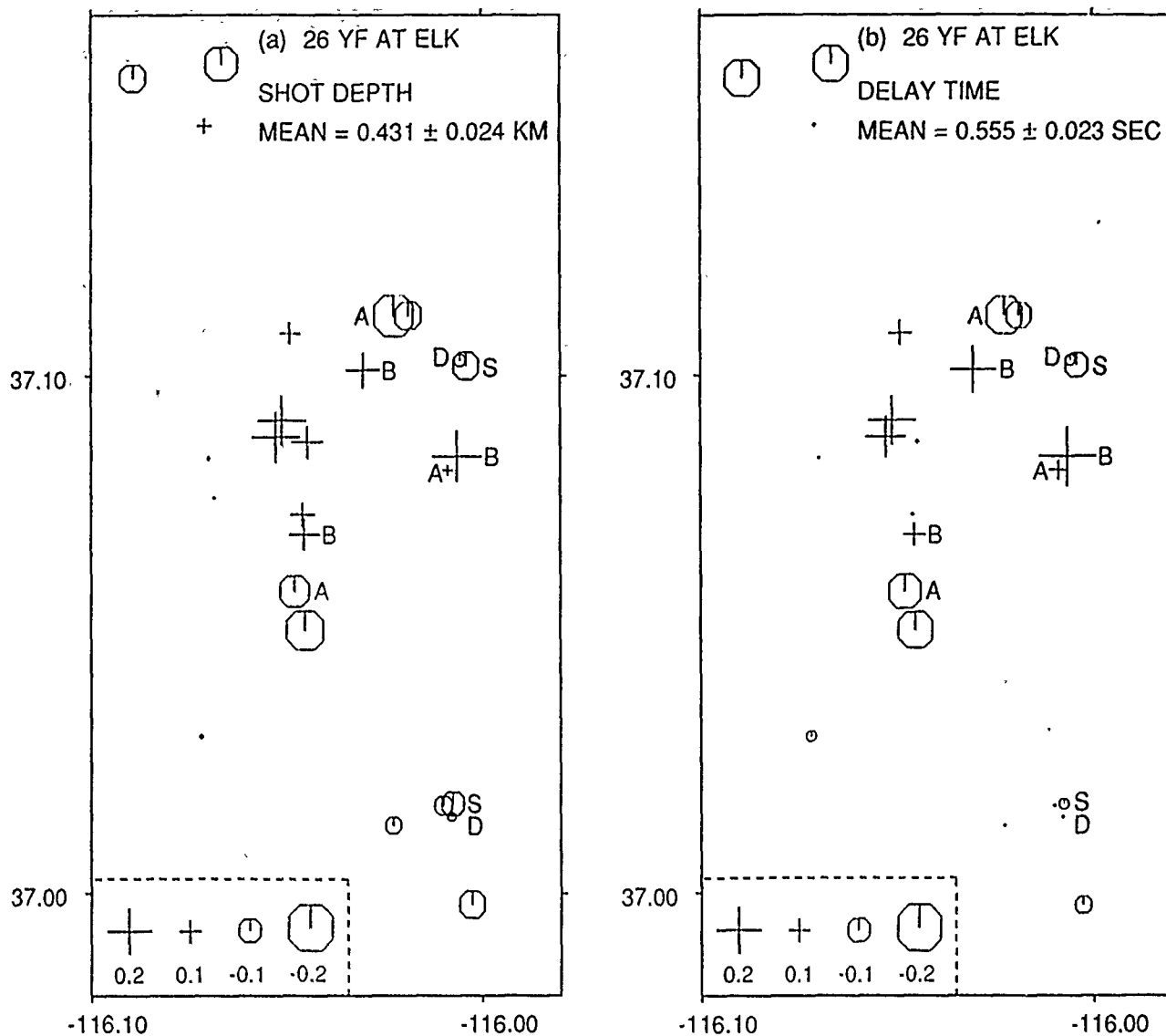
Figure 10. Similar to Figure 8 for 26 Yucca Flat shots for (a) shot depth and (b) delay time. Note similarity of the two figures.
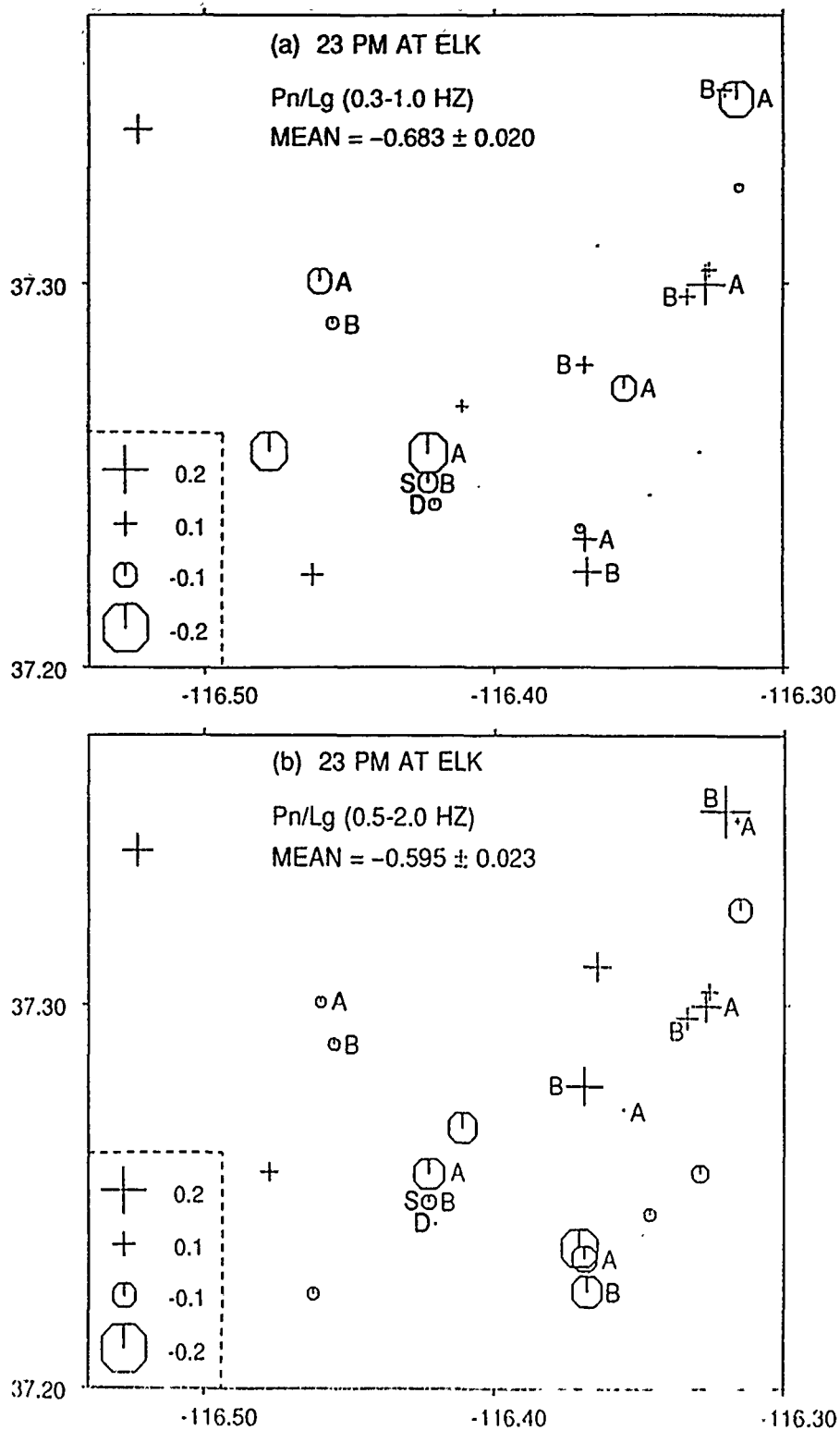
Figure 11. Similar to Figure 8 for Pn/Lg for 23 Pahute Mesa shots. Six pairs of closely spaced A and B shots and one pair of S and D shots are identified. For nearly all pairs, the deeper shot (B or D) has larger Pn/Lg than the shallower (A or S) explosion.

Figure 12. Similar to Figure 8 for Pg/Lg for 23 Pahute Mesa shots. For nearly all pairs, the deeper shot (B or D) has larger Pg/Lg than the shallower (A or S) explosion.
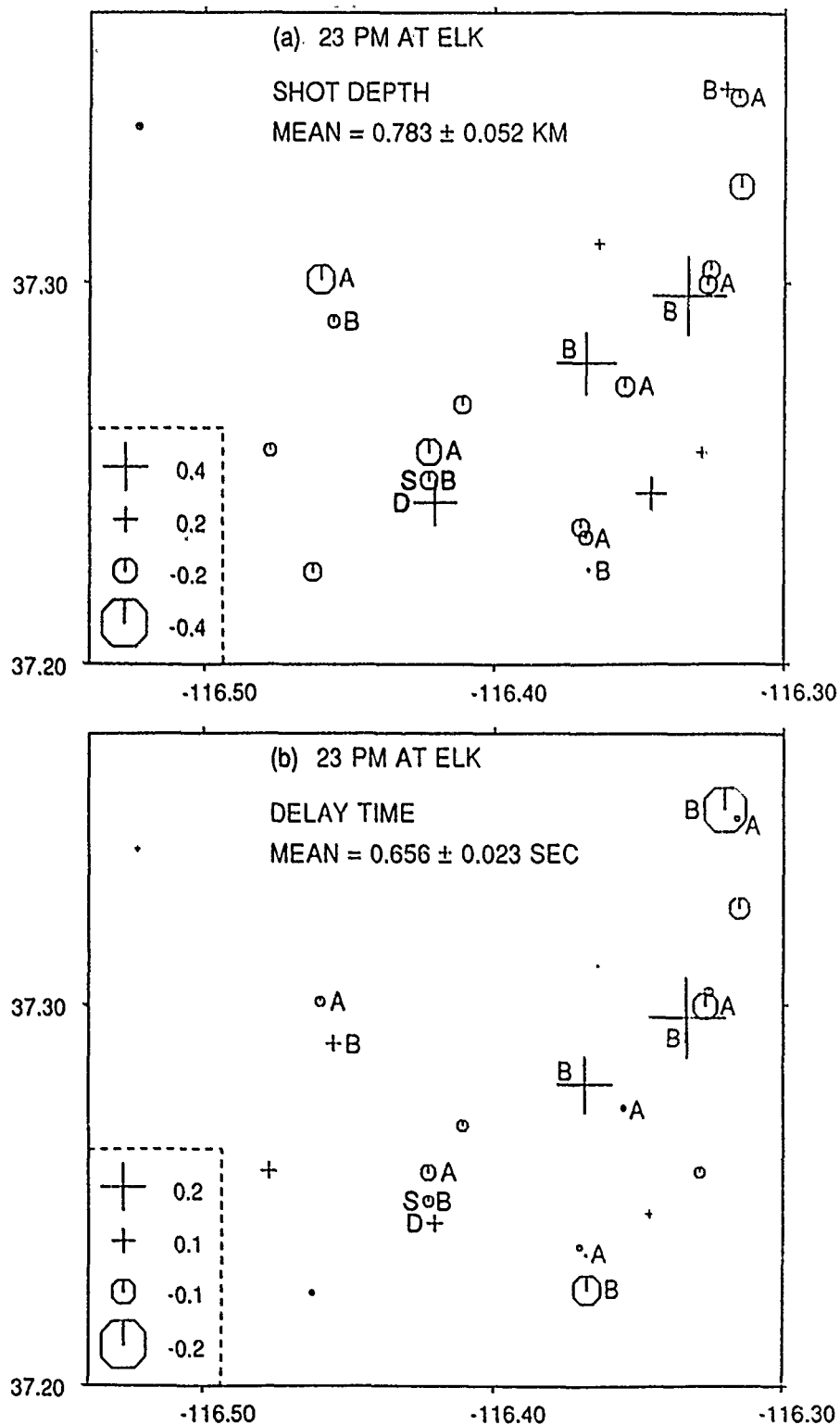
Figure 13. Similar to Figure 8 for 23 Pahute Mesa shots for (a) shot depth and (b) delay time. Note the relative lack of similarity between the two figures, especially for two pairs of closely spaced explosions (MAST and HOSTA, INLET and BACKBEACH).

between plots of shot depth and delay time for Yucca Flat explosions (Figures 10a and 10b), the Pahute Mesa plots (Figures 13a and 13b) show much less similarity. In fact, for two pairs of closely spaced AWT and BWT explosions (MAST and HOSTA, INLET and BACK-BEACH), the shot depth and delay time have opposite trends. As mentioned earlier, extremely large lateral variations in medium velocity are responsible for this. Figures 11, 12, and 13 include data from 7 pairs of closely spaced explosions such that 6 pairs include AWT and BWT shots (denoted by the letters A and B, respectively) and the remaining pair (denoted by S and D) consists of two BWT shots. A comparison of the four plots in Figures 11 and 12 with the shot depth plot in Figure 13a show a great deal of similarity, especially for the relative differences among closely spaced shots. As observed for Yucca Flat shots, the deeper shots (marked B and D) almost always have relatively larger values of both Pn/Lg and Pg/Lg for both ranges of frequency than those for the shallower shots (denoted by A and S). Once again, it seems that, for closely spaced shots, the observed values of Pn/Lg and Pg/Lg are in agreement with the theoretically expected dependence on shot depth and the lack of a linear relationship for Pahute Mesa data points in Figures 5 and 7 are mainly due to the strong lateral variations in the geology of the Pahute Mesa region.

Plots of all available amplitude ratios Pn/Lg and Pg/Lg (averaged over the frequency ranges of 0.3-1.0 Hz and 0.5-2.0 Hz) versus shot depth, delay time, and estimated delay time, derived from 51 NTS shots (including 28 from Yucca Flat) recorded at KNB, are shown in Figures 14 through 17. The correlations are poor in some cases and good in some others. The results are therefore similar to those for the recording station ELK (Figures 4 through 7). All available values of Pn/Lg and Pg/Lg derived from KNB are plotted at their epicentral locations in Figures 18, 19, 21, and 22 whereas the corresponding values of shot depth and

47
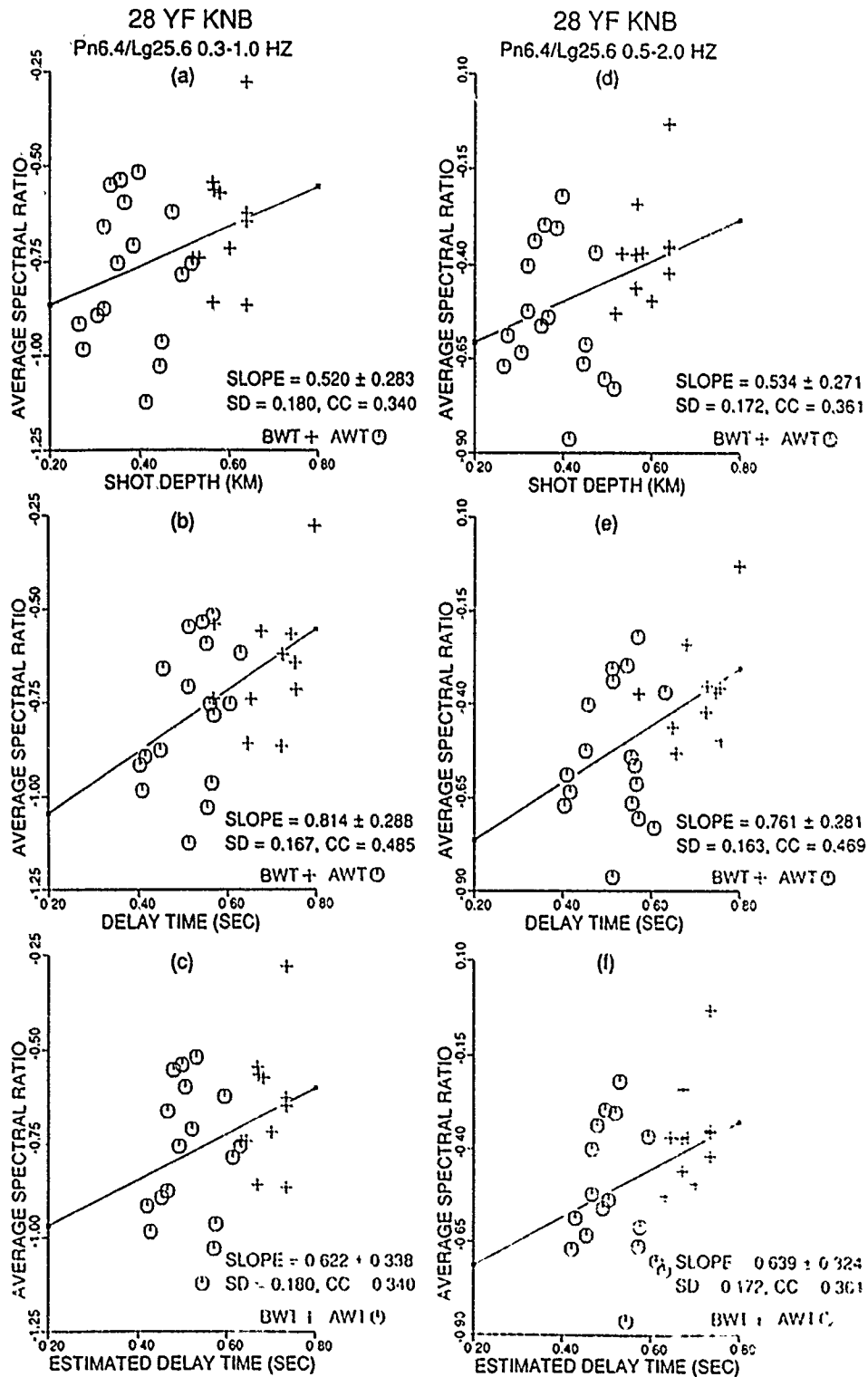
Figure 14. Similar to Figure 4 for 28 Yucca Flat shots recorded at KNB.

48

51 NTS KNB Pn6.4/Lg25.6 0.3-1.0 HZ
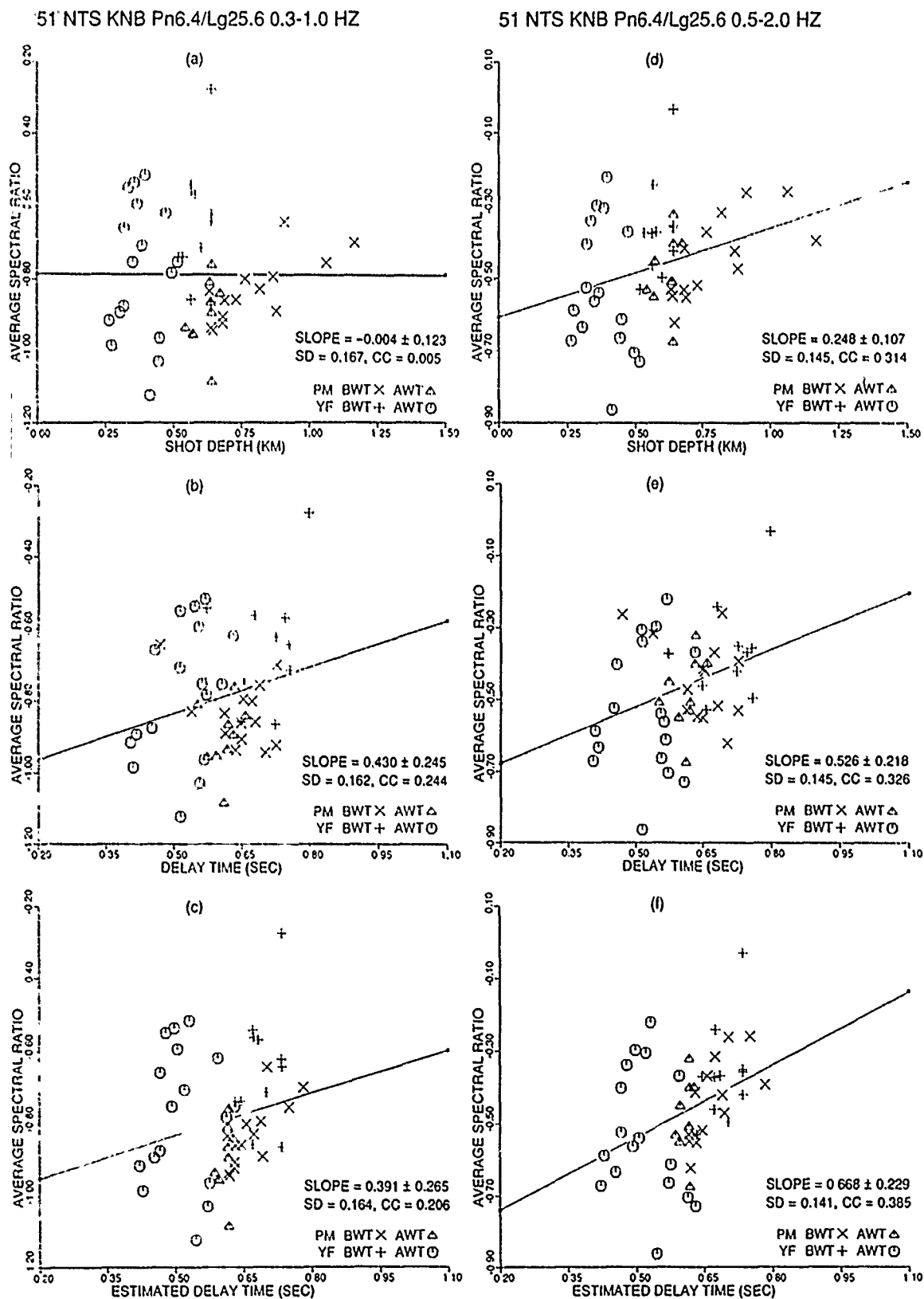
51 NTS KNB Pn6.4/Lg25.6 0.5-2.0 HZ

Figure 15. Similar to Figure 4 derived from 51 NTS (28 Yucca Flat and 23 Pahute Mesa) shots recorded at KNB.
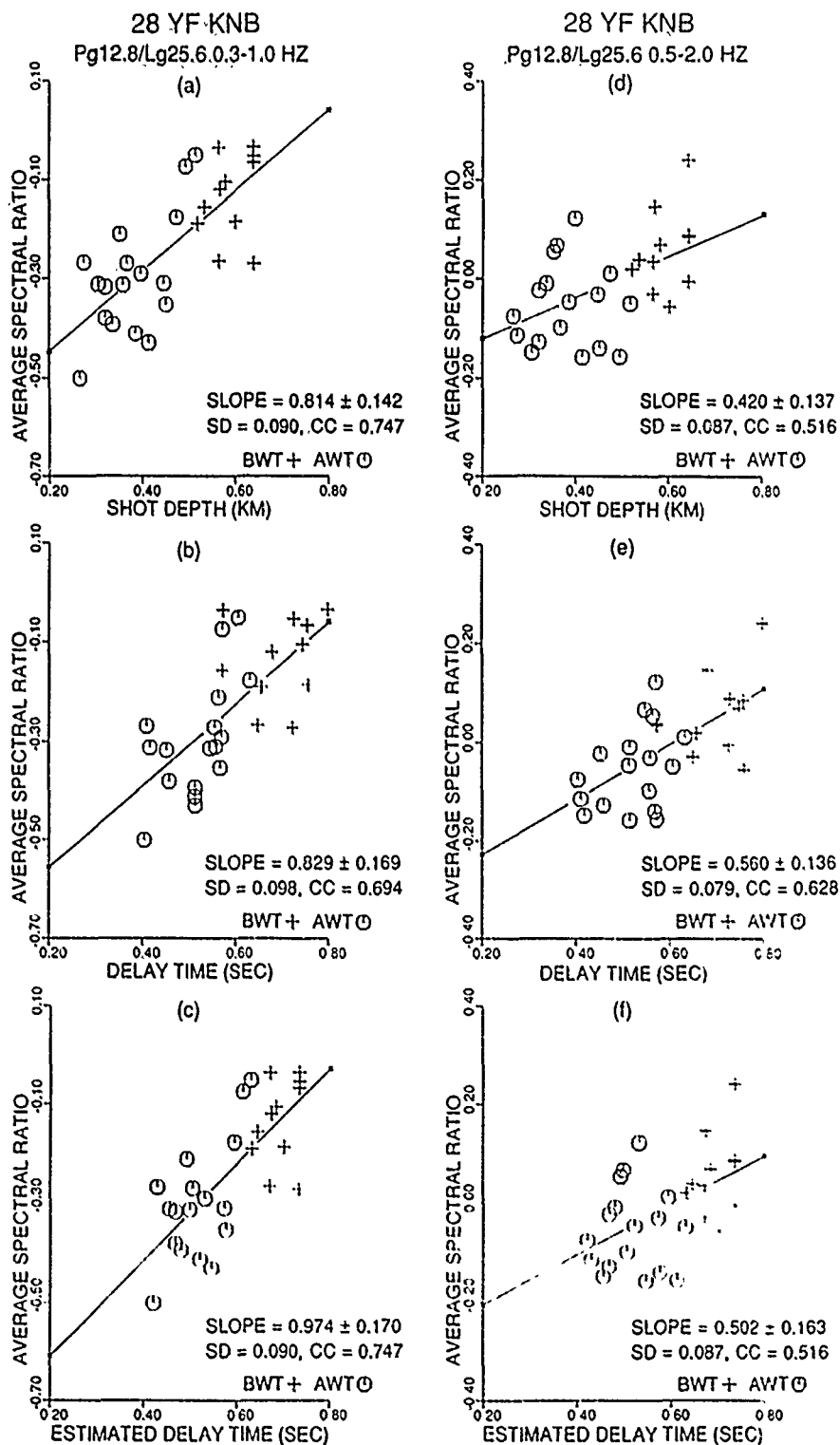
Figure 16. Similar to Figure 4 for Pg/Lg derived from 28 Yucca Flat shots recorded at KNB.
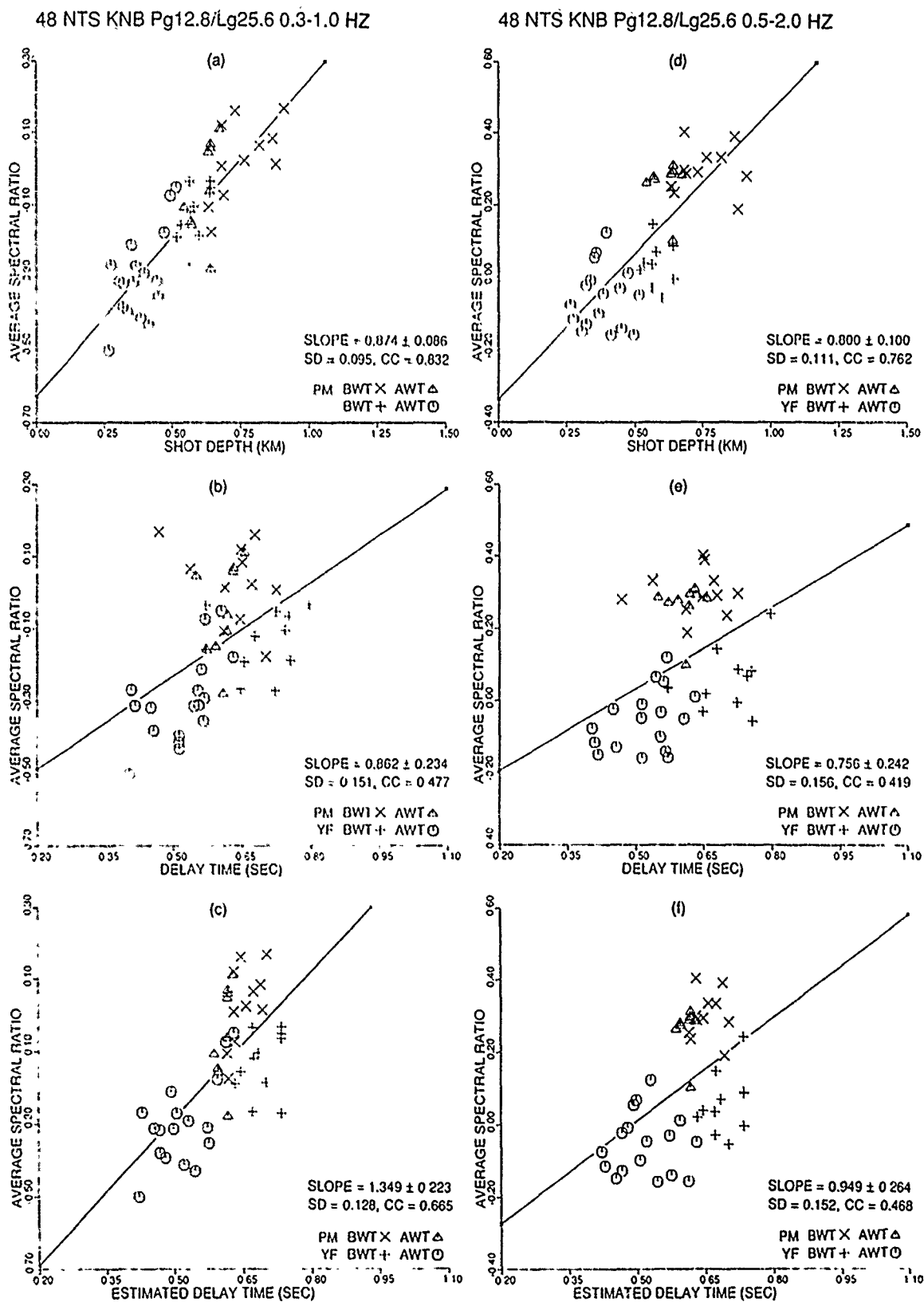
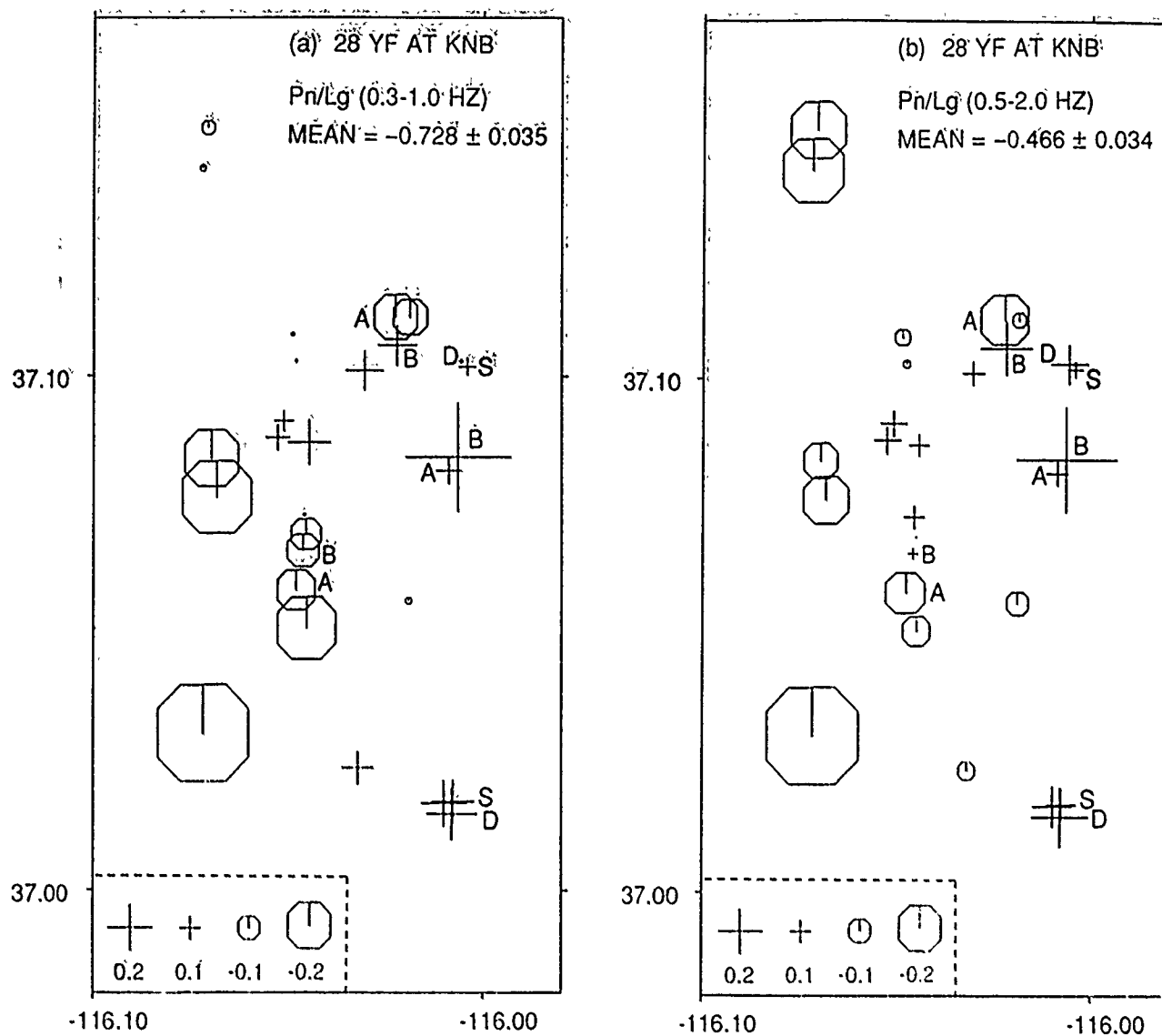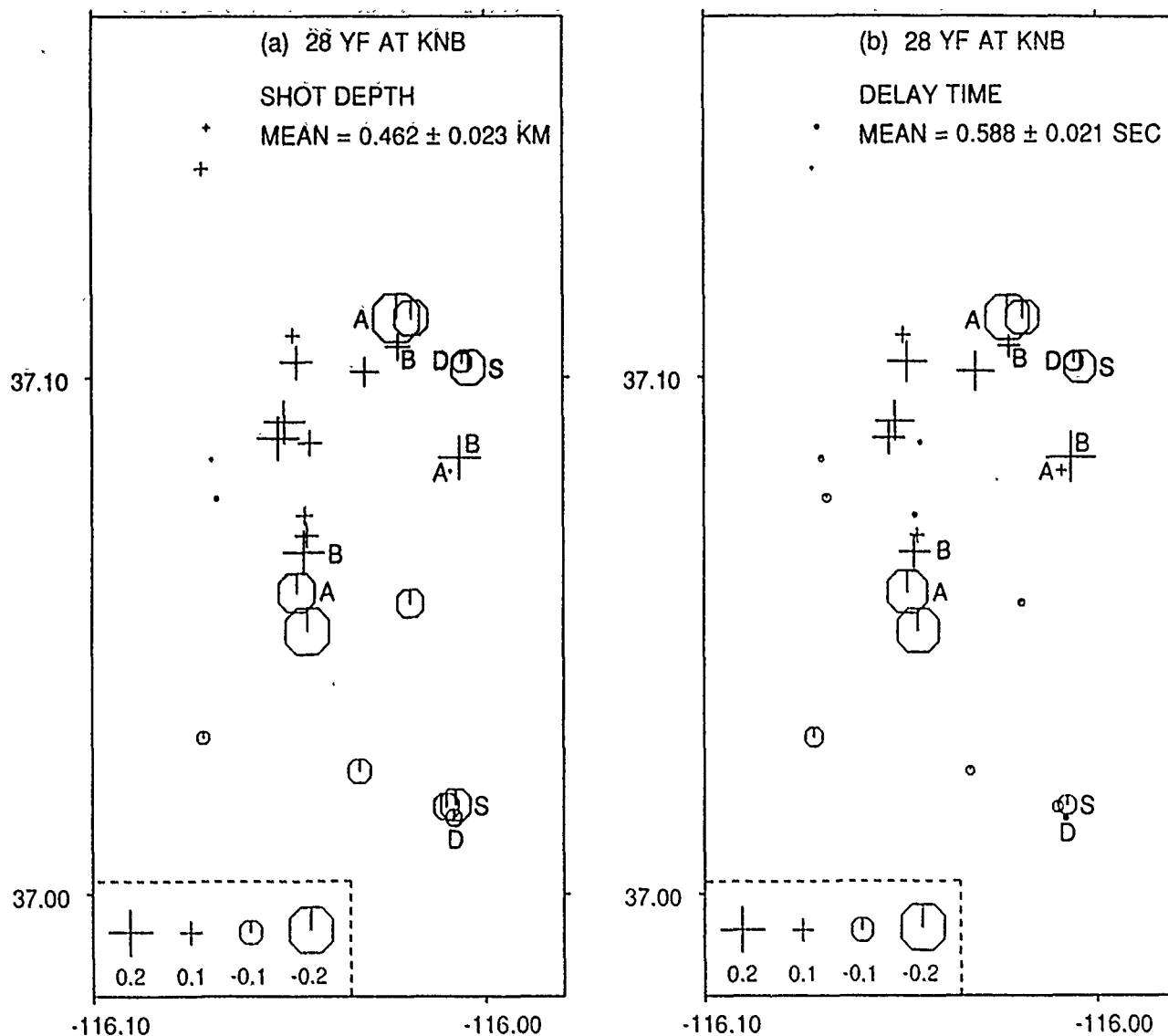Figure 17. Similar to Figure 4 for Pg/Lg derived from 48 NTS (28 Yucca Flat and 20 Pahute Mesa) shots recorded at KNB.

51

Figure 18. Similar to Figure 8 for 28 Yucca Flat shots recorded at KNB. For nearly all pairs, the deeper shot (B or D) has relatively larger Pn/Lg than the shallower (A or S) explosion.
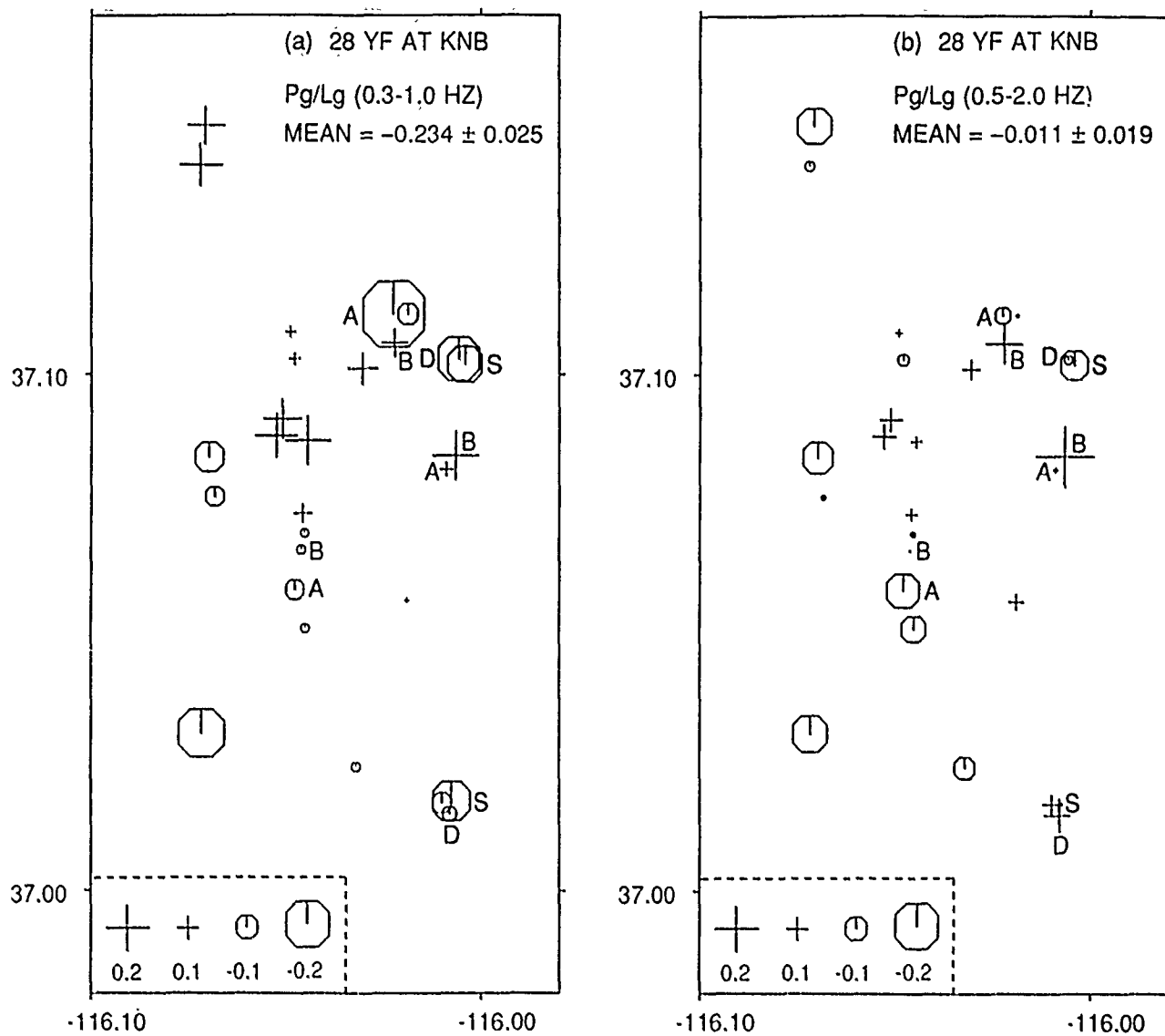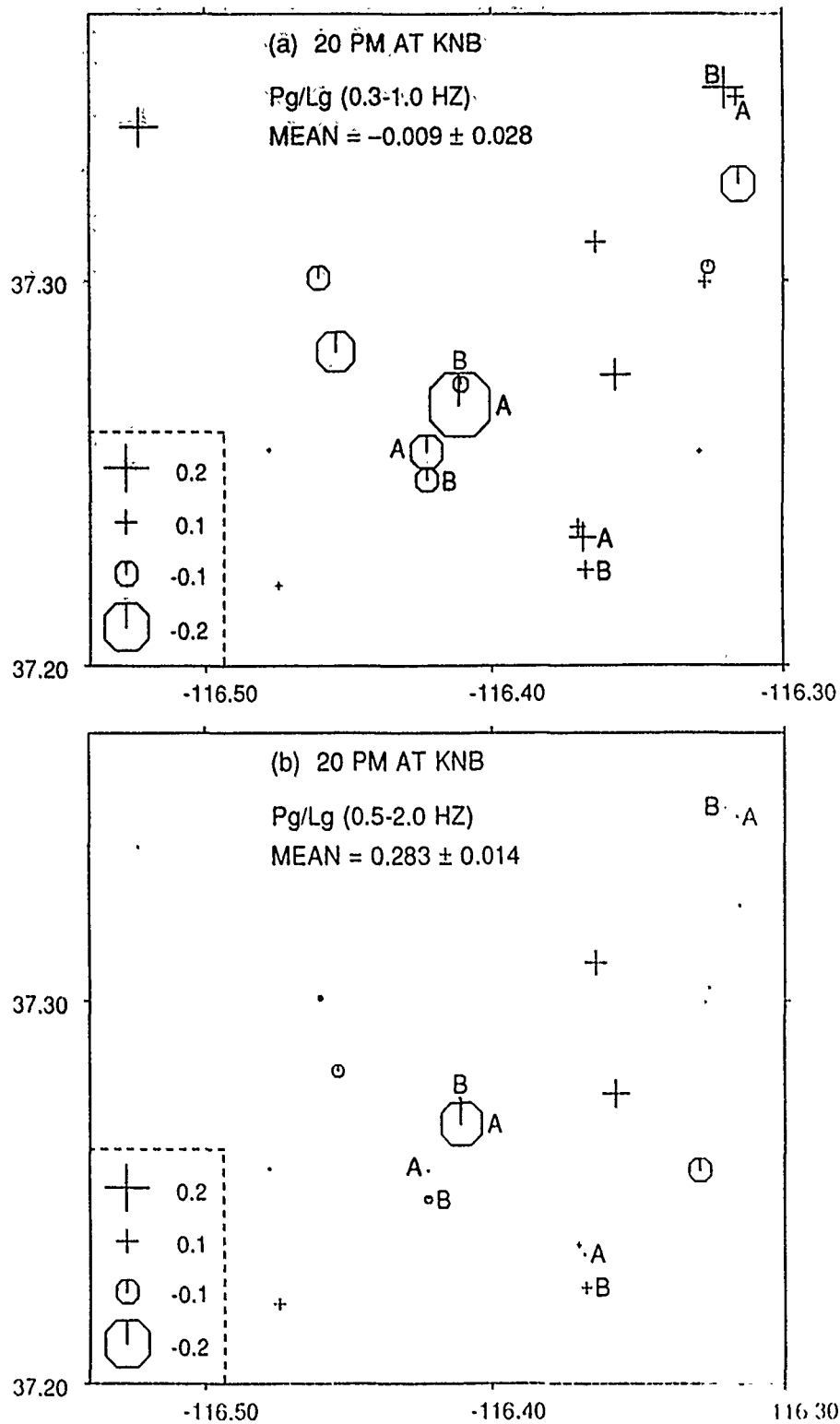
Figure 19. Similar to Figure 8 for Pg/Lg derived from 28 Yucca Flat shots recorded at KNB. For nearly all pairs, the deeper shot (B or D) has relatively larger Pg/Lg than the shallower (A or S) explosion.
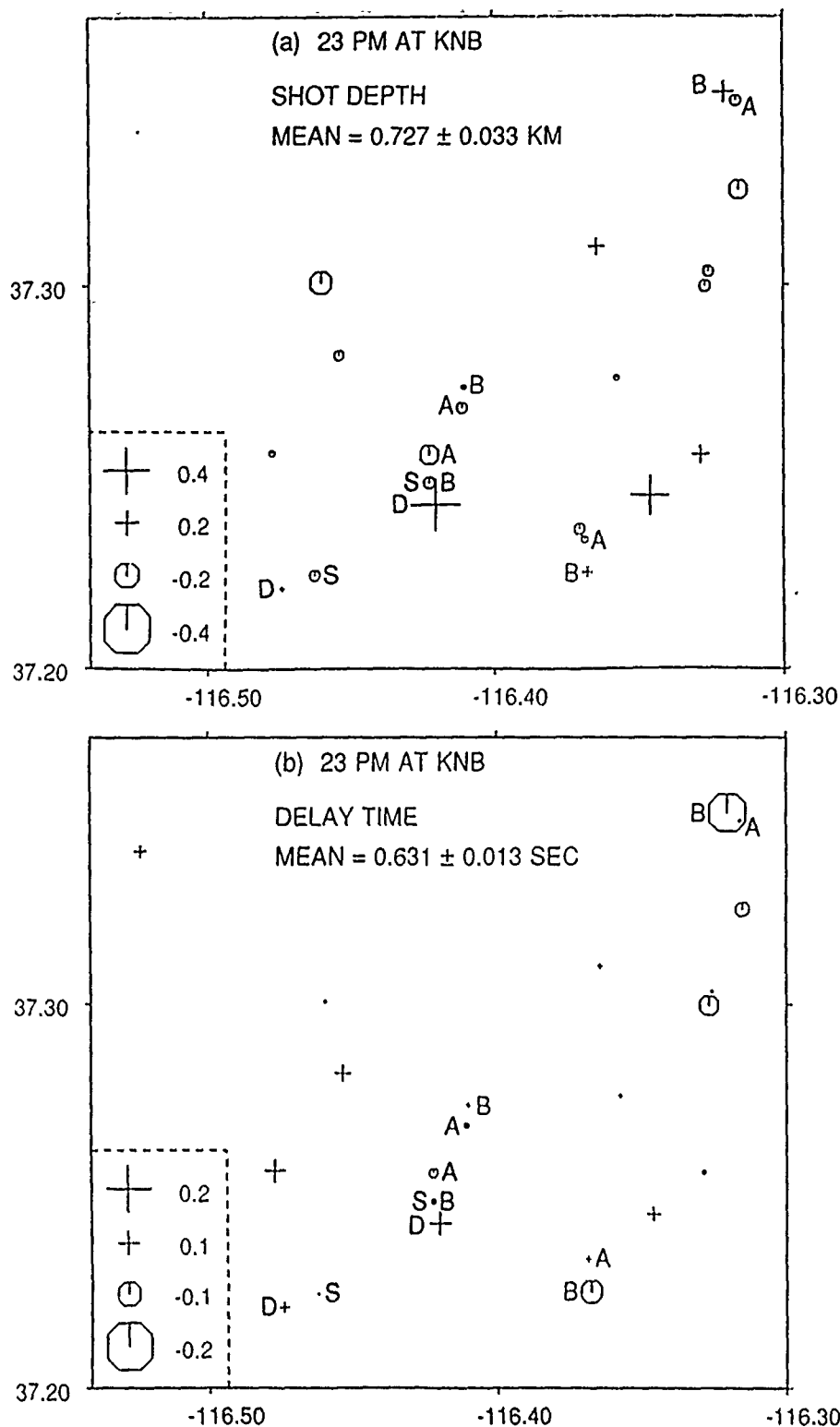
Figure 20. Similar to Figure 8 for 28 Yucca Flat shots recorded at KNB for (a) shot depth and (b) delay time. Note similarity of the two figures.
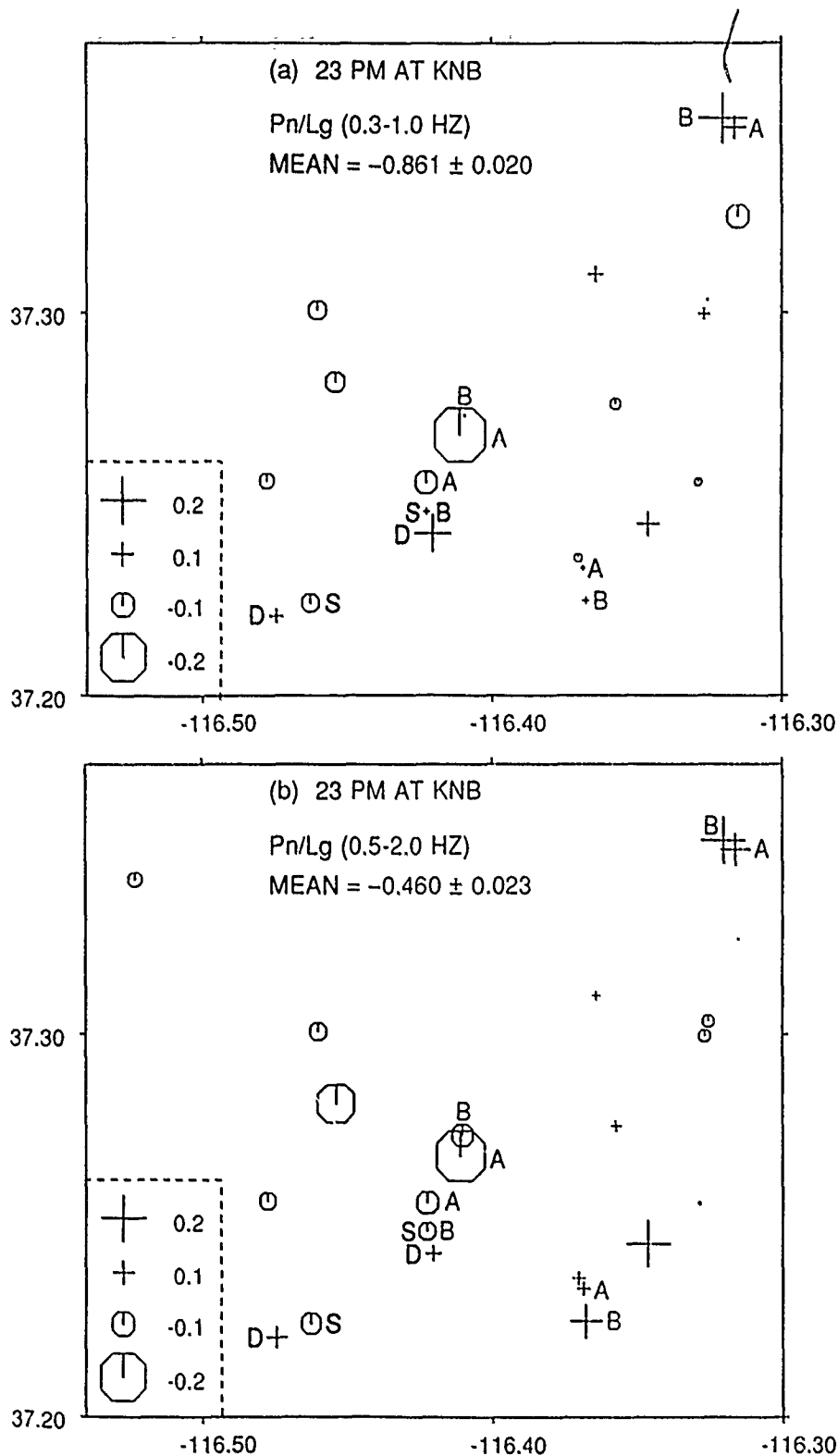
Figure 21. Similar to Figure 8 for 23 Pahute Mesa shots recorded at KNB. Four pairs of closely spaced A and B shots and two pairs of S and D shots are identified. For nearly all pairs, the deeper shot (B or D) has relatively larger Pn/Lg than the shallower (A or S) explosion.

Figure 22. Similar to Figure 8 for Pg/Lg derived from 20 Pahute Mesa shots recorded at KNB. For nearly all pairs, the deeper shot (B) has relatively larger Pg/Lg than the shallower (A) explosion.

56

(a) 23 PM AT KNB

SHOT DEPTH
MEAN = 0.727 ± 0.033 KM

(b) 23 PM AT KNB

DELAY TIME
MEAN = 0.631 ± 0.013 SEC

Figure 23. Similar to Figure 8 for 23 Pahute Mesa shots recorded at KNB for (a) shot depth and (b) delay time. Note the relative lack of similarity between the two figures, especially for two pairs of closely spaced explosions (MAST and HOSTA, INLET and BACKBEACH).

delay times are shown in Figures 20 and 23. These figures include data from as many as 5 pairs of closely spaced shots (denoted by A,B and S,D) for the Yucca Flat region and 5 pairs for the Pahute Mesa region. Nearly all closely spaced shots show differences in Pn/Lg and Pg/Lg that agree well with the theoretically expected dependence. The results from KNB are therefore again similar to those from ELK (Figures 8 through 13). The similarity of results from ELK and KNB indicates that the observed dependence of Pn/Lg and Pg/Lg on shot depth is not significantly influenced by path effects and is mainly due to near-source scattering of the depth-dependent Rg.

COMPARISON OF ELK AND KNB RESULTS FOR COMMON SHOTS

In order to understand the influence of variations in the propagation path on the low-frequency spectra of regional phases, a comparison was made of the spectral ratios Pn/Lg and Pg/Lg derived from ELK and KNB records of common Yucca Flat shots. Average values of Pn/Lg and Pg/Lg, over the frequency range of 0.5 to 2.0 Hz, were plotted versus the estimated delay time for 22 shots recorded at both ELK and KNB, and the residuals with respect to the least squares linear regression were computed. Residuals for various shots recorded at ELK and KNB are plotted at their epicentral locations in Figures 24 and 25 for Pn/Lg and Pg/Lg, respectively. A comparison of the residuals at ELK and KNB for either Pn/Lg or Pg/Lg do not show much similarity. In fact, many explosions show opposite trends. Figure 26 shows residuals at ELK plotted versus those at KNB for both Pn/Lg and Pg/Lg. The opposite trend, suggested by the negative mean slopes, is much better established for Pg/Lg than for Pn/Lg. It is hard to explain these large and rather systematic variations with direction on the basis of spall which mainly represents an axisymmetric source. On the other hand, theoretical (e.g. Stead and Helmberger, 1988) as well as observational (e.g. Gupta *et al.*, 1990) studies of explosion sources in the Yucca Flat region have suggested strong directional effects associated with the scattering of Rg.
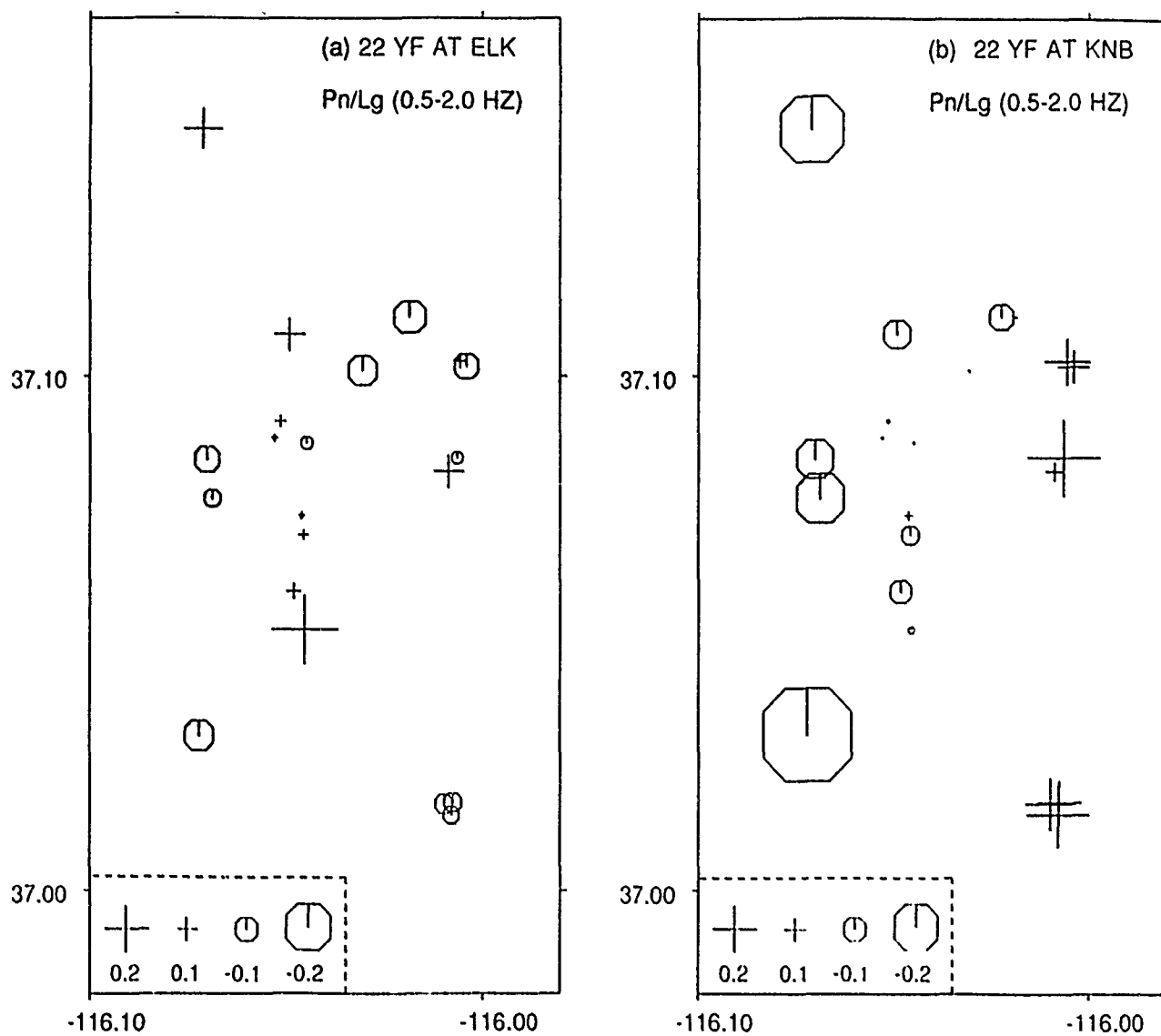
Figure 24. Similar to Figure 8 for residuals of linear regression of Pn/Lg (0.5-2.0 Hz) versus estimated delay time derived from 22 Yucca Flat shots recorded at (a) ELK and (b) KNB.
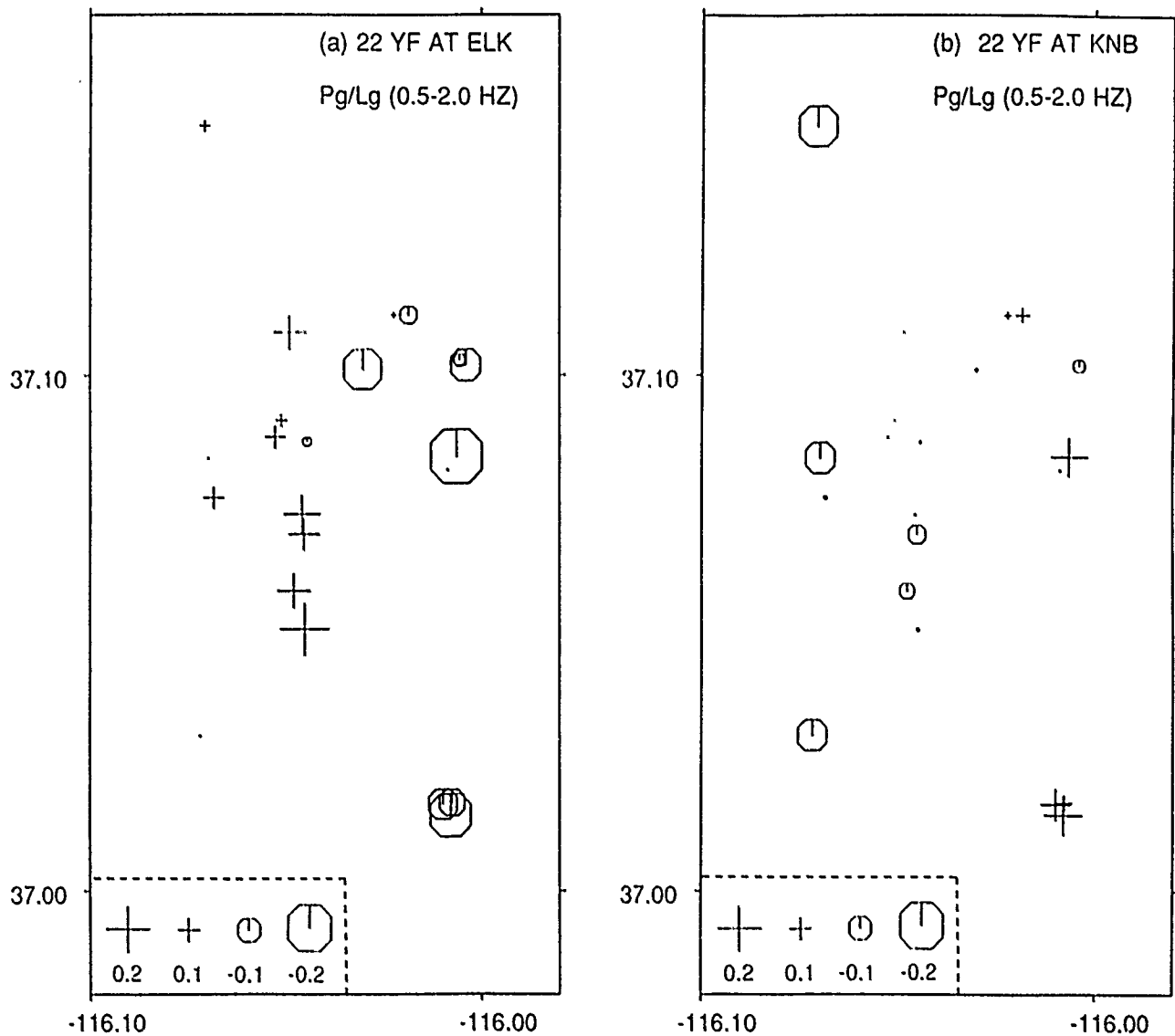
Figure 25. Similar to Figure 8 for residuals of linear regression of Pg/Lg (0.5-2.0 Hz) versus estimated delay time derived from 22 Yucca Flat shots recorded at (a) ELK and (b) KNB.
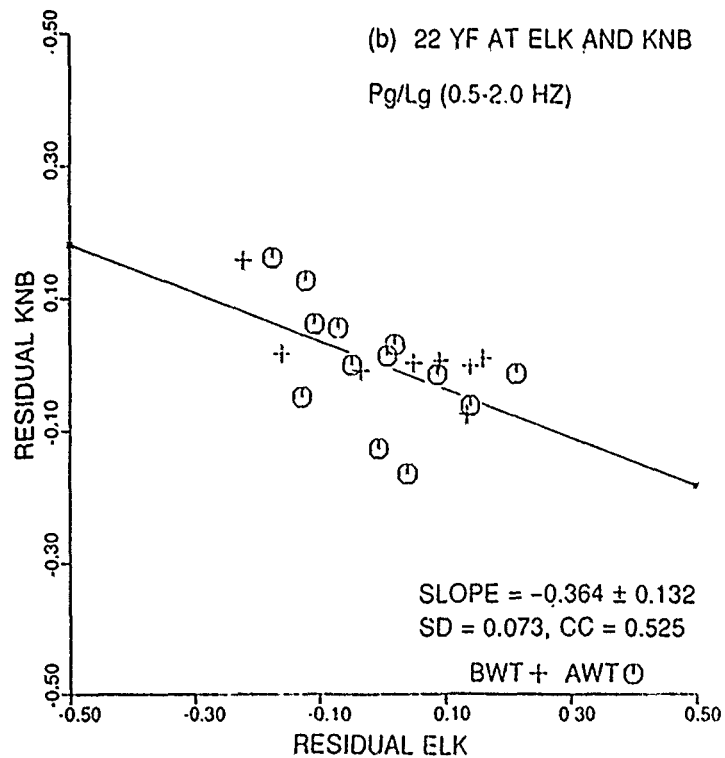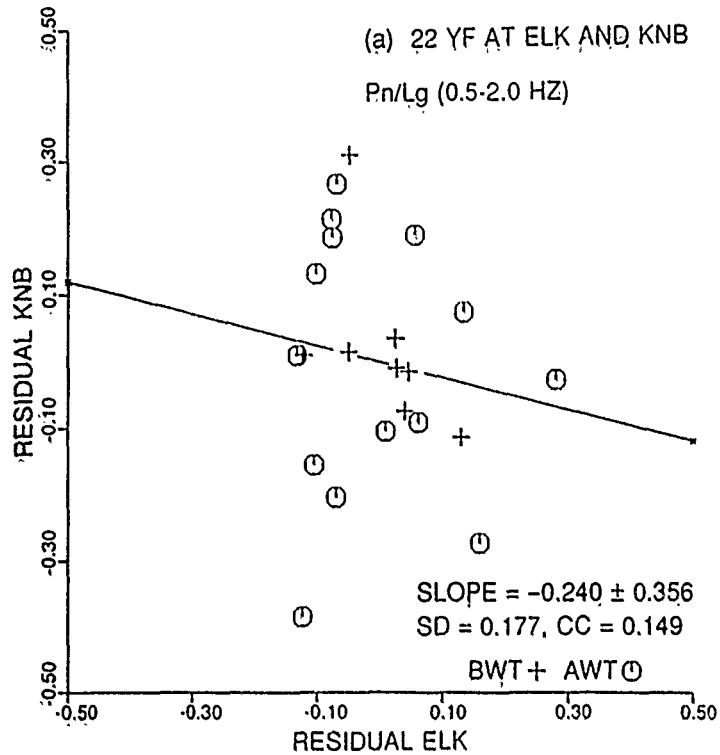
Figure 26. Residuals of linear regression of (a) Pn/Lg and (b) Pg/Lg versus estimated delay time derived from 22 Yucca Flat shots recorded at KNB plotted against similar residuals from ELK. Note the opposite correlation (indicated by negative mean slope) in both cases.

SPECTRAL RATIOS OF NORMAL AND OVERBURIED SHOTS

Figures 27 and 28 show spectral ratios between two pairs of closely spaced normal and overburied explosions. BASEBALL and BORREGO (overburied) have the same shot depth and are less than 500 m apart (Figure 1). The overburied shot, TECHADO, is only 15 m deeper than ROUSANNE and the two are separated by less than 300 m. On the basis of their m_b values (Table 1), yields of the two overburied shots are at least a factor of about 25 smaller than their neighboring explosions. The spectral ratios are based on the use of S/N = 1.5 and five-point smoothing. Results from the three stations ELK, KNB, and LAC are rather similar and show the low-frequency Lg from the normal shots to be significantly larger than that from the overburied shots whereas such behavior is mostly not observed for the other two phases Pn and Pg. It is generally agreed that the normal nuclear shots are associated with a large non-linear zone and it is much more realistic to regard them as volume sources rather than point sources. Since most of the non-linear zone is above the shot point, the "effective" shot depth may be considerably smaller than the emplacement depth. On the other hand, the non-linear zone associated with an overburied shot is expected to be much smaller so that its effective shot depth may be close to its emplacement depth. Thus the observed spectral ratios for the low-frequency Lg in Figures 27 and 28 can be explained by the scattering of explosion-generated Rg into S.

Theoretical studies of the generation of Lg by spall from a normal explosion indicate a sharply peaked spectrum (compared to the broadband explosion signal) which falls-off rapidly for frequencies above 2 Hz and below about 0.5 Hz (Barker *et al.*, 1990; McLaughlin, *et al.*, 1990). Spall from an overburied explosion is significantly less important than from a normal shot (McLaughlin *et al.*, 1990). It follows therefore that the amplitude ratio of Lg for a
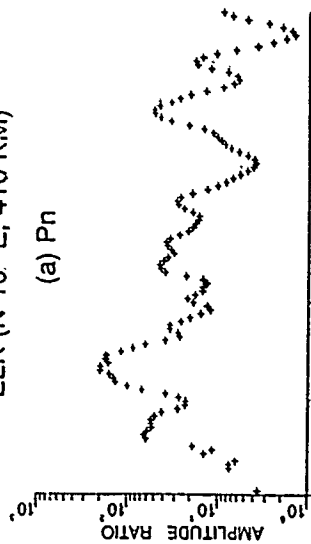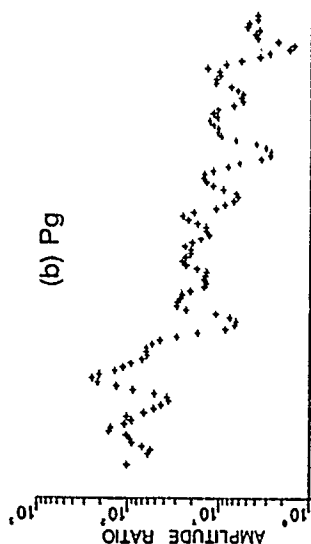
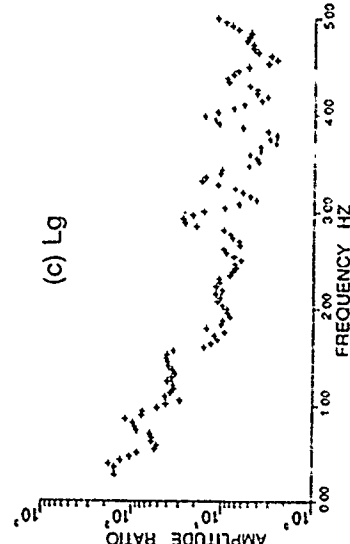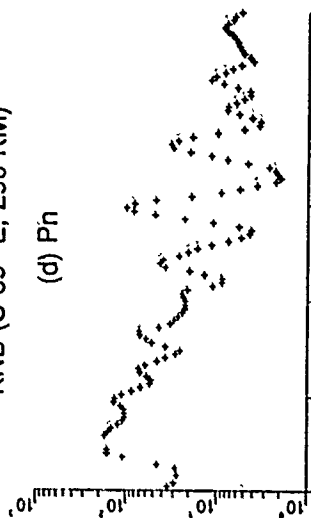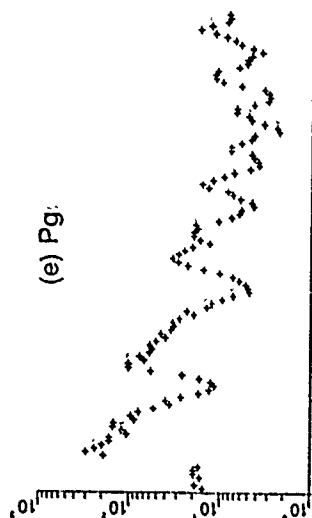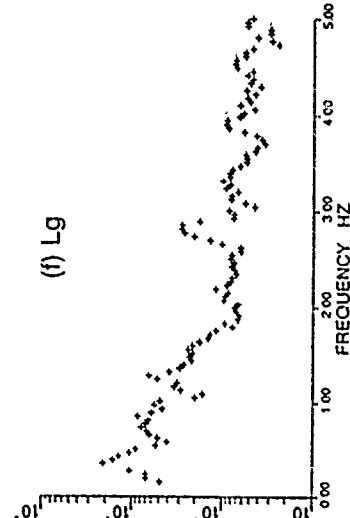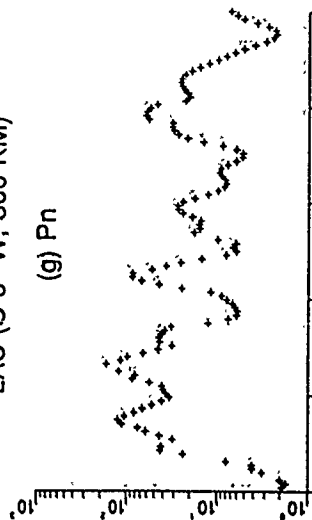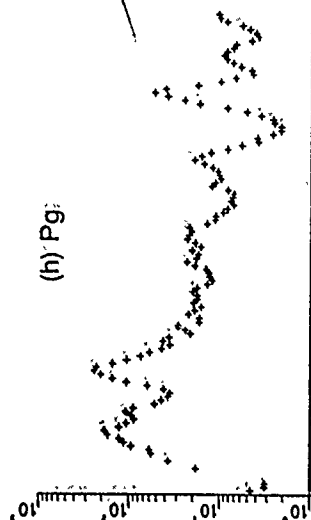Figure 27. Spectral ratios of closely spaced explosions BASEBALL and BORREGO (over-buried) for phases Pn, Pg, and Lg at stations ELK, KNB, and LAC. Note the relatively larger low-frequency Lg for BASEBALL at all three recording stations.

64

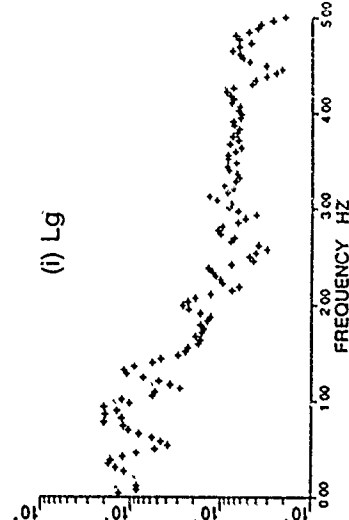Figure 28. Spectral ratios of closely spaced explosions ROUSANNE and TECHADO (over-buried) for phases Pn, Pg, and Lg at stations ELK, KNB, and LAC. Note the relatively larger low-frequency Lg for ROUSANNE at all three recording stations.
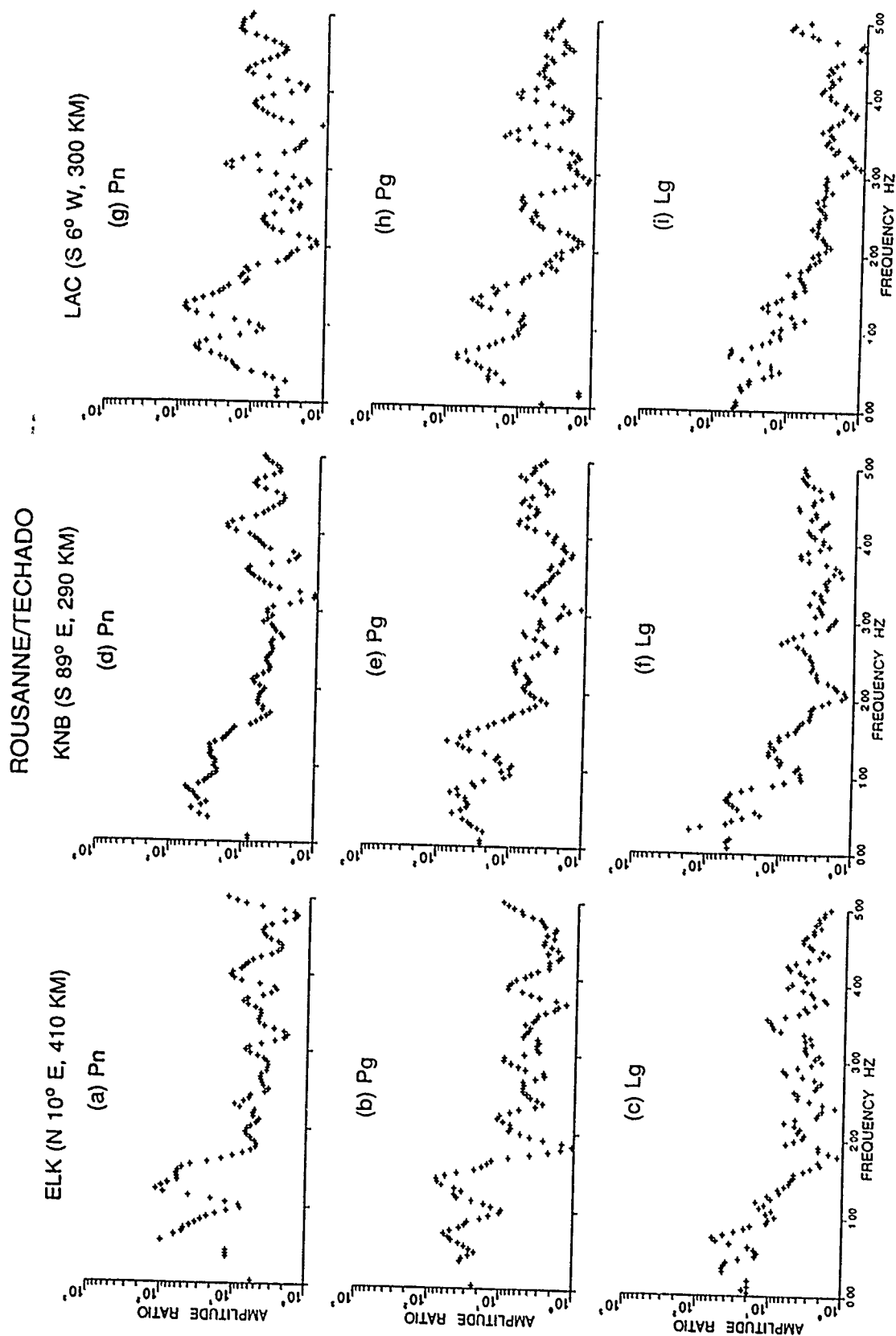
65

normal to an overburied shot should *decrease* as the frequency approaches 0 Hz. Our observations (Figures 27c, f, i and 28c, f, i) clearly indicate an opposite trend.

CONCLUSIONS

The observed variations of Pn/Lg and Pg/Lg with shot depth and delay time, especially for closely spaced shots for which the scattering functions are likely to be similar, suggest that the low-frequency Lg from Yucca Flat and Pahute Mesa (NTS) explosions is mainly due to the scattering of explosion-generated Rg into S. The observed dependence of the amplitude ratios Pn/Lg and Pg/Lg on shot depth is mostly in agreement with the dependence on depth of explosion-generated Rg. A better quantitative agreement with theory is not expected because of the extensive lateral variations in physical parameters that exist for most NTS shots. The known stability of Lg as an estimator of explosive yield may be explained by scattering taking place over a large volume of the shallow crust.

ACKNOWLEDGMENTS

REFERENCES

Barker, T. G., S. M. Day, K. L. McLaughlin, B. Shkoller, and J. L. Stevens (1990). An analysis of the effects of spall on regional and teleseismic waveforms using two-dimensional numerical modeling of underground explosions, *GL-TR-90-0126*, Geophysics Laboratory, Hanscom Air Force Base, Massachusetts. ADA226921

Bolt, B. A. (1978). Incomplete formulations of the regression of earthquake magnitude with surface fault rupture length, *Geology 6*, 233-235.

Campillo, M., M. Bouchon, and B. Massinon (1984). Theoretical study of the excitation, spectral characteristics, and geometrical attenuation of regional seismic phases, *Bull. Seism. Soc. Am. 74*, 79-90.

Gupta, I. N. and R. R. Blandford (1983). A mechanism for generation of short-period transverse motion from explosions, *Bull. Seism. Soc. Am. 73*, 571-591.

Gupta, I. N., W. W. Chan, and R. A. Wagner (1991). A comparison of regional phases from underground nuclear explosions at East Kazakh and Nevada Test Sites, *Bull. Seism. Soc. Am. 81* (in press).

Gupta, I. N., C. S. Lynnes, T. W. McElfresh, and R. A. Wagner (1990). F-k analysis of NORESS array and single-station data to identify sources of near-receiver and near-source scattering, *Bull. Seism. Soc. Am. 80*, 2227-2241.

Gutowski, P. R., F. Hron, D. E. Wagner, and S. Treitel (1984). S*, *Bull. Seism. Soc. Am. 74*, 61-78.

Hays, W. W. and J. R. Murphy (1971). The effect of Yucca Fault on seismic wave propagation, *Bull. Seism. Soc. Am. 61*, 697-706.

Langston, C. A. (1982). Aspects of Pn and Pg propagation at regional distances, *Bull. Seism. Soc. Am. 72*, 457-471.

Lilwall, R. C. (1988). Regional $m_b{:}M_s$, Lg/Pg amplitude ratios and Lg spectral ratios as criteria for distinguishing between earthquakes and explosions: a theoretical study, *Geophys. J. 93*, 137-147.

McLaughlin, K. L., T. G. Barker, and S. M. Day (1990). Implications of explosion-generated spall models: regional seismic signals, *GL-TR-90-0133*, Geophysics Laboratory, Hanscom Air Force Base, Massachusetts. ADA227273

Murphy, J. R. and T. J. Bennett (1982). A discrimination analysis of short-period regional seismic data recorded at Tonto Forest Observatory, *Bull. Seism. Soc. Am. 72*, 1351-1366.

Ramspott, L. D. and N. W. Howard (1975). Average properties of nuclear test areas and media at the USERDA Nevada Test Site, *UCRL-51948*, Lawrence Livermore Laboratory, Livermore, California.

Stead, R. J. and D. V. Helmberger (1988). Numerical-analytical interfacing in two dimensions with applications to modeling NTS seismograms, *PAGEOPH 128*, Nos. 1/2, 157-193.

Taylor, S. R. and G. E. Randall (1989). The effects of spall on regional seismograms, *Geophys. Res. Lett. 16*, 211-214.

SECTION C

AN ARRAY STUDY OF THE EFFECTS OF A KNOWN LOCAL SCATTERER

ON REGIONAL PHASES

INTRODUCTION

Until recently, very few studies of teleseismic PPP waveforms had been successful in identifying and locating specific sources of scattering from observed seismograms. One of the most convincing analyses has been the identification of scattered arrivals from the region of Moffat Water, a narrow lake in Scotland about 8 miles long, which lies at the bottom of a 600 ft deep valley (Key, 1967). Broadband f-k analysis of EKA recordings of both U.S. and Soviet nuclear explosions further confirmed the secondary seismic source to be from Moffat Water (Gupta *et al.*, 1990a). Residual seismograms obtained by subtracting the beamed record from each array channel (Blandford *et al.*, 1976) significantly improved identification of the sources of locally scattered arrivals.

Our recent f-k analyses of data from the high-frequency seismic array NORESS (Norway) first suggested the presence of a local scatterer about 25-30 km southwest of the array, in the region of Lake Mjosa near Skreikampen in Figure 1 (Gupta *et al.*, 1989; Gupta *et al.*, 1990a, 1990b). Soviet and U.S. nuclear explosions and an earthquake were used as the seismic sources, providing significantly different source-receiver azimuthal directions. Two new f-k techniques based on the use of residual seismograms and f-k power difference plots improved identification of the scatterer. Similar results were obtained by polarization analysis of three-component NORESS data. Our deterministic location of a prominent scatterer near Skreikampen has been duplicated by later studies (e.g. Bannister *et al.*, 1990; Hedlin *et al.*,
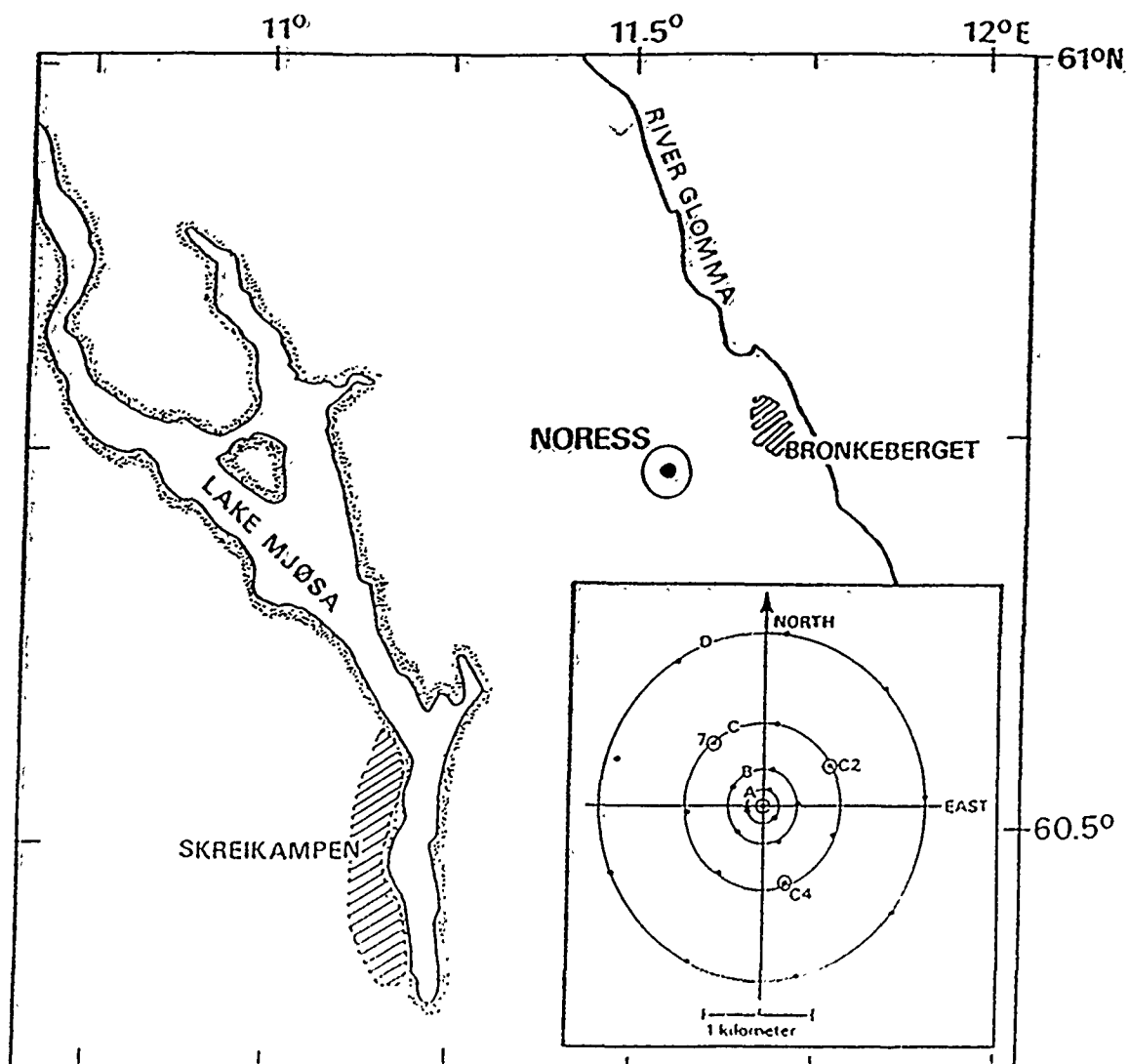
71

Figure 1. The NORESS array region with the two scattering locations Skreikampen and Bronkeberget hatched. The array configuration is given in the lower right insert where encircled stations indicate three-component sites.

1991). We also located another scatterer about 10 km east of NORESS, near Bronkeberget in Figure 1 (Gupta *et al.*, 1989) and this too has been confirmed by later research (Bannister *et al.*, 1990; Hedlin *et al.*, 1991). In this study, we investigate the effects of the well established prominent scatterer associated with Lake Mjosa on array recordings of the regional phases Pn, Pg, and Lg.

In order to make best possible use of array data, it is important to understand the characteristics of various arrivals from both teleseismic and regional seismic sources. Both near-receiver and near-source scattering play important roles in the monitoring of underground nuclear tests. For example, the Lg phase from explosions, known to be strongly influenced by scattering (e.g., Gupta and Blandford, 1983), is often used for the detection, source discrimination, and yield determination of underground nuclear explosions.

F-K ANALYSIS OF REGIONAL DATA FROM A MINE BLAST

Our study of several regional events recorded at NORESS suggested that near-receiver scattering exerts significant influence on the regional phases Pn, Pg, and Lg by generating observable scattered arrivals (Gupta et al. 1990c). Results from the mine blast of 4 February 1986 (59.3° N, 24.4° E, $m_b \approx$ 2.6, distance 734 km, backazimuth 97°; Jurkevics, 1988) are shown in Figures 2 and 3. As with teleseismic data, the use of residual seismograms derived by subtracting the beamed record from each array channel provided an effective method for isolating the secondary source from the primary source. The beamed record for each regional phase was obtained by incorporating steering delays based on the known azimuthal direction and phase velocity from the f-k analysis of raw data. Figure 2a shows f-k results for the 6.4 sec long window with the largest amplitude Lg, Lg_{max}. It indicates a phase velocity of about 4.6 km/sec and a backazimuth of about 96°. Knowing the location of the Skreikampen scatterer and assuming a group velocity of 3.5 km/sec for Lg, the scattered Lg-to-Rg arrival should arrive about 14 sec after Lg_{max}; the corresponding normal f-k plot is shown in Figure 2b. F-k plots from residual seismograms obtained by subtracting the beamed Lg from each array channel provided the results shown in Figures 2c to 2f in which plots for both later windows (Figures 2d and 2f) clearly indicate the expected Lg to Rg arrivals along the expected direction and with phase velocity appropriate for Rg. A comparison of power on the normal and residual f-k plots suggests that amplitude of the Lg-to-Rg scattered phase is a significant fraction of the on-azimuth Lg. For example, in the Lg_{max} + 14 sec window (Figure 2d), the prominent scattered arrival has power only about 3 db smaller than that of the on-azimuth Lg (Figure 2b).
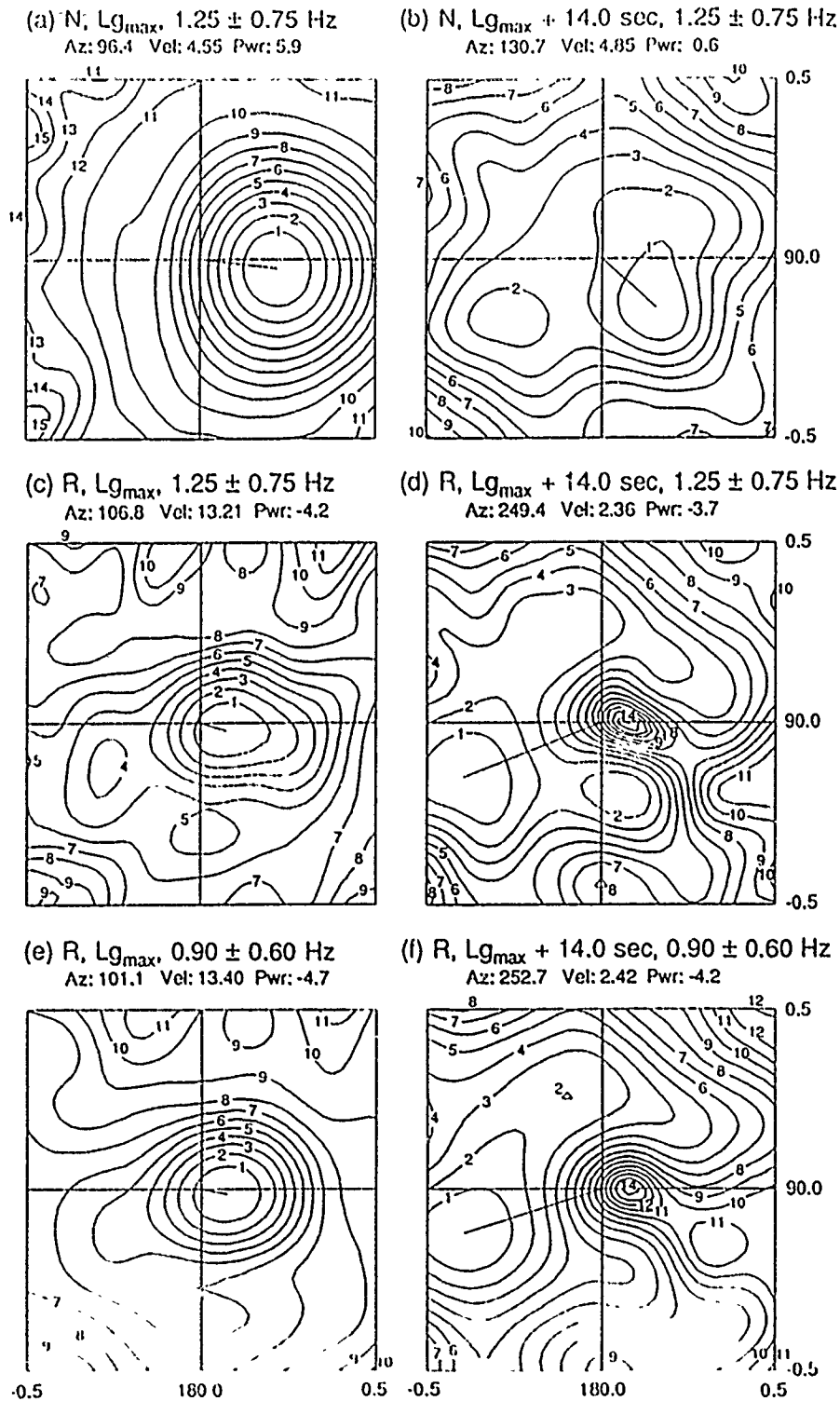
Figure 2. Frequency-slowness spectral estimates of the mine blast of 4 February 1986 with a maximum slowness of 0.5 sec/km and use of Lg windows. The numbers on top of each plot indicate backazimuth (deg), phase velocity (km/sec), and signal power (dB), respectively of the highest-amplitude arrival which is shown connected to the plot origin. The signal windows and frequency passbands are indicated on each plot. Plots (a) and (b) are based on the use of normal (N) seismograms whereas (c) to (f) are derived from the residual (R) seismograms. Both (d) and (f) indicate prominent scattered Rg arrivals from the direction of Skreikampen.
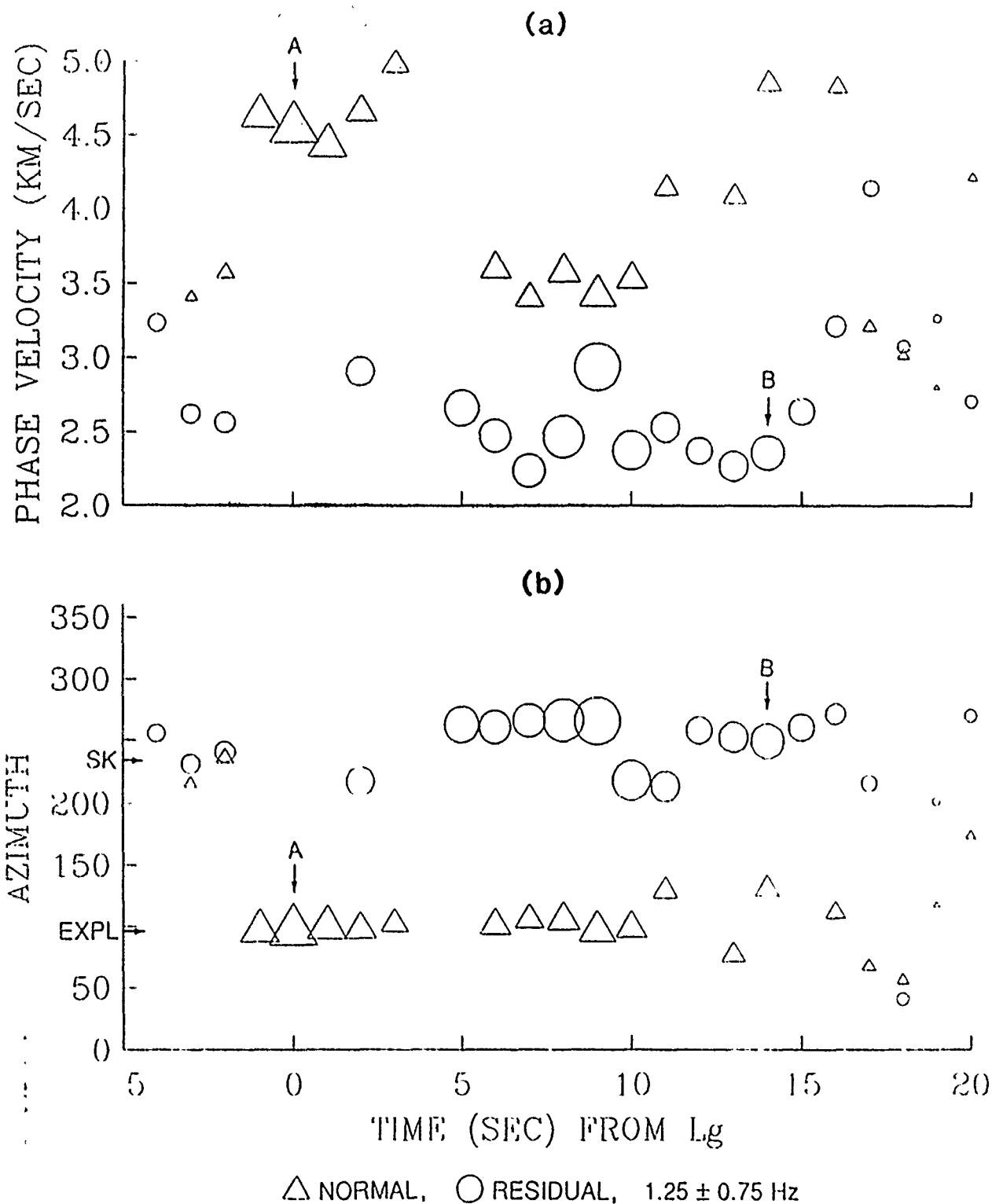
Figure 3. Plots of (a) phase velocity and (b) backazimuth of the dominant arrivals in f-k plots of 25 sec of Lg derived from normal and residual seismograms of the mine blast of 4 February 1986. The size of the symbol is proportional to the power in each dominant arrival. Backazimuths to the explosion and Skreikampen are denoted by EXPL and SK, respectively. Arrows marked A and B represent results from windows corresponding to Lg_{max} and the expected Lg_{max}-to-Rg scattered phase from Skreikampen, respectively. Results from the residual seismograms indicate prominent Rg arrivals from the direction of Skreikampen.

76

F-k plots from both normal and residual seismograms were obtained for 25 consecutive windows, starting 5 sec before Lg_{max} and with incremental shift of 1 0 sec. As before, each window was 6.4 sec long. Results using only those f-k plots which indicated the phase velocity of the dominant arrival to be within the range of 2.0 to 5.0 km/sec are shown in Figure 3. The size of symbols is proportional to the power in each dominant arrival but the maximum power for normal and residual f-k plots differ by about 25 db. In Figure 3a, the phase velocities of dominant arrivals on normal f-k plots show considerable variation whereas the phase velocities of most prominent arrivals on residual f-k plots are restricted to velocities close to 2.5 km/sec, suggesting Rg . Similarly, Figure 3b indicates nearly all dominant arrivals on the normal f-k plots arriving from directions close to the backazimuth to the source and most dominant arrivals on the residual f-k plots coming from the direction of Skreikampen. The arrows marked by the letters A and B denote prominent arrivals in windows corresponding to Lg_{max} and Lg_{max} + 14 sec. The second (B) arrival is associated with a phase velocity expected for Rg and agrees remarkably well with the expected backazimuth and arrival time of Lg-to-Rg scattered from Skreikampen. The large number of prominent arrivals, with phase velocity typical of Rg and azimuthal direction close to Skreikampen, observed on residual f-k plots (Figure 3) suggests that a significant fraction of the seismic energy directly reaching Skreikampen is continuously scattered into Rg recorded at NORESS.

# F-K ANALYSIS OF REGIONAL DATA FROM TWO LOCAL EARTHQUAKES

Results of similar analysis of NORESS data from the earthquake of 1 April 1986 (56.42° N, 12.10° E, $m_b \approx 3.6$, distance 482 km, backazimuth 176°; Jurkevics, 1988) are shown in Figures 4 and 5. F-k results for the 6.4 sec long window with the largest amplitude Lg, Lg_{max}, shown in Figure 4a, indicate a phase velocity of about 3.7 km/sec and a backazimuth of about 169°. Based on known location of the Skreikampen scatterer, the scattered Lg-to-Rg arrival should arrive about 6 sec after Lg_{max}; the corresponding normal f-k plot is shown in Figure 4b. F-k plots from residual seismograms provided results shown in Figures 4c to 4f in which plots for both later windows (Figures 4d and 4f) clearly indicate the expected Lg-to-Rg arrivals along the expected direction and with phase velocity appropriate for Rg. In addition to Lg-to-Rg arrivals from the direction of Skreikampen, Figures 2d and 2f also suggest prominent arrivals from a direction close to that of Bronkeberget and with phase velocity expected of Rg. These secondary arrivals are therefore probably due to the scattering of Lg-to-Rg in the vicinity of Bronkeberget. A comparison of the power on the normal (Figure 4b) and residual (Figure 4d) f-k plots again suggests that the amplitude of the scattered Lg is not insignificant.

Similar to the analysis of data from the mine blast, f-k plots from both normal and residual seismograms were obtained for 25 sec of Lg, starting 5 sec before Lg_{max}. Results based on f-k plots with the phase velocity of the dominant arrival limited to 2.0-5.0 km/sec are shown in Figure 5. The size of symbols is again proportional to the power in each dominant arrival but the maximum powers for normal and residual f-k plots differ by about 25 db. All dominant arrivals on the normal f-k plots are observed to be from directions close to the backazimuth to the source whereas most dominant arrivals on the residual f-k plots appear to
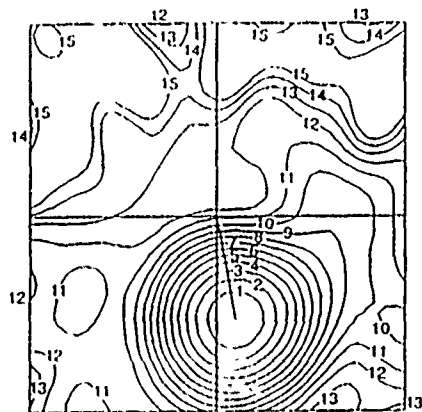
78
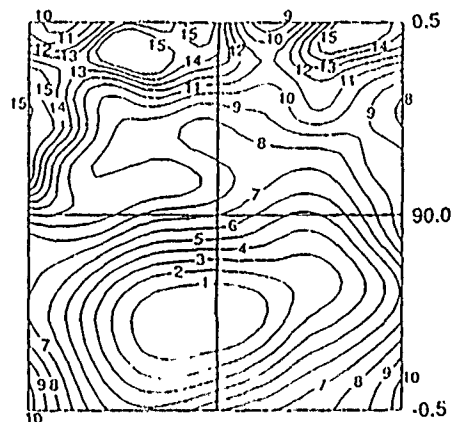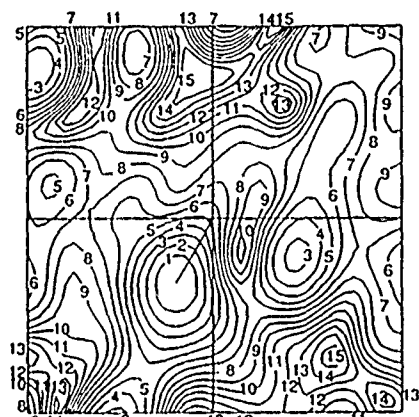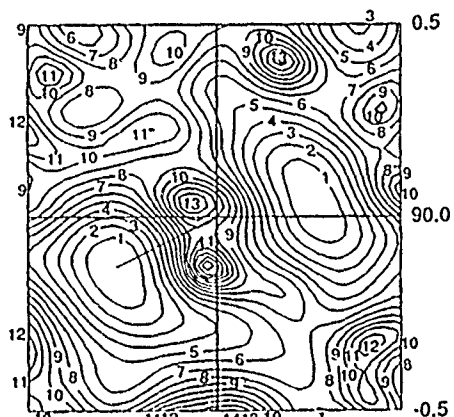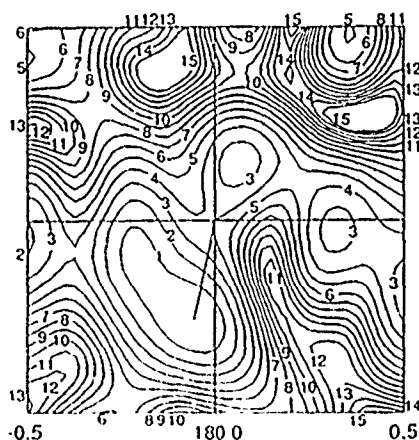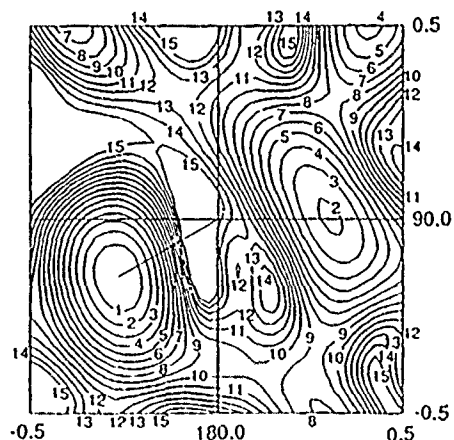
Figure 4. Similar to Figure 2 for the regional earthquake of 1 April 1986. Both (d) and (f) indicate prominent scattered arrivals from directions close to Skreikampen and Bronkeberget.

(a)

(b)

△ NORMAL, ○ RESIDUAL, 1.25 ± 0.75 Hz
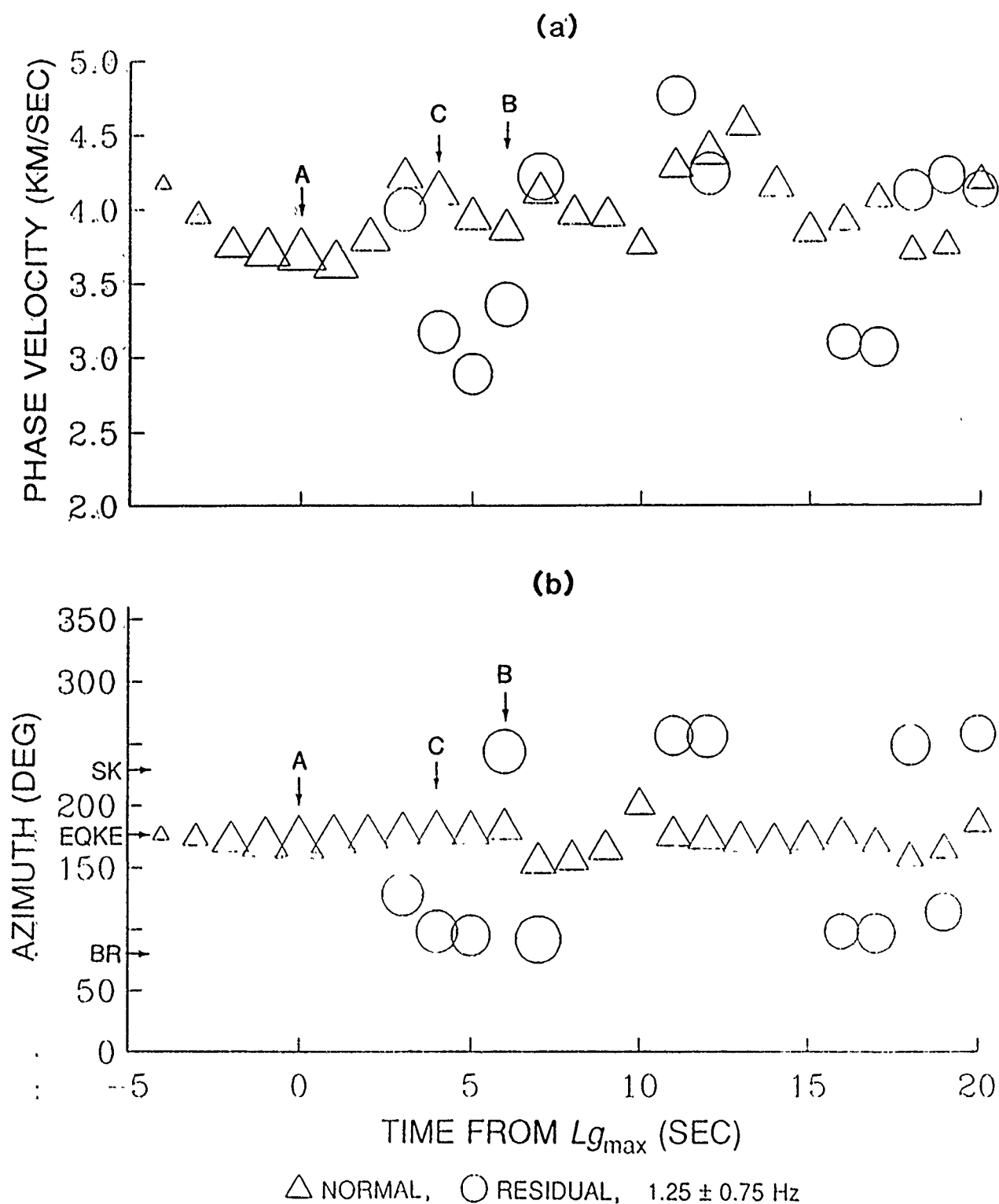
Figure 5. Similar to Figure 3 for the regional earthquake of 1 April 1986. Backazimuths to the earthquake, Skreikampen, and Bronkeberget are denoted by EQKE, SK, and BR, respectively. Arrows marked A, B, and C denote windows corresponding to Lg$_{max}$ and the expected Lg$_{max}$-to-Rg scattered phases from Skreikampen and Bronkeberget, respectively. Results from the residual seismograms indicate Rg arrivals from azimuthal directions close to those of Skreikampen and Bronkeberget.

be from directions close to those of the two scattering regions associated with Skreikampen and Bronkeberget. The arrows denoted by the letters A, B, and C denote windows corresponding to Lg_{max}, Lg_{max} + 6 sec, and Lg_{max} + 4 sec, respectively. The last two arrival times are associated with phase velocities expected for Rg and agree remarkably well with the expected backazimuth and arrival times of Lg-to-Rg scattered from Skreikampen and Bronkeberget, respectively.

F-k plots were also obtained for 6.4 sec long windows containing the Pn, Pg_{max} and later arrivals. Results from normal seismograms containing the Pn and Pg_{max} windows are shown in Figures 6a and 6d, respectively. The residual f-k plots for the Pn + 6 sec and Pg_{max} + 6 sec windows indicated dominant arrivals from the south-west direction (Figures 6c and 6f) although the corresponding normal f-k plots (Figures 6b and 6e) suggested dominant arrivals directly from the source region. Considering the phase velocities and the various distances involved, it seems that the primary arrivals observed on the two residual plots in Figures 6c and 6f are probably be due to the scattering near Skreikampen of Pn-to-Rg and Pg_{max}-to-Rg, respectively.

Similar analyses were carried on the NORESS data for another earthquake that occurred along a considerably different azimuthal direction. Results from the earthquake of 5 February 1986 (62.81° N, 4.86° E, $m_b \approx 4.7$, distance 422 km, backazimuth 306°; Jurkevics, 1988), based on the use of Pn and Pg windows, are shown in Figures 7 and 8, respectively. Lg from this relatively larger event was clipped so that scattering of Lg-to-Rg could not be investigated. Pn from this event was rather weak but Pg was strong and impulsive. In Figure 7, only the f-k plot with the lowest frequency passband (Figure 7f) shows prominent Rg arrival from the direction of Skreikampen, probably because of the low amplitude of Pn. However,

(a) N, Pn + 1.0 sec, 0.90 ± 0.60 Hz
Az: 194.0 Vel: 6.76 Pwr: 0.1

(b) N, Pn + 6.0 sec, 0.90 ± 0.60 Hz
Az: 161.4 Vel: 9.71 Pwr: 2.8

(c) R, Pn + 6.0 sec, 0.90 ± 0.60 Hz
Az: 231.0 Vel: 3.23 Pwr: -4.1

(d) N, Pg$_{max}$, 0.90 ± 0.60 Hz
Az: 177.8 Vel: 5.41 Pwr: 14.7

(e) N, Pg$_{max}$ + 6.0 sec, 0.90 ± 0.60 Hz
Az: 177.1 Vel: 7.91 Pwr: 8.3

(f) R, Pg$_{max}$ + 6.0 sec, 0.90 ± 0.60 Hz
Az: 248.2 Vel: 3.05 Pwr: 3.8

Figure 6. Similar to Figure 2 but based on use of Pn and Pg windows on records of the regional earthquake of 1 April 1986. Plots (a), (b), (d), and (e) are obtained by using normal (N) seismograms. Plots (c) and (f), derived from residual (R) seismograms, indicate prominent scattered arrivals from the direction of Skreikampen, probably due to the scattering of Pn-to-Rg and Pg$_{max}$-to-Rg, respectively.

82

(a) N, Pn + 1.0 sec, 1.25 ± 0.75 Hz
Az: 304.4 Vel: 8.28 Pwr: 26.4

(b) N, Pn + 9 0 sec, 1.25 ± 0.75 Hz
Az: 307.4 Vel: 6.99 Pwr: 31.9

(c) R, Pn + 1.0 sec, 1.25 ± 0.75 Hz
Az: 287.6 Vel: 2.79 Pwr: 10.1

(d) R, Pn + 9.0 sec, 1.25 ± 0.75 Hz
Az: 111.3 Vel: 2.76 Pwr: 19.2

(e) R, Pn + 1.0 sec, 0.90 ± 0.60 Hz
Az: 282.5 Vel: 2.30 Pwr: 6.8

(f) R, Pn + 9.0 sec, 0.90 ± 0.60 Hz
Az: 257.3 Vel: 3.24 Pwr: 13.9

Figure 7. Similar to Figure 2 but based on use of Pn windows on records of the regional earthquake of 5 February 1986. Only the lowest-frequency passband (f) indicates prominent scattered arrival from the direction of Skreikampen, probably due to the scattering of Pn-to-Rg.

83

(a) N, Pg$_{max}$, 1.25 ± 0.75 Hz
Az: 305.9 Vel: 6.57 Pwr: 54.9

(b) N, Pg$_{max}$ + 8.0 sec, 1.25 ± 0.75 Hz
Az: 298.2 Vel: 6.72 Pwr: 43.6

(c) R, Pg$_{max}$, 1.25 ± 0.75 Hz
Az: 37.6 Vel: 75.32 Pwr: 41.7

(d) R, Pg$_{max}$ + 8.0 sec, 1.25 ± 0.75 Hz
Az: 252.1 Vel: 2.88 Pwr: 39.7

(e) R, Pg$_{max}$, 0.90 ± 0.60 Hz
Az: 57.8 Vel: 17.36 Pwr: 36.2

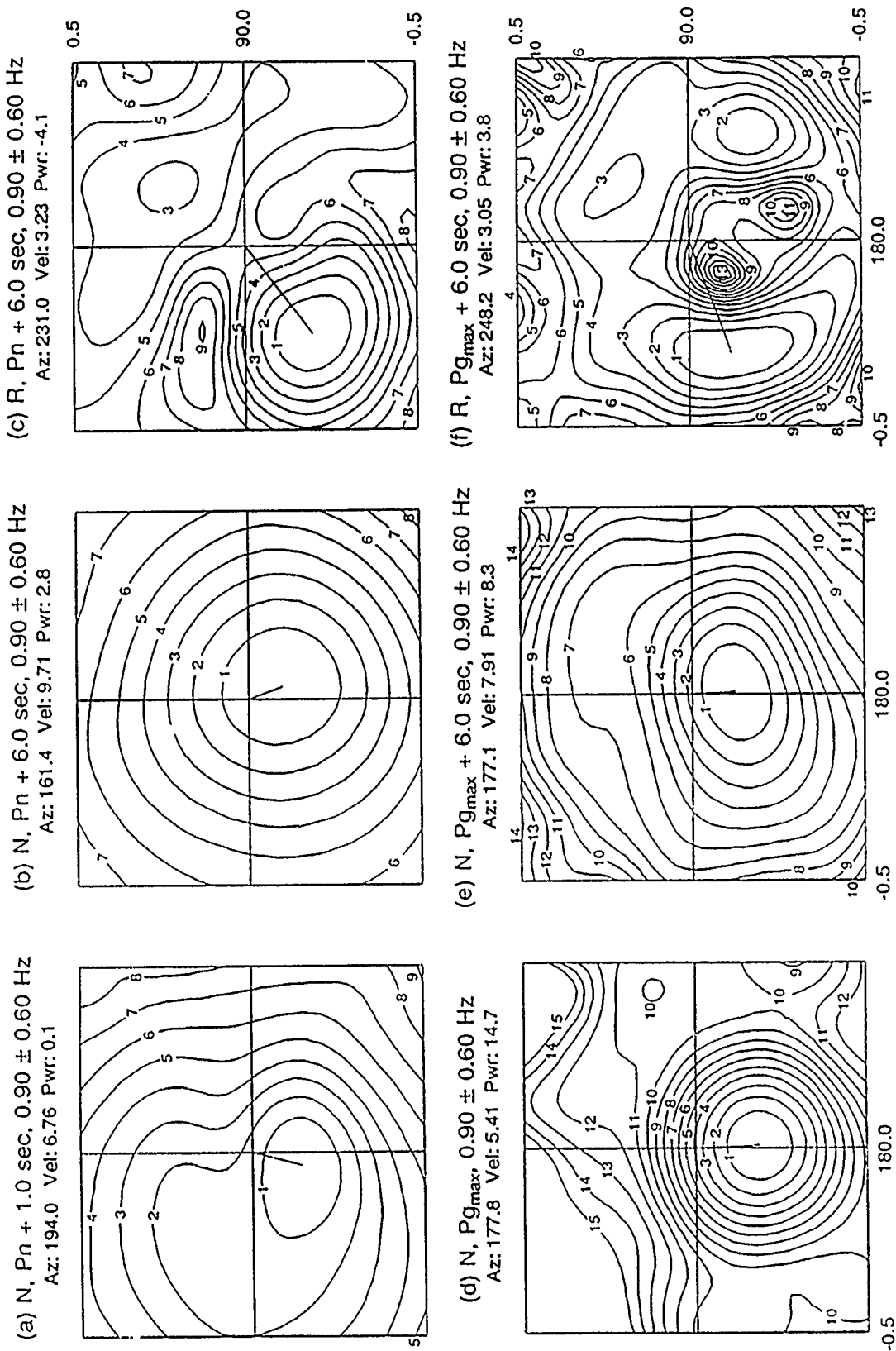(f) R, Pg$_{max}$ + 8.0 sec, 0.90 ± 0.60 Hz
Az: 251.6 Vel: 2.83 Pwr: 36.2

Figure 8. Similar to Figure 2 but based on use of Pg windows on records of the regional earthquake of 5 February 1986. Both (d) and (f) indicate prominent scattered Rg arrivals from the direction of Skreikampen, probably due to the scattering of Pg$_{max}$-to-Rg.

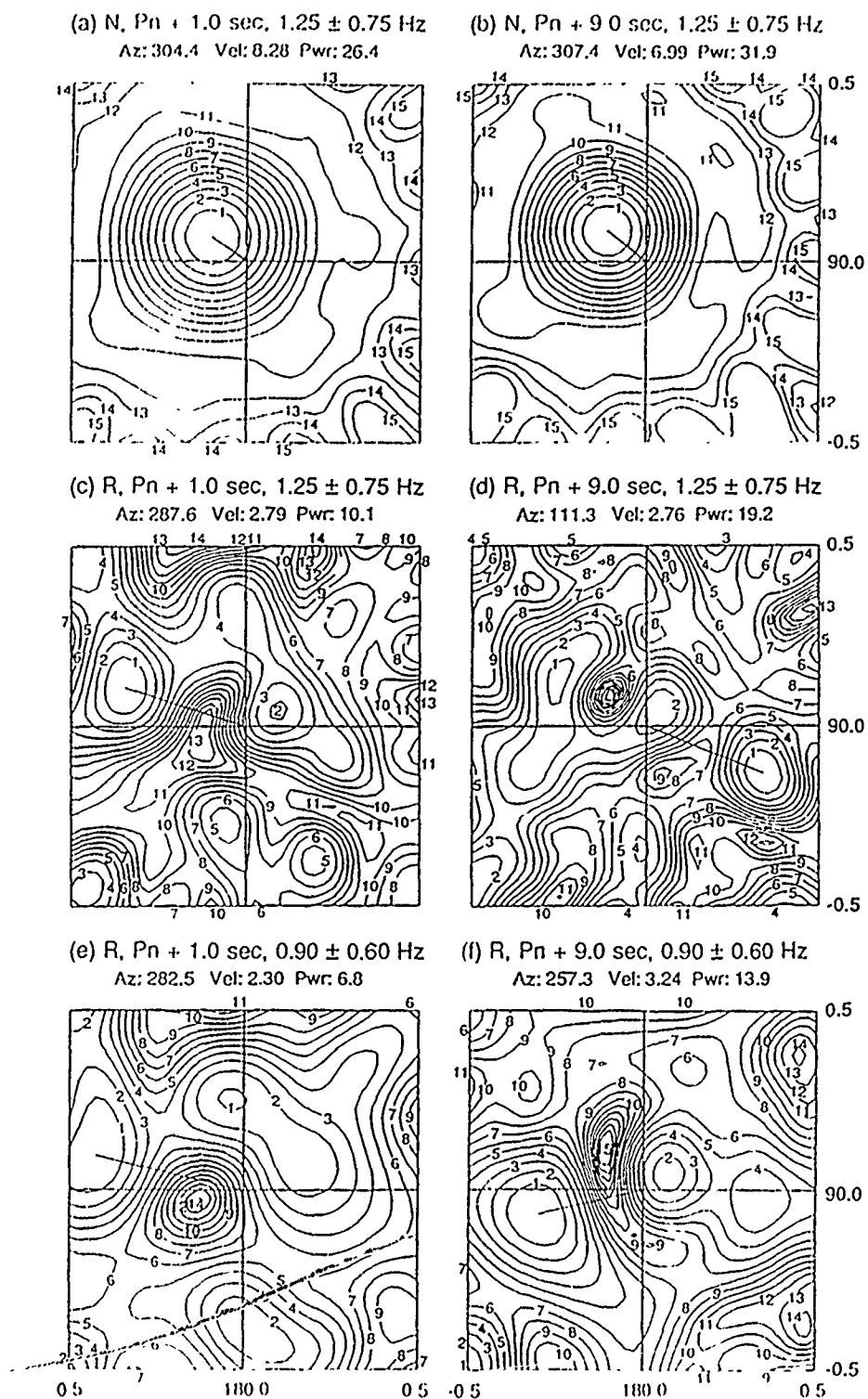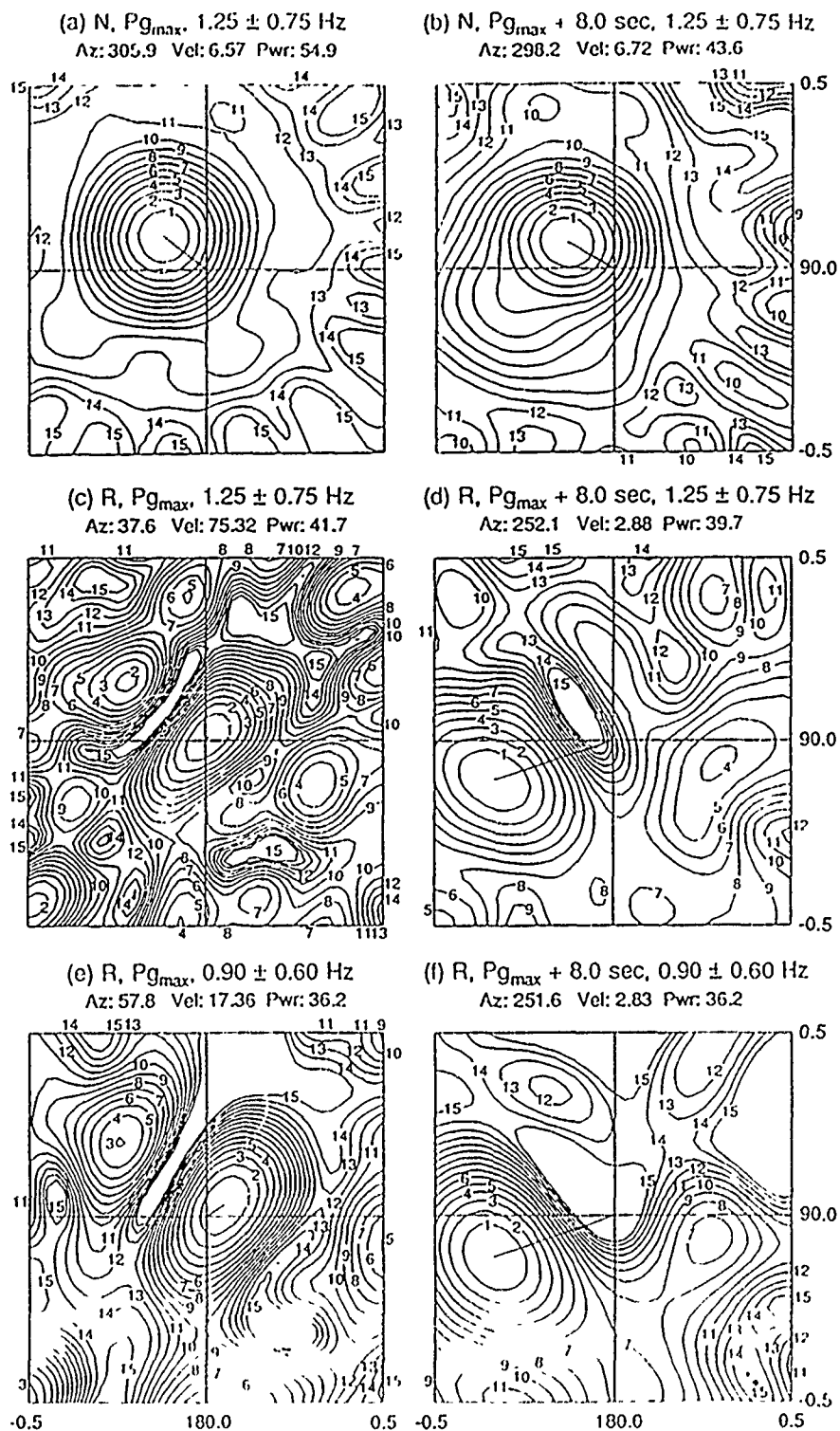plots in both Figures 8d and 8f, based on the use of Pg windows, show clear evidence of Rg arrivals from the direction of Skreikampen.

In addition to these two events, several other earthquake and explosion sources along various azimuthal directions to NORESS also provided evidence for scattered arrivals Pn-to-Rg, Pg-to-Rg, and Lg-to-Rg, originating mainly from the two scattering source regions near Skreikampen and Bronkeberget. These scattered arrivals are observed with remarkable clarity and closeness to the expected arrival times and are rich in low frequencies, as expected for Rg. Their presence in various regional phases indicates that near-receiver scattering plays an important role in the composition of regional phases.

POSSIBLE EFFECT OF SCATTERING ON ESTIMATION OF SOURCE AZIMUTH

Suteau-Henson (1990) examined azimuth and slowness estimates by polarization analysis of the first several seconds of P arrivals on three-component recordings of regional events recorded at NORESS. The epicentral locations of these events were known from the Intelligent Monitoring System Bulletins. Results for azimuth differences (defined as azimuth from polarzation minus azimuth from the IMS Bulletins) versus the IMS azimuth for the four three-component sensors, NRA0, NRC2, NRC4, and NRC7 are shown in Figure 9 (after Figure 9b of Suteau-Henson, 1990). Although NRC7, which has the largest number of observations, shows considerably more deviations than the other three sensors, the generally large deviation at azimuths of about 90° and 230° − 300° for all sensors may, at least in part, be due to the scattering at Bronkeberget and Skreikampen, respectively, which lie along nearly the same azimuthal directions (see Figure 1).

Assuming isotropic scattering, the contribution of secondary arrivals (such as Pn-to-Rg) due to scattering at Bronkeberget is expected to be the earliest (about 2 sec after the first Pn) for seismic sources lying east of NORESS. This may contaminate the Pn phase particle motion, producing larger errors in azimuth estimates of events east of NORESS. A similar reason for larger azimuthal errors may apply to events lying along the azimuthal direction of Skreikampen. A detailed study may lead to azimuth-dependent corrections for the improvement of azimuth estimates from three-component data recorded at NORESS.

Odegaard et al. (1990) investigated the effects of surface topography within a few km of NORESS and ARCESS on slowness and azimuth anomalies for signals recorded at the two arrays. Surface topography was found to explain about half of the observed anomalies in the three-component solutions.
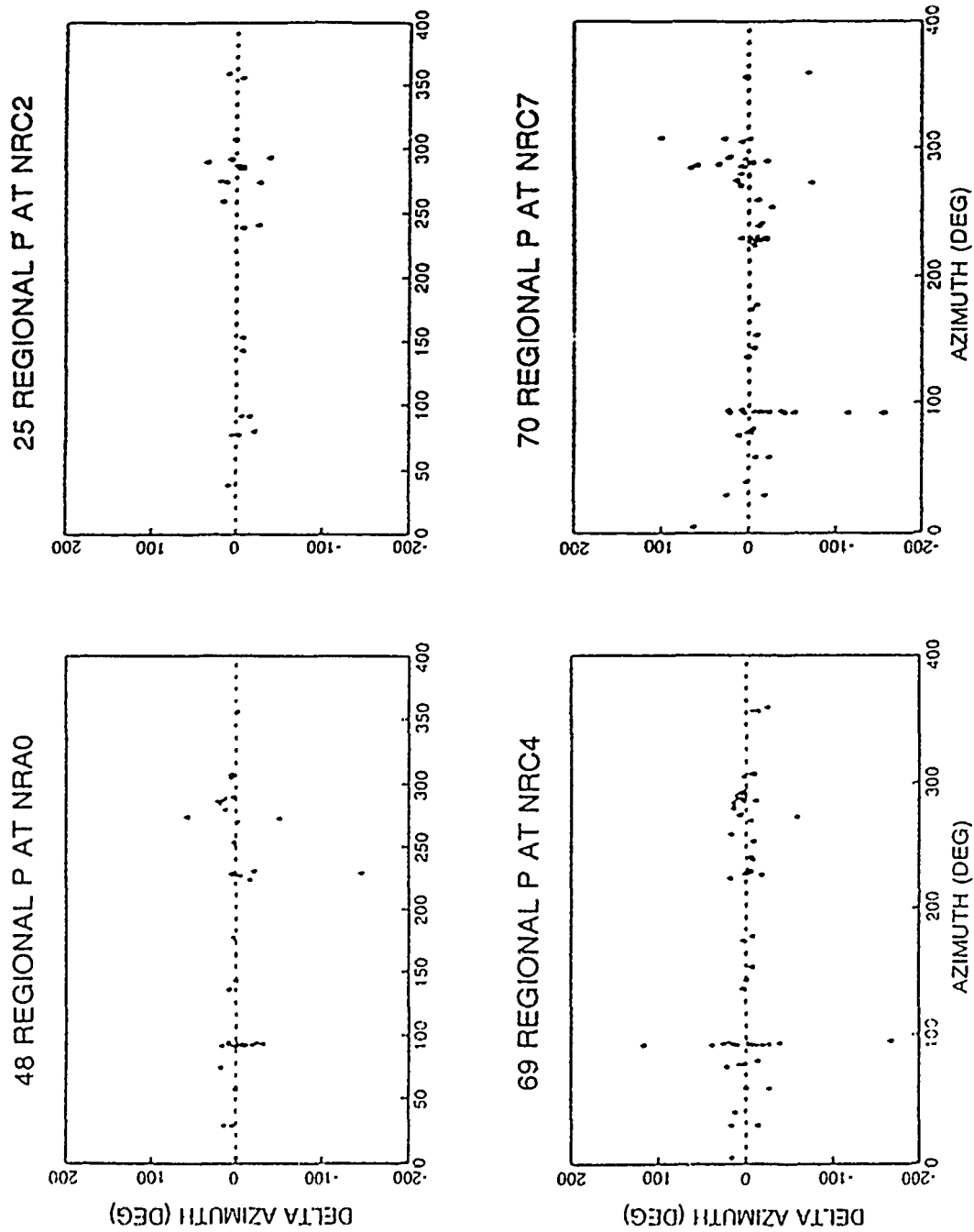
86

Figure 9. Azimuth differences versus theoretical azimuth for regional P arrivals at the four NORESS three-component sensors. Note the generally larger differences along azimuths corresponding to Bronkeberget and Skreikampen.

87

DISCUSSION

Use of data from arrays such as NORESS is essential for monitoring decoupled and low-yield coupled nuclear explosions because of the significant improvement in S/N provided by multi-channel data. Array measurements of Lg have also been known to provide remarkably precise measurements of yields of USSR nuclear explosions. It is therefore important to investigate methods which can further improve measurements of regional phases at arrays. Our recently developed methods including the use of residual seismograms have already demonstrated their effectiveness in determining locations of prominent scatterers near NORESS. A knowledge of the contribution of near-receiver scattering associated with various seismic sources (underground nuclear explosions and earthquakes) makes it possible to correct the observed Lg for the effects of local (near-receiver) scattering. The improved estimates of Lg should lead to improvement in Lg-based yield estimates and source discrimination.

CONCLUSIONS

F-k analyses of NORESS array recordings of teleseismic events have indicated a prominent secondary source about 25-30 km southwest of the array, in the region of Lake Mjosa, with large topographical relief. Both earthquake and explosion sources at regional distances and along various azimuthal directions to NORESS provide evidence for easily observed scattered phases Pn-to-Rg, Pg-to-Rg, and Lg-to-Rg, originating from the same region of Lake Mjosa. This implies that scattering due to known scatterers near NORESS exerts significant influence on the regional phases Pn, Pg, and Lg and a detailed investigation should be useful in improving location and yield determination of regional events. Similar studies of the influence of discrete local scatterers on regional phases should be carried out for other arrays such as ARCESS and GERESS. The results are useful not only in the understanding of various arrivals on regional seismograms but also in improving yield estimates and source location and discrimination.

ACKNOWLEDGMENTS

REFERENCES

Bannister, S. C., E. S. Husebye, and B. O. Ruud (1990). Teleseismic P-coda analyzed by three-component and array techniques - deterministic location of topographic P-to-Rg scattering near the NORESS array, *Bull. Seism. Soc. Am. 80*, 1969-1986.

Blandford, R., T. Cohen, and J. Woods (1976). An iterative approximation to the mixed-signal processor, *Geophys. J. 45*, 677-687.

Gupta, I. N. and R. R. Blandford (1983). A mechanism for generation of short-period transverse motion from explosions, *Bull. Seism. Soc. Am. 73*, 571-591.

Gupta, I. N., C. S. Lynnes, R. S. Jih, and R. A. Wagner (1989). A study of teleseismic P and P-coda from U.S. and Soviet nuclear explosions, paper presented at the 11th Annual DARPA/AFGL Seismic Research Symposium, San Antonio, Texas. GL-TR-90-0301, ADA229228

Gupta, I. N., C. S. Lynnes, and R. A. Wagner (1990a). Broadband f-k analysis of array data to identify sources of local scattering, *Geophys. Res. Lett. 17*, 183-186.

Gupta, I. N., C. S. Lynnes, T. W. McElfresh, and R. A. Wagner (1990b). F-k analysis of NORESS array and single-station data to identify sources of near-receiver and near-source scattering, *Bull. Seism. Soc. Am. 80*, 2227-2241.

Gupta, I. N., C. S. Lynnes, and R. A. Wagner (1990c). An array study of the effects of a known local scatterer on regional phases - preliminary results, *EOS 71 (17)*, 565 (abstract).

Hedlin, M. A. H., J. B. Minster, and J. A. Orcutt (1991). Beam-stack imaging using a small aperture array, *Geophys. Res. Lett. 18*, 1771-1774.

Jurkevics, A., 1988. Polarization analysis of three-component array data, *Bull. Seism. Soc. Am. 78*, 1725-1743.

Key, F. A. (1967). Signal-generated noise recorded at the Eskdalemuir seismometer array station, *Bull. Seism. Soc. Am. 57*, 27-37.

Odegaard, E., D. J. Doornbos, and T. Kvaerna (1990). Surface topographic effects at arrays and three-component stations, *Bull. Seism. Soc. Am. 80*, 2214-2226.

Suteau-Henson, A. (1990). Estimating azimuth and slowness from three-component and array stations, *Tech. Report C89-02*, 2-50 - 2-87, Center for Seismic Studies, Arlington, Virginia.

Prof. Thomas Ahrens
Seismological Lab, 252-21
Division of Geological & Planetary Sciences
California Institute of Technology
Pasadena, CA 91125

Prof. Keiiti Aki
Center for Earth Sciences
University of Southern California
University Park
Los Angeles, CA 90089-0741

Prof. Shelton Alexander
Geosciences Department
403 Deike Building
The Pennsylvania State University
University Park, PA 16802

Dr. Ralph Alewine, III
DARPA/NMRO
3701 North Fairfax Drive
Arlington, VA 22203-1714

Prof. Charles B. Archambeau
CIRES
University of Colorado
Boulder, CO 80309

Dr. Thomas C. Bache, Jr.
Science Applications Int'l Corp.
10260 Campus Point Drive
San Diego, CA 92121 (2 copies)

Prof. Muawia Barazangi
Institute for the Study of the Continent
Cornell University
Ithaca, NY 14853

Dr. Jeff Barker
Department of Geological Sciences
State University of New York
 at Binghamton
Vestal, NY 13901

Dr. Douglas R. Baumgardt
ENSCO, Inc
5400 Port Royal Road
Springfield, VA 22151-2388

Dr. Susan Beck
Department of Geosciences
Building #77
University of Arizona
Tuscon, AZ 85721

Dr. T.J. Bennett
S-CUBED
A Division of Maxwell Laboratories
11800 Sunrise Valley Drive, Suite 1450
Reston, VA 22091

Dr. Robert Blandford
AFTAC/TT, Center for Seismic Studies
1330 North 17th Street
Suite 1450
Arlington, VA 22209-2308

Dr. G.A. Bollinger
Department of Geological Sciences
Virginia Polytechnical Institute
21044 Derring Hall
Blacksburg, VA 24061

Dr. Stephen Bratt
Center for Seismic Studies
1300 North 17th Street
Suite 1450
Arlington, VA 22209-2308

Dr. Lawrence Burdick
Woodward-Clyde Consultants
566 El Dorado Street
Pasadena, CA 91109-3245

Dr. Robert Burridge
Schlumberger-Doll Research Center
Old Quarry Road
Ridgefield, CT 06877

Dr. Jerry Carter
Center for Seismic Studies
1300 North 17th Street
Suite 1450
Arlington, VA 22209-2308

Dr. Eric Chael
Division 9241
Sandia Laboratory
Albuquerque, NM 87185

Prof. Vernon F. Cormier
Department of Geology & Geophysics
U-45, Room 207
University of Connecticut
Storrs, CT 06268

Prof. Anton Dainty
Earth Resources Laboratory
Massachusetts Institute of Technology
42 Carleton Street
Cambridge, MA 02142

Prof. Steven Day
Department of Geological Sciences
San Diego State University
San Diego, CA 92182

Dr. Art Frankel
U.S. Geological Survey
922 National Center
Reston, VA 22092

Marvin Denny
U.S. Department of Energy
Office of Arms Control
Washington, DC 20585

Dr. Cliff Frolich
Institute of Geophysics
8701 North Mopac
Austin, TX 78759

Dr. Zoltan Der
ENSCO, Inc.
5400 Port Royal Road
Springfield, VA 22151-2388

Dr. Holly Given
IGPP, A-025
Scripps Institute of Oceanography
University of California, San Diego
La Jolla, CA 92093

Prof. Adam Dziewonski
Hoffman Laboratory, Harvard University
Dept. of Earth Atmos. & Planetary Sciences
20 Oxford Street
Cambridge, MA 02138

Dr. Jeffrey W. Given
SAIC
10260 Campus Point Drive
San Diego, CA 92121

Prof. John Ebel
Department of Geology & Geophysics
Boston College
Chestnut Hill, MA 02167

Dr. Dale Glover
Defense Intelligence Agency
ATTN: ODT-1B
Washington, DC 20301

Eric Fielding
SNEE Hall
INSTOC
Cornell University
Ithaca, NY 14853

Dr. Indra Gupta
Teledyne Geotech
314 Montgomery Street
Alexanderia, VA 22314

Dr. Mark D. Fisk
Mission Research Corporation
735 State Street
P.O. Drawer 719
Santa Barbara, CA 93102

Dan N. Hagedon
Pacific Northwest Laboratories
Battelle Boulevard
Richland, WA 99352

Prof Stanley Flatte
Applied Sciences Building
University of California, Santa Cruz
Santa Cruz, CA 95064

Dr. James Hannon
Lawrence Livermore National Laboratory
P.O. Box 808
L-205
Livermore, CA 94550

Dr. John Foley
NER-Geo Sciences
1100 Crown Colony Drive
Quincy, MA 02169

Dr. Roger Hansen
HQ AFTAC/TTR
Patrick AFB, FL 32925-6001

Prof. Donald Forsyth
Department of Geological Sciences
Brown University
Providence, RI 02912

Prof. David G. Harkrider
Seismological Laboratory
Division of Geological & Planetary Sciences
California Institute of Technology
Pasadena, CA 91125

Prof. Danny Harvey
CIRES
University of Colorado
Boulder, CO 80309

Prof. Donald V. Helmberger
Seismological Laboratory
Division of Geological & Planetary Sciences
California Institute of Technology
Pasadena, CA 91125

Prof. Eugene Herrin
Institute for the Study of Earth and Man
Geophysical Laboratory
Southern Methodist University
Dallas, TX 75275

Prof. Robert B. Herrmann
Department of Earth & Atmospheric Sciences
St. Louis University
St. Louis, MO 63156

Prof. Lane R. Johnson
Seismographic Station
University of California
Berkeley, CA 94720

Prof. Thomas H. Jordan
Department of Earth, Atmospheric &
  Planetary Sciences
Massachusetts Institute of Technology
Cambridge, MA 02139

Prof. Alan Kafka
Department of Geology & Geophysics
Boston College
Chestnut Hill, MA 02167

Robert C. Kemerait
ENSCO, Inc.
445 Pineda Court
Melbourne , FL 32940

Dr. Max Koontz
U.S. Dept. of Energy/DP 5
Forrestal Building
1000 Independence Avenue
Washington, DC 20585

Dr. Richard LaCoss
MIT Lincoln Laboratory, M-200B
P.O. Box 73
Lexington, MA 02173-0073

Dr. Fred K. Lamb
University of Illinois at Urbana-Champaign
Department of Physics
1110 West Green Street
Urbana, IL 61801

Prof. Charles A. Langston
Geosciences Department
403 Deike Building
The Pennsylvania State University
University Park, PA 16802

Jim Lawson, Chief Geophysicist
Oklahoma Geological Survey
Oklahoma Geophysical Observatory
P.O. Box 8
Leonard, OK 74043-0008

Prof. Thorne Lay
Institute of Tectonics
Earth Science Board
University of California, Santa Cruz
Santa Cruz, CA 95064

Dr. William Leith
U.S. Geological Survey
Mail Stop 928
Reston, VA 22092

Mr. James F. Lewkowicz
Phillips Laboratory/GPEH
Hanscom AFB, MA 01731-5000(2 copies)

Mr. Alfred Lieberman
ACDA/VI-OA State Department Building
Room 5726
320-21st Street, NW
Washington, DC 20451

Prof. L. Timothy Long
School of Geophysical Sciences
Georgia Institute of Technology
Atlanta, GA 30332

Dr. Robert Masse
Denver Federal Building
Bos 25046, Mail Stop 967
Denver, CO 80225

Dr. Randolph Martin, III
New England Research, Inc.
76 Olcott Drive
White River Junction, VT 05001

3

Dr. Gary McCartor
Department of Physics
Southern Methodist University
Dallas, TX 75275

Dr. Bao Nguyen
HQ AFTAC/TTR
Patrick AFB, FL 32925

Prof. Thomas V. McEvilly
Seismographic Station
University of California
Berkeley, CA 94720

Prof. John A. Orcutt
IGPP, A-025
Scripps Institute of Oceanography
University of California, San Diego
La Jolla, CA 92093

Dr. Art McGarr
U.S. Geological Survey
Mail Stop 977
U.S. Geological Survey
Menlo Park, CA 94025

Prof. Jeffrey Park
Kline Geology Laboratory
P.O. Box 6666
New Haven, CT 06511-8130

Dr. Keith L. McLaughlin
S-CUBED
A Division of Maxwell Laboratory
P.O. Box 1620
La Jolla, CA 92038-1620

Dr. Howard Patton
Lawrence Livermore National Laboratory
L-025
P.O. Box 808
Livermore, CA 94550

Stephen Miller & Dr. Alexander Florence
SRI International
333 Ravenswood Avenue
Box AF 116
Menlo Park, CA 94025-3493

Dr. Frank Pilotte
HQ AFTAC/TT
Patrick AFB, FL 32925-6001

Prof. Bernard Minster
IGPP, A-025
Scripps Institute of Oceanography
University of California, San Diego
La Jolla, CA 92093

Dr. Jay J. Pulli
Radix Systems, Inc.
2 Taft Court, Suite 203
Rockville, MD 20850

Prof. Brian J. Mitchell
Department of Earth & Atmospheric Sciences
St. Louis University
St. Louis, MO 63156

Dr. Robert Reinke
ATTN: FCTVTD
Field Command
Defense Nuclear Agency
Kirtland AFB, NM 87115

Mr. Jack Murphy
S-CUBED
A Division of Maxwell Laboratory
11800 Sunrise Valley Drive, Suite 1212
Reston, VA 22091 (2 Copies)

Prof. Paul G. Richards
Lamont-Doherty Geological Observatory
 of Columbia University
Palisades, NY 10964

Dr. Keith K. Nakanishi
Lawrence Livermore National Laboratory
L-025
P.O. Box 808
Livermore, CA 94550

Mr. Wilmer Rivers
Teledyne Geotech
314 Montgomery Street
Alexandria, VA 22314

Dr. Carl Newton
Los Alamos National Laboratory
P.O. Box 1663
Mail Stop C335, Group ESS-3
Los Alamos, NM 87545

Dr. George Rothe
HQ AFTAC/TTR
Patrick AFB, FL 32925-6001

Dr. Alan S. Ryall, Jr.
DARPA/NMRO
3701 North Fairfax Drive
Arlington, VA 22209-1714

Dr. Richard Sailor
TASC, Inc.
55 Walkers Brook Drive
Reading, MA 01867

Prof. Charles G. Sammis
Center for Earth Sciences
University of Southern California
University Park
Los Angeles, CA 90089-0741

Prof. Christopher H. Scholz
Lamont-Doherty Geological Observatory
 of Columbia University
Palisades, CA 10964

Dr. Susan Schwartz
Institute of Tectonics
1156 High Street
Santa Cruz, CA 95064

Secretary of the Air Force
(SAFRD)
Washington, DC 20330

Office of the Secretary of Defense
DDR&E
Washington, DC 20330

Thomas J. Sereno, Jr.
Science Application Int'l Corp.
10260 Campus Point Drive
San Diego, CA 92121

Dr. Michael Shore
Defense Nuclear Agency/SPSS
6801 Telegraph Road
Alexandria, VA 22310

Dr. Matthew Sibol
Virginia Tech
Seismological Observatory
4044 Derring Hall
Blacksburg, VA 24061-0420

Prof. David G. Simpson
IRIS, Inc.
1616 North Fort Myer Drive
Suite 1400
Arlington, VA 22209

Donald L. Springer
Lawrence Livermore National Laboratory
L-025
P.O. Box 808
Livermore, CA 94550

Dr. Jeffrey Stevens
S-CUBED
A Division of Maxwell Laboratory
P.O. Box 1620
La Jolla, CA 92038-1620

Lt. Col. Jim Stobie
ATTN: AFOSR/NL
Bolling AFB
Washington, DC 20332-6448

Prof. Brian Stump
Institute for the Study of Earth & Man
Geophysical Laboratory
Southern Methodist University
Dallas, TX 75275

Prof. Jeremiah Sullivan
University of Illinois at Urbana-Champaign
Department of Physics
1110 West Green Street
Urbana, IL 61801

Prof. L. Sykes
Lamont-Doherty Geological Observatory
 of Columbia University
Palisades, NY 10964

Dr. David Taylor
ENSCO, Inc.
445 Pineda Court
Melbourne, FL 32940

Dr. Steven R. Taylor
Los Alamos National Laboratory
P.O. Box 1663
Mail Stop C335
Los Alamos, NM 87545

Prof. Clifford Thurber
University of Wisconsin-Madison
Department of Geology & Geophysics
1215 West Dayton Street
Madison, WS 53706

Prof. M. Nafi Toksoz
Earth Resources Lab
Massachusetts Institute of Technology
42 Carleton Street
Cambridge, MA 02142

Dr. Larry Turnbull
CIA-OSWR/NED
Washington, DC 20505

Dr. Gregory van der Vink
IRIS, Inc.
16116 North Fort Myer Drive
Suite 1440
Arlington, VA 22209

Dr. Karl Veith
EG&G
5211 Auth Road
Suite 240
Suitland, MD 20746

Prof. Terry C. Wallace
Department of Geosciences
Building #77
University of Arizona
Tuscon, AZ 85721

Dr. Thomas Weaver
Los Alamos National Laboratory
P.O. Box 1663
Mail Stop C335
Los Alamos, NM 87545

Dr. William Wortman
Mission Research Corporation
8560 Cinderbed Road
Suite 700
Newington, VA 22122

Prof. Francis T. Wu
Department of Geological Sciences
State University of New York
 at Binghamton
Vestal, NY 13901

AFTAC/CA
(STINFO)
Patrick AFB, FL 32925-6001

DARPA/PM
3701 North Fairfax Drive
Arlington, VA 22203-1714

DARPA/RMO/RETRIEVAL
3701 North Fairfax Drive
Arlington, VA 22203-1714

DARPA/RMO/SECURITY OFFICE
3701 North Fairfax Drive
Arlington, VA 2203-1714

HQ DNA
ATTN: Technical Library
Washington, DC 20305

Defense Intelligence Agency
Directorate for Scientific & Technical Intelligence
ATTN: DTIB
Washington, DC 20340-6158

Defense Technical Information Center
Cameron Station
Alexandria, VA 22314 (2 Copies)

TACTEC
Battelle Memorial Institute
505 King Avenue
Columbus, OH 43201 (Final Report)

Phillips Laboratory
ATTN: XPG
Hanscom AFB, MA 01731-5000

Phillips Laboratory
ATTN: GPE
Hanscom AFB, MA 01731-5000

Phillips Laboratory
ATTN: TSML
Hanscom AFB, MA 01731-5000

Phillips Laboratory
ATTN: SUL
Kirtland, NM 87117 (2 copies)

Dr. Michel Bouchon
I.R.I.G.M.-B.P. 68
38402 St. Martin D'Heres
Cedex, FRANCE

Dr. Michel Campillo
Observatoire de Grenoble
I.R.I.G.M.-B.P. 53
38041 Grenoble, FRANCE

Dr. Kin Yip Chun
Geophysics Division
Physics Department
University of Toronto
Ontario, CANADA

Prof. Hans-Peter Harjes
Institute for Geophysic
Ruhr University/Bochum
P.O. Box 102148
4630 Bochum 1, GERMANY

Prof. Eystein Husebye
NTNF/NORSAR
P.O. Box 51
N-2007 Kjeller, NORWAY

David Jepsen
Acting Head, Nuclear Monitoring Section
Bureau of Mineral Resources
Geology and Geophysics
G.P.O. Box 378, Canberra, AUSTRALIA

Ms. Eva Johannisson
Senior Research Officer
National Defense Research Inst.
P.O. Box 27322
S-102 54 Stockholm, SWEDEN

Dr. Peter Marshall
Procurement Executive
Ministry of Defense
Blacknest, Brimpton
Reading FG7-FRS, UNITED KINGDOM

Dr. Bernard Massinon, Dr. Pierre Mechler
Societe Radiomana
27 rue Claude Bernard
75005 Paris, FRANCE (2 Copies)

Dr. Svein Mykkeltveit
NTNT/NORSAR
P.O. Box 51
N-2007 Kjeller, NORWAY (3 Copies)

Prof. Keith Priestley
University of Cambridge
Bullard Labs, Dept. of Earth Sciences
Madingley Rise, Madingley Road
Cambridge CB3 OEZ, ENGLAND

Dr. Jorg Schlittenhardt
Federal Institute for Geosciences & Nat'l Res.
Postfach 510153
D-3000 Hannover 51, GERMANY

Dr. Johannes Schweitzer
Institute of Geophysics
Ruhr University/Bochum
P.O. Box 1102148
4360 Bochum 1, GERMANY